DEVELOPMENT OF THERAPEUTIC SYSTEMS TO TREAT THE INFARCTED HEART

A Dissertation
Presented to
The Academic Faculty

by

Warren Dale Gray

In Partial Fulfillment
of the Requirements for the Degree
Doctor of Philosophy in the
Wallace H. Coulter Department of Biomedical Engineering

Georgia Institute of Technology
May 2014

DEVELOPMENT OF THERAPEUTIC SYSTEMS TO TREAT THE INFARCTED HEART

Approved by:

Dr. Michael E. Davis, Advisor
Department of Biomedical Engineering
Georgia Institute of Technology &
Emory University

Dr. Ying Luo, Advisor
Department of Biomedical Engineering
Peking University &
Georgia Institute of Technology

Dr. Julie A. Champion
School of Chemical & Biomolecular Engineering
Georgia Institute of Technology

Dr. Hanjoong Jo
Department of Biomedical Engineering
Georgia Institute of Technology &
Emory University

Dr. Charles Searles, Jr.
School of Medicine
Emory University

Date Approved: 5 March 2014

To my parents,
Raymond and Kim Gray,
who taught me to explore

ACKNOWLEDGMENTS

Shortly after starting my graduate degree, my plans included working in three labs at three campuses, so I realized that I would need the support of many people if I wanted to survive. In this section, I would like to send a big thank you to all of the people who have made this experience successful (pending my committee's decision!)—and enjoyable.

First, I would like to thank my research advisors. Dr. Michael Davis has helped me through it all, and in addition to shaping my research skills, has provided a perfect balance between guidance and freedom, and has brought levity to many difficult situations. My advisor at PKU, Dr. Ying Luo, took a chance on me when she accepted me into her lab based merely on email interactions. During my stay, she provided fine examples of how to re-examine and refine hypotheses and approaches. Dr. Niren Murthy was instrumental in teaching me chemical synthesis research and taught me how to evaluate research novelty.

I would also like to thank my thesis committee members: Julie Champion, Hanjoong Jo, and Charles Searles. Even though the committee was formed relatively late in the phD process due to logistical complications, the committee members have nonetheless provided invaluable feedback that hugely shaped my projects.

Niren's lab provided an ideal situation for my chemical synthesis crash course, and I would like to thank all of his researchers (Abhinav Acharya, Madhuri Dasari, Yash Kolambkar, Kousik Kundu, Dongwoon Lee, Jason Lee, Xinghai Ning, and Scott Wilson). Special thanks to Scott for telling me to keep swimming, Madhuri for patiently explain reaction mechanisms, and Xinghai for his carbohydrate chemistry wizardry.

Not having met Ying's lab members before going to China, I was nervous that things might not "click" well and that I would feel like a foreigner outside of lab and in. To the complete contrary, however, they welcomed me with open arms. We learned science and culture from each other, and along the way you all became my brothers and sisters (Liyang Jiang, Jiaying Liu, Jie Liu, Xiaopeng Liu, Bing Lv, Jinyang Wang, Kai Wang, Ruo Jia Wu, Xiang Yin, and Wei Zhang). I would especially like to acknowledge 妹妹 Jie and Liyang for showing me the ropes in lab and 弟弟 Kai.

The majority of my time was spent in Mike's lab, and I want to thank the lab members (Srishti Bhutani, Arhana Boopathy, Milton Brown, Bernadette Cabigas, Pauline Che, Kristen French, Shohini Ghosh- Chadhary, Gokul Iyer, Katie Maiellaro-Rafferty, Mario Martinez, Karl Pendergrass, Jay Sy Amanda Smith, and Inthu Somasuntharam) for providing thought-provoking scientific questions and guidance as well as an enjoyable work environment. The many sounds of pipetting, cell splitting, and centrifuging was matched by plentiful laughter, and going to conferences with y'all made me giddy like a grade-school boy.

The undergraduate researchers with whom I worked deserve many thanks for all their help and letting me develop some mentoring skills. Dave Bhaumik (Murthy & Davis labs) imaged hundreds of heart cross sections. Ruo Jia Wu and Xiang Ying (Luo Lab) plated thousands of cells, ran qRT-PCR, and evaluated cytotoxicity. Shohini Ghosh-Chaudhary worked with four cell types, ran qRT-PCR, cultured millions of cells, troublshot apoptosis assays, and imaged tube formation. I feel fortunate to have worked with such dedicated folks.

Also, I would like to thank labs with which we have collaborated and affiliated: Dr. Platt's, Dr. Jo's, Dr. Taylor's, and Dr. Searles'.

There are several people on the administrative side who deserve thanks. Leita Young at Emory always kindly helped figure out the Emory side of things and reimbursements. Jialei Luo at PKU was crucial for getting everything sorted out for my exchange there. Dr. Cheng Zhu also was vital to fitting my year in China into my graduate program. Sally Gerrish at GT has provided both invaluable advice and a listening ear. Shannon Sullivan, our self-titled “big sister,” has not only helped me navigate paperwork and milestones, but has been there to chat about life and release steam.

I have been fortunate to receive funding during my graduate experience. Thank you to: Drug Design, Delivery, and Development Grant; the Whitaker Seed Grant for the PKU Program; Whitaker International Fellowship that funded my year in China, and the Achievement Award for College Scientists (ARCS) Foundation Fellowship.

I would like to thank support faculty and staff who have trained or provided scientific services: Lu Hilenski (microscopy), Neil Anthony (microscopy), Ben Isett (miR array), Leslie Gelbaum (SEM), Bob Karaffa (flow cytometry), Nikolay Patrushev (ultracentrifugation), Aaron Rae (flow cytometry), Dave Smith (glycan array), and Hong Yi (TEM).

In addition to graduate research, my life has been full of additional “balancing” experiences. I would like to acknowledge my running friends (Art, Brandy, Cameron, Cory, Don, Jessica, Katie, Kristen, Kristin, Laura, MaryAnn, Mike, Natalie, Niki, Patrick, Riley, Tim, and Walter) for runs around Atlanta and across the states of Georgia and Tennessee. Ballet with Mara, Jessie, and Renee has given me a fantastic artistic and physical outlet. Also, interactions with my church friends (Bryan, Brooke, Carolyn, Carrie, Kristen, Jen, Jenn, Jessica, Joe, Julia, and Robbie) have reminded me to keep things in an eternal perspective.

When I was visiting grad schools, I knew that I would want to spend the following 4-6 years with friends. To the BME cohort of 2009 (Akhil, Alice, Brian, Eric, Inthu, Jason, Kristin, Kaitao, Marilyn, Mengchen, Tanu, Sean, and Yanni), I knew I'd met a match when we toured Tech, Emory, and Atlanta together. I feel immensely fortunate that our lives intertwined for these years. Tanu and I spent our year in China together, finding the best campus dining halls, trying to not botch the language, and weekend adventuring. When Inthu and I started in Mike and Niren's labs together, we (or at least I) were a tad anxious about what we'd gotten into. We've been best buds, there to discuss research goals and relationships, and to remind each other to turn in BME support forms!

Finally, I give sincerest thanks to my closest set of friends and allies: my family. My parents and siblings have an inexhaustible amount of faith in my abilities. My in-laws intently discuss my research and life goals with me. And to my wife of a just a few months, thank you for starting this journey with me. Together, we will triumph through life's many adventures.

TABLE OF CONTENTS

LIST OF FIGURES

LIST OF ABBREVIATIONS

ACE	angiotensin-converting enzyme
ANOVA	analysis of variance
Bcl-2	B-cell lymphoma 2
Bcl-xL	B-cell lymphoma-extra large
BMB	1,4-bis(maleimido)butane
BSA	bovine serum albumin
^{13}C-NMR	carbon-nuclear magnetic resonance
CABG	coronary artery bypass graft
CEC	cardiac endothelial cell
CGGRGD	cysteine-glycine-glycine-arginine-glycine-aspartic acid-serine
CGNKRTRGC	cysteine-glycine-asparagine-lysine-arginine-threonine-arginine-glycine-cysteine
CKMB	creatine kinase MB
CM	cardiomyocyte
CMFDA	5-chloromethylfluorescein diacetate
CMRA	9'-(4-(and 5)-chloromethyl-2-carboxyphenyl)-7'-chloro-6'-oxo-1,2,2,4-tetramethyl-1,2-dihydropyrido [2',3'-6]xanthene
CPC	cardiac progenitor cell
CREKA	cysteine-arginine-glutamic acid-lysine-alanine
CVD	cardiovascular disease
CXCL12	chemokine (C-X-C motif) ligand 12
DAPI	4',6-diamidino-2-phenylindole
DEPC	diethylpyrocarbonate
DLS	dynamic light scattering
DMEM	Dulbecco's Modified Eagle Medium
DMSO	dimethyl sulfoxide
DNA	deoxyribonucleic acid
DOTA	1,4,7,10-tetraazacyclododecane-1,4,7,10-tetraacetic acid
DPBS	Dulbecco's phosphate buffered saline
DTNB	5,5’-dithio-bis-(2-nitrobenzoic acid)

ECG	echocardiogram
ECM	endothelial cell medium
EDTA	ethylenediaminetetraacetic acid
EGFR	epidermal growth factor receptor
exc/emi	excitation/emission
FAB	fast atom bombardment
FBS	fetal bovine serum
FDA	Food & Drug Administration
FITC	fluorescein isothiocyanate
FS	fractional shortening
g2P	generation 2 poly(amidoamine)
g4P	generation 4 poly(amidoamine)
g4P-BMB	generation 4 poly(amidoamine)-1,4-bis(maleimido)butane
GalNAc	*N*-acetylagalatosamine
GAPDH	glyceraldehyde 3-phosphate dehydrogenase
GlcNAc	*N*-acetylglucosamine
GRAS	generally regarded as safe
^{1}H-NMR	hydrogen-nuclear magnetic resonance
HBSS	Hanks Balanced Salt Solution
HOXA9	homeobox A9
HRMS	high resolution mass spectra
HUVEC	human vascular endothelial cell
IR	ischemia-reperfusion
IS/AAR	infarct size/area-at-risk
ITS	insulin-transferrin-selenium
IV	intravenous
JNK	c-jun N-terminal kinase
LIF	Leukemia Inhibitory Factor
LV	left ventricle
m/z	mass/charge
MAPK	mitogen-activated protein kinases
MCF-7	Michigan Cancer Foundation-7
MI	myocardial infarction
miR	micro ribonucleic acid

mRNA	messenger ribonucleic acid
MWCO	molecular weight cut off
NCBI	National Center for Biotechnology Information
NMR	nuclear magnetic resonance
O-GlcNAc	O-linked *N*-acetylglucosamine
OCT	Optimum Cutting Temperature
OGT	O-linked *N*-acetylglucosamine transferase
PAMAM	poly(amidoamine)
PBS	phosphate buffered saline
PC	principle component
PCADK	poly(cyclohexane-1,4-diyl acetone dimethylene ketal)
PCR	polymerase chain reaction
PEG	polyethylene glycol
PEI	polyethylenimine
PFA	paraformaldehyde
PI3K	phosphatidylinositol-4,5-bisphosphate 3-kinase
PIK3R2	phosphoinositide-3-kinase, regulatory subunit 2 (beta)
PK	poly(cyclohexane-1,4-diyl acetone dimethylene ketal)
PK-CMRA	poly(cyclohexane-1,4-diyl acetone dimethylene ketal)-9'-(4-(and 5)-chloromethyl-2-carboxyphenyl)-7'-chloro-6'-oxo-1,2,2,4-tetramethyl-1,2-dihydropyrido[2',3'-6]xanthene
PK-GlcNAc	poly(cyclohexane-1,4-diyl acetone dimethylene ketal)-*N*-acetylglucosamine
PK-GlcNAc-CMFDA	poly(cyclohexane-1,4-diyl acetone dimethylene ketal)-*N*-acetylglucosamine-5-chloromethylfluorescein diacetate
PK-GlcNAc-CMRA	poly(cyclohexane-1,4-diyl acetone dimethylene ketal)-*N*-acetylglucosamine-5-chloromethylfluorescein diacetate
PK-GlcNAc-SB	poly(cyclohexane-1,4-diyl acetone dimethylene ketal)-*N*-acetylglucosamine-SB239063
PLSR	partial least squares regression
polyR	arginine-arginine-arginine-arginine-arginine-arginine-arginine-arginine-arginine
ppm	parts per million
PVA	polyvinyl alcohol

qRT-PCR	quantitative real-time polymerase chain reaction
RCPLSHSLICY	arginine-cysteine-proline-leucine-serine-histadine-serine-leucine-isoleucine-cysteine-tyrosine
Rg	radius of gyration
RGD	arginine-glycine-aspartic acid
RGD-bowtie	arginine-glycine-aspartic acid-decorated dendrimer
RISC	ribonucleic acid-induced silencing complex
RNA	ribonucleic acid
Rnase	ribonuclease
SB	SB239063
SD	standard deviation
SD	standard deviation
SDS-PAGE	sodium dodecyl sulfate polyacrylamide gel electrophoresis
SEM	scanning electron microscopy
SEM	standard error of the mean
SLS	static light scattering
$SM(PEG)_2$	succinimidyl-([N-maleimido propionamido]-diethylene glycol) ester
SOD	superoxide dismutase
SPRED1	Sprouty-related, EVH1 domain-containing protein 1
Tat	glycine-arginine-lysine-lysine-arginine-arginine-glutamine-arginine-arginine-arginine-proline-glutamine
TBE	tris-borate-ethylenediaminetetraacetic acid
TCEP	tris(2-carboxyethyl) phosphine
TMR	tetramethylrhodamine
TNF	tumor necrosis factor
TNF-a	tumor-necrosis factor-alpha
TOM1	Target of Myb protein 1
TRAIL	TNF-related apoptosis-inducing factor
TTC	triphenyltetrazolium chloride
TUNEL	terminal deoxynucleotidyl transferase dUTP nick end labeling
WIFPWIQL	tryptophan-isoleucine-phenylalanine-tryptophan-isoleucine-glutamine-leucine
XIAP	X-linked inhibitor of apoptosis protein

SUMMARY

Cardiovascular disease (CVD) is the leading cause of morbidity and mortality in developed nations, and heart disease is predicted to remain the leading killer for the foreseeable future. Acute myocardial infarctions (MI)—1.2 million annually occurring in the U.S. alone—are the major CVD subgroup. Blood supply to the heart is occluded during MI, and the ensuing hypoxic and anemic hypoxia triggers deleterious responses within the affected tissue, affecting cardiomyocyte (CM) and endothelial cell function and viability. Largely non-regenerative, the pressure overload leads to non-contractile scar formation and the infarcted heart undergoes a degenerative process toward heart failure. Beyond immediate treatments to restore coronary blood flow, the medical community lacks therapeutic strategies to effectively intervene in the long-term progression of cardiac dysfunction.

The first section of this thesis examines two synthetic drug delivery vehicles to mitigate myocyte cell death and enhance vasculogenesis. The second part focuses on amplifying endogenous cardiac signals to treat the heart, and elucidating clues from said signals for bio-inspired therapeutics.

Although many drugs exist that may aid ischemic myocytes, intracellular delivery of such drugs remains a hurdle, owing to the non-phogocytic nature of myocytes. Here, we describe a novel drug delivery system that relies on surface decoration with *N*-acetylglucosamine (GlcNAc) to induce internalization. We tested the ligand with an acid-degradable polymeric nanoparticle poly(cyclohexane-1,4-diyl acetone dimethylene ketal) (PCADK) encapsulating an anti-apoptotic small molecule, SB239063. The vehicle mitigated the effects of MI in a rat model: it reduced cell death *in vivo* and improved cardiac function. We also developed a dendrimeric delivery vehicle that exhibited region-selective decoration with the internalizing tripeptide arginine-glycine-aspartic acid (RGD)

and loaded it with the angiogenic microRNA, miR-126. This vehicle promoted vasculogenesis *in vitro* and may prove useful in enhancing blood flow within the infarcted cardiac zone.

A small population of stem cells resides in the heart, termed cardiac progenitor cells (CPCs). We collected the exosomes secreted in various conditions and treated cardiac endothelial and fibroblast cell lines with concentrated doses of the exosomes. The hypoxic exosomes enhanced tube formation of endothelial cells and attenuated cytokine stimulation of fibroblasts, indicating that they may restore blood flow to the infarct and mitigate excessive scar formation in the heart. We characterized the miR signature that CPCs release in response to hypoxic conditions and found several to be upregulated in secreted exosomes. Statistical analysis revealed clusters of co-varying miRs and predicted their physiological response, laying groundwork for development of rationally bio-inspired therapeutics.

CHAPTER 1

INTRODUCTION

1.1 Motivation

The National Institutes of Health estimates that among the current population, 7.9 million Americans have suffered acute MI.[1] Current treatments are limited to immediate intervention, including angioplasty and thrombolysis, which serve to restore blood flow to the infarcted region and thereby mitigate further damage, but fail to regenerate tissue. During the ischemic injury and in subsequent reperfusion,[2] deleterious signaling cascades in the affected tissue are triggered, leading to localized death at the cellular level.[3] As adult CMs are terminally differentiated[4] and relatively non-proliferative,[5] the ischemic insult leads to eventual dysfunction and failure at the organ level[6]; rather than regenerate, the heart forms a non-contractile fibrotic scar in the infarct region that is key to subsequent degeneration. Because the initial cell death is primarily regional,[7] localized therapy to target and reverse the damage by protecting or regenerating CMs or restoring blood flow to the injured myocardium is quite promising.

Apoptotic pathways are complex and include many molecules, including whose activation either promote or inhibit cell death, such as Bcl-2,[8, 9] Bcl-xL,[10] and XIAP.[11] Other proteins outside of apoptotic pathways also improve cell survival, such as superoxide dismutase (SOD) and catalase that attenuate oxidative stress produced during ischemia–reperfusion (IR) injury.[12] Furthermore, expression and activity of these proteins are regulated by intracellular signaling molecules. Whereas many of these

kinases have specific small molecule inhibitors, delivery and toxicity concerns due to the need for large systemic doses preclude their use.

The development of miR-based pharmaceuticals holds exciting promise for improving the status quo of medicine.[13] Traditional pharmaceuticals have faced significant limitations: protein-based therapeutics are generally restricted to extracellular receptors; and small-molecule drugs modulate only certain functions of their targeted protein and are limited in specificity. In contrast, by exploiting endogenous translational machinery by delivering synthetic miR mimics, genetic pathways can be regulated selectively.[14] The range of miR-based pharmaceuticals is wide, with potential applications ranging from cancer to diabetes and heart failure. Furthermore, some miRs associated with cardiac development, endothelial cell proliferation, vascular integrity, and CM and vascular smooth muscle cell differentiation have been identified and could be applied as therapeutics.[15-17]

While overexpressing anti-apoptotic proteins and antioxidants in CMs has shown functional improvements in animal models,[18, 19] many delivery hurdles prevent clinical translation. The short circulation half-life of these proteins and small molecules[20] precludes systemic delivery due to the need for extended exposure to large amounts of therapeutics needed. To address this concern, many studies have been performed using biomaterials for sustained, local delivery.[21, 22] Despite some successes, methods to deliver drugs to the infarct currently rely on passive release into the interstitium from delivery vehicles or internalization by phagocytic cells. As the majority of phagocyctic cells accumulate 24–72 hr following ischemia-reperfusion (IR) injury,[23] delivery vehicles that rely on passive macrophage-mediated release do not inhibit the excessive apoptosis that occurs in CMs during the initial 72 hr.

Drug delivery vehicles that target CMs are virtually nonexistent, owing largely to the non- phagocytic nature of these cells. However, recent studies have implicated GlcNAc as a viable candidate for a drug delivery system targeted to CMs, demonstrating the ability of CMs to bind to and internalize GlcNAc-decorated liposomes.[24, 25]

Challenges exist in the development of RNAi therapies, such as protecting the miR molecules from ribonucleases (RNases),[14] and difficulty inducing cellular uptake by the target cell population. RNases that are present in bodily fluids readily degrade miR, requiring protective measures such as encapsulation of the miR[26] or the use of chemically modified RNA.[27] The highly charged backbone and size of nucleic acids precludes passive cell penetration,[14, 28] necessitating incorporation of a mechanism for cellular uptake in most cell types.

Solid particles have long been researched as delivery vehicles for bioactive molecules, to prevent delivery to unintended targets, convey therapeutic doses to tissue, and to shield cargo from recognition and degradation. However, the effects that spent vehicles or carrier degradation products may have on cells and tissue may disqualify the use of vehicles. Formulations of poly(lactic-co-glycolic acid) have been extensively used as micro-and nanoparticles, but degrade into acidic products that may elicit an inflammatory response.[29] The recent development of polyketals as acid-degradable carriers provides a strategy for delivering therapeutics to cells and tissue where an inflammatory response would be undesirable;[22, 29-32] for example PCADK degrades in acidic conditions—such as in the developing endosome—into acetone and 1,4-cyclohexanedimethanol, both of which exhibit excellent biocompatibility. Already, polyketals have been shown to efficiently encapsulate small molecules and proteins, form micro- or nanoparticles, serve as extra- or intra-cellular delivery vehicles, and function compatibly in heart and lung applications.[22, 29-32]

Dendrimers, a class of radially symmetric, regularly branched polymers, have been extensively studied as delivery agents for a variety of drugs.[33-35] One well studied dendrimer is poly(amido amine) (PAMAM), which generally consists of an ethylenediamine core that is reacted alternatively with methyl acrylate and ethylenediamine to form a size-tuned dendrimer commonly with amino termini.[35] Traditional strategies have largely consisted of physical entrapment of drugs within the relatively hydrophobic dendrimer core, with conjugated targeting moieties distributed among the dendrimer terminal groups. As such, dendrimers are attractive multi-functional nanomaterials despite some side effects, such as cytotoxicity.[36] Recent studies have extended dendrimer applications to siRNA- and miR- based therapeutics.[35, 37, 38] The suitability of a dendrimer-based RNAi therapeutic lies in part with the amino groups present at the termini and within the dendrimer that afford electrostatic interactions with—and thereby encapsulation and protection of—anionic miR mimics.[37] The terminal amines of many dendrimers can be readily conjugated with biomolecular ligands, which “decorate” the dendrimer with signals to potentially enhance cell targeting and uptake. Studies have indicated that varying the number of ligands on the vehicle surface elicits different binding and internalization kinetics, and dendrimeric materials can handily exert these “multivalent effects” by presenting an increased number, density, and arrangement of ligands.[34, 38-40] The use of dendrimers for targeted miR delivery, however, is largely undeveloped, and novel architectures are needed that can bind sufficient amounts of miR with presenting adequate ligand density to trigger internalization.

Until fairly recently, the heart was thought to be devoid of regenerative potential; endogenous mammalian cardiac regeneration declines rapidly after birth, but a small population of ckit+ cardiac-resident stem-like cells have been identified within the past decade.[41] While not fully understood, researchers have induced the differentiation of

these CPCs into CMs, endothelial, and smooth muscle cells.[42] These and other stem cell types have been attractive candidates for cell-based therapies wherein transplanted cells in the myocardium would differentiate and regenerate the damaged tissue. Results have been mixed: injected CPCs regenerated the myocardium and improved cardiac performance in rat and canine MI models;[41, 43] and early human clinical trials demonstrated improved cardiac function resulting from injected stem cells,[44, 45] although relatively few cells were retained within the myocardium, suggesting that regenerative or protective effects may occur through paracrine mechanisms rather than cardiogenesis. Studies have begun to explore stem cell-exerted paracrine effects: injection of conditioned media[46, 47] or exosomes[48] secreted from mesenchymal stem cells improved cardiac function and infarct size following IR.

1.2 Specific Aims

The need exists for therapeutic drug delivery systems that can mitigate tissue damage within and around the infarcted territory. Despite substantial development in the general field of nano-vehicles to deliver beneficial molecular cargo to cells, further research regarding vehicular architecture and targeting capabilities to suit delivery to cardiac-specific cells is needed. Furthermore, although stem cells are known to exert beneficial effects on the infarcted heart, the paracrine network of miR intercellular transfer from such cells has yet to be elucidated or exploited. We hypothesize that specially designed therapeutic systems will ameliorate the MI heart by featuring characteristics suitable for the delivery of cardio-protective and pro-regenerative agents. We propose investigation through the following aims:

Specific Aim 1: Evaluate efficacy of a polymeric nanoparticle system featuring a surface-decorated carbohydrate ligand to enhance uptake by CMs. A molecular tether was synthesized to decorate PCADK nanoparticles with GlcNAc, a saccharide that

triggers internalization by otherwise non-phagocytic CMs. Functionalized nanoparticles (300-400 nm) loaded with anti-apoptotic p38 mitogen-activated protein kinase (MAPK) inhibitor SB239063 were injected into the myocardium directly following occlusion and reperfusion of the left descending coronary artery in a rat model of MI. The effectiveness of the proposed therapeutic system in mitigating cardiac dysfunction was determined by evaluation of CM apoptosis in infarcted tissue, ejection fraction, and infarct size.

Specific Aim 2: Synthesize and validate novel dendrimeric vehicle featuring hemispheric-selective decoration of bioactive ligands for miR-based therapy. A vehicle design based on PAMAM architecture provided a platform to deliver therapeutic miR. It featured a region of one-half the structure devoted to nucleic acid binding and the other half to high-density ligand presentation that induced multivalent cell interactions. Human vascular endothelial cells (HUVECs) were treated with such “bowtie” structures loaded with the angiogenic miR-126 and decorated with poly(arginine)$_9$ (poly(R)) or RGD peptides. Delivery system suitability was evaluated by quantifying cell proliferation and tube formation, two hallmarks of angiogenesis.

Specific Aim 3: Evaluate cardioprotective/regenerative potential of exosomes secreted from hypoxic CPCs. The differential release of miR-containing RNA from CPCs subjected to hypoxia was evaluated by miR array and reviewed for pro-regenerative application. The protective/regenerative effects of the hypoxic exosomes were evaluated in relevant cardiac cells by evaluating angiogenic potential and mitigation of fibroblast stimulation. Furthermore, we employed statistical modeling (principle component (PC) and partial least squares regression (PLSR) analyses) to identify co-varying miRs and their physiological response to elucidate clues for bio-inspired cardiac therapeutics.

CHAPTER 2

BACKGROUND

2.1 Myocardial infarction

2.1.1 Statistics

According to the American Heart Association,[49] 83.6 million Americans (>1 in 3) have at least one type of CVD. A major subgroup of coronary heart disease, MI, affects 7.6 million Americans. Cardiovascular diseases accounted for 31.9% of US deaths in 2010, which is more than any other major cause of death, and is greater than combined deaths from cancer and chronic lower pulmonary disease. In 2010, US direct and indirect costs of CVD totaled $315.4 billion, and costs are projected to increase to $918 billion, when 43.9% of the US population is expected to have CVD.

2.1.2 Pathogenesis

Acute MI is most frequently a manifestation of coronary artery disease.[50] It is commonly triggered by disruption of an atherosclerotic plaque in an epicardial coronary artery, which leads to clotting and occlusion of the artery. When unstable, plaques may also rupture and promote an occluding thrombus. Arterial occlusion prevents blood from flowing to part of the heart, and muscle is injured due to the resulting ischemia, or lack of oxygen and nutrients. Injured heart tissue conducts electrical impulses more slowly than healthy tissue, creating a difference in conductance velocity and leading to lethal arrhythmias. Symptoms of MI include pain in the chest, upper extremity, and jaw, as well as shortness of breath, excessive sweating, nausea, or fainting. However, these symptoms are not specific to MI, and proper diagnosis may include evaluation by echocardiogram (ECG), biomarkers, and cardiac imaging.[51]

2.1.3 Diagnosis

Diagnosis criteria for acute MI includes detection of increased levels of biomarkers (such as tryponin or creatine kinase) with symptoms of ischemia, changes in ECG readout including development of pathological Q waves, or imaging evidence of loss of viable myocardium.[51] The term MI may include qualifiers, such as the amount of myocardial loss (infarct size), circumstances that lead to the infarct (whether spontaneous or medical procedure-related), and the timing of the necrosis and observation (evolving, healing, or healed).[52] Immediate treatments for suspected MI include aspirin to prevent further blood clotting, and nitroglycerin to treat chest pain. Some immediate treatment regimens include oxygen, but that has been shown to be deleterious to the heart. Reperfusion therapy includes angioplasty and thrombolysis, and multiple blockages may require coronary artery bypass graft surgery (CABG). There are no definitive treatments for MI to repair or regenerate the heart.[51]

2.1.4 Pathophysiology

The pathology of MI includes myocardial cell death due to ischemia, either through oncosis (ischemic cell death) or apoptosis. After the onset of MI, cell death is not immediate but takes a period of time to develop (as little as 20 min). Complete necrosis of the affected myocardial cells takes several hours, and is a function of collateral circulation to the to the ischemic zone, arterial occlusion, sensitivity of myocytes to ischemia, pre-conditioning of cells, and individual demand of cells for oxygen and nutrients. The size of MI can be classified as microscopic, small (<10% of left ventricle (LV) myocardium), moderate (10-30% of LV), or large (>30% of LV).[51]

The stages of MI are acute, healing, or healed. In acute MI, affected myocardium features the presence of polymorphonuclear leukocytes. The absence of polymorphonuclear leukocytes, and presence of mononuclear cells and fibroblasts

characterize the healing infarction. The healed infarction features scar tissue without cellular infiltration. The temporal characterization of MI may be classified as evolving (<6 hr), acute (6 hr – 7 days), healing (7 days – 28 days), and healed (29 days and beyond).[52]

2.1.5 Biomarkers

A preferred method for diagnosis includes detection of biomarkers in the circulation, as myocardial cell death increases the appearance of different proteins in the blood, such as myoglobin, troponin (I and T), creatine kinase (CKMB) and others.[52] However, an increase in such biomarkers reflects necrosis, and not necessarily acute MI. Other conditions that may raise biomarkers include congestive heart failure, aortic dissection, aortic valve disease, hypertrophic cardiomyopathy, renal failure, stroke, sepsis, extreme exertion, and burns.[53, 54] As troponin is nearly absolutely specific to myocardial tissue and exhibits high clinical sensitivity, it is the preferred biomarker for myocardial necrosis. Its sensitivity can reflect even microscopic zones of myocardial necrosis.[55]

2.1.6 Imaging techniques

Imaging techniques allow for great evaluation and characterization of MI. Important parameters include perfusion, myocyte viability, myocardial thickness, motion, and effects of fibrosis on kinetics of radiolabelled and paramagnetic contrast agents. Commonly used imaging techniques include echocardiography,[56] radionuclide ventriculography,[57] myocardial perfusion scintigraphy, and magnetic resonance imaging.[58] Positron emission tomography and X-ray computed tomography are less commonly used.[59, 60]

2.1.7 Risk factors and recurrence prevention

Risk factors for acute MI include existing CVD, age, tobacco smoking, high low-density lipoprotein blood levels, low high-density lipoprotein levels, diabetes, high blood pressure, lack of physical activity, obesity, chronic kidney disease, and excessive alcohol consumption.[55] The risk of MI recurrence includes strict blood pressure management, ceasing tobacco smoking, exercise, healthy diet, and limitation of alcohol intake. Medications for recurrence prevention include antiplatelets (such as aspirin), beta blockers, angiotensin-converting enzyme (ACE) inhibitors, statin therapy, aldosterone antagonists, and heparin.

2.2 pH-Sensitive polymers

2.2.1 Polymers for drug delivery

The decreasing pH of the maturing endosome provides for two strategies by which the endosome can be disrupted: hydrolysis and protonation.[33] In the first camp are acetal and orthoester hydrolysis (Figure 2.1). In use, these functional groups link two molecules together (such as polyethylene glycol (PEG) to increase water solubility and a hydrophobic molecule), which provides for convenient characteristics for the overall compound. As the endosomal pH decreases, the acetal or orthoester linker is cleaved, creating a scenario where the endosomal membrane is disturbed, such as a hydrophobic molecule becoming embedded into and rupturing the membrane.

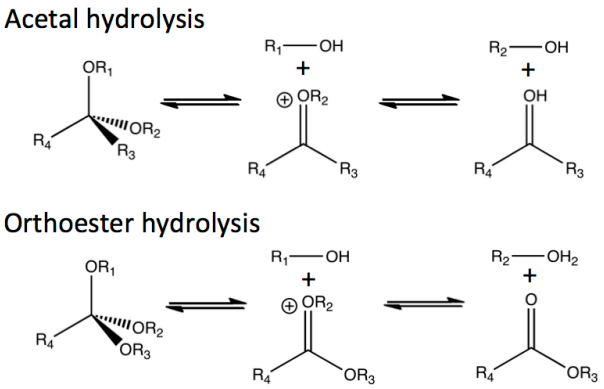

Figure 2.1. Depiction of acetal and orthoester hydrolysis.

Protonation of the primary amines in polyethylenimine (PEI) (Figure 2.2), as well as imidazole and carboxyl groups, is the other general strategy to disrupt the endosome. The mechanism by which the first two approaches work is described by the "proton sponge" hypothesis.[33] That is, that only a percentage of these groups are protonated at physiological pH, and that as the endosome becomes more acidic, the amines and imidazoles act as a buffer by binding to the incoming hydrogen ions. The ATPase enzyme, which actively transports protons into the endosome from the cytosol, then transports more hydrogen ions in order to reach lysosomal pH. However, an influx of counter ions ensues to balance the increased number of protons. It is this increased ion concentration which leads to osmotic pressure in the endosome, and ultimately swelling and rupturing of the endosomal membrane. As every third atom of PEI is nitrogen, there is a high density of amines, only 15-20% of which are protonated at physiological pH (the pKa of primary amines in PEI is ~5.5). Polyethylenimine is commercially available and was an early method for gene delivery, but the cytotoxicity of PEI limits its use, though conjugation of molecules resulting in greater biocompatibility is an option.[61]

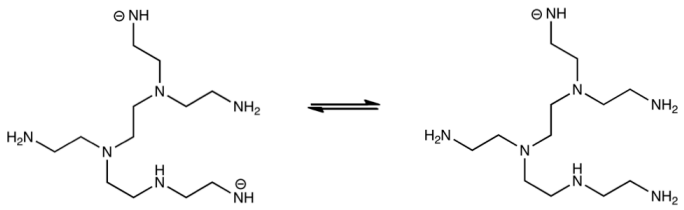

Figure 2.2. Depiction of polyethylenimine protonation.

Imidazole protonation (Figure 2.3) relies on the "proton sponge" theory, yet it is significantly less cytotoxic than PEI.[61] The pKa of imidazole is ~6.0, providing an appropriate buffer between physiological and lysosomal pH.

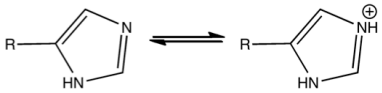

Figure 2.3. Depiction of imidazole protonation.

The third major approach to endosomal disruption by protonation is carboxyl protonation (Figure 2.4), which converts an overall hydrophilic polymer into a hydrophobic polymer.[62] In this scenario, hydrophobic molecules are conjugated to a polymer that also includes carboxyl groups, some of which remain unprotonated at physiological pH. Examples of such polymers include polyethylacrylic acid (PEAAc) and polypropylacrylic acid (PPAAc).[62, 63] As the pH drops in the maturing endosome, the number of protonated carboxyl groups increases, leading to the conformation change of the polymer. This causes the hydrophobic tails of the polymer to partition into and rupture the endosomal membrane.

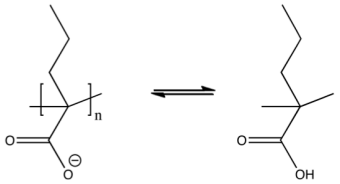

Figure 2.4. Depiction of polypropylacrylic acid.

2.2.2 Acid-cleavable acetal and orthoester bonds

Use of therapeutic-loaded liposomes as a method of cytoplasmic drug delivery has been studied extensively for the past 30 years.[64, 65] Upon internalization by endocytosis, the destabilization of pH-sensitive liposomes in the acidic endosome and redistribution of the bilayer components leads to destabilization of the endosomal membrane. This allows for the contents of the liposome to leak into the cytoplasm. Alternatively, lipids can be used to create lipoplexes. Of the several types of lipid pH-sensitivity, acetal and orthoester linkages will be discussed.

Acetals can be synthesized from primary, secondary, and tertiary alcohols.[65, 66] The rate of hydrolysis is first order relative to the hydronium ion. Therefore, per unit decrease in pH, the rate of hydrolysis increases ten times. It is worth noting that the rate of hydrolysis can be tuned according to the structure of the acetal, something which can be useful for temporal control of hydrolysis in the maturing endosome.[67]

Unlike phospholipids, glycolipids (Figure 2.5) are not usually charged, which can ease synthesis and removes the potential for ionic interaction with the biological system.[68, 69] Additionally, the hydroxyl groups on the sugar group allows for surface modification. Song, *et al.* synthesized a glycolipid conjugate of glucose and two palmitoyl chains connected by an acetal bond.[70]

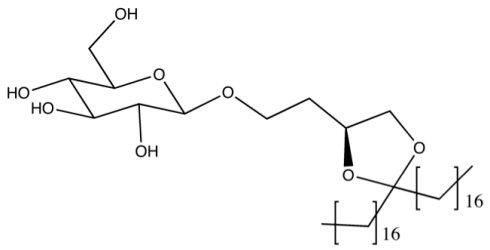

Figure 2.5. Structure of example glycolipid.

However, the researchers found that the acetal hydrolyzed rapidly at pH 4, but relatively slowly at pHs 5 to 7. The fact that only late endosomes and lysosomes reach an adequately low pH indicates that this lipid may not be a strong candidate for drug delivery.

In another approach, Wong, *et al.* included the acid-labile acetal linkage in their synthesis of a PEG lipid, which they used as a lipopolyplex to deliver DNA.[71] They included a cationic group because previous research has indicated that such groups can interact with anionic cell surface receptors and enhance the endosomal release rate of drugs. The presence of PEG can shield the cation from interaction with other compounds or proteins. Their synthetic scheme follows in Figure 2.6.

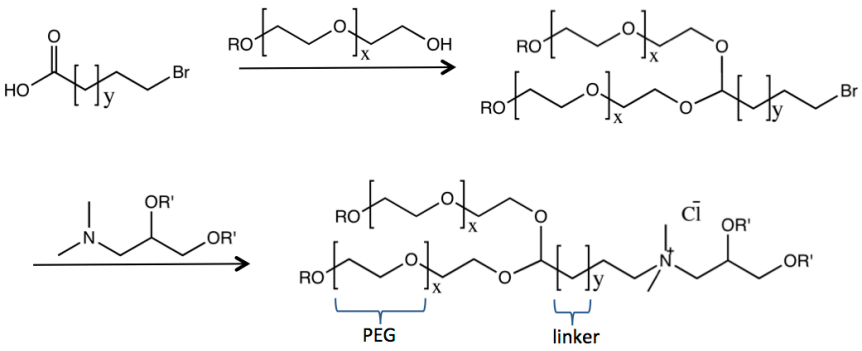

Figure 2.6. Synthetic scheme of example polyethylene glycol-modified lipid.

That the acetal linker of lipids of similar structures hydrolyzes as varying pHs provides means by which drug delivery can be tailored depending on the progression of endosomal maturation.

Orthoesters are known to be one of the most acid-sensitive functional groups, and due to a stable reaction intermediate, are generally expected to hydrolyze more quickly than acetals in response to a decrease in pH.[72] Hydrolysis of the orthoester in a lipid cleaves the headgroup, leading to the collapse of the liposome and release of its contents.

Zhu *et al*. produced a cationic lipid containing an orthoester functional group (Figure 2.7).[73]

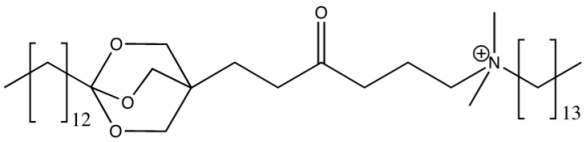

Figure 2.7. Structure of example orthoester lipid.

Liposomes including this lipid demonstrated the ability to encapsulate and then—in 10 min at pH 3.5—release fluorescent molecules. To fully cleave the headgroup, the mechanism undergoes two fast hydrolysis steps of the orthoester, but complete fragmentation of the lipid requires the slow final step of hydrolysis in the cleavage of an ester group. Incorporation of a single orthoester functional group in a lipid for drug delivery then may be most appropriate for collapse of the liposome in a mature endosome.

To promote faster cleavage of the headgroup, Guo *et al.* designed a lipid that incorporated a diorthoester functional group.[69, 74] The benefit of this approach is that the

fast first step of hydrolysis of the diorthoester completely fragments the lipid, leading to liposome collapse (Figure 2.8).

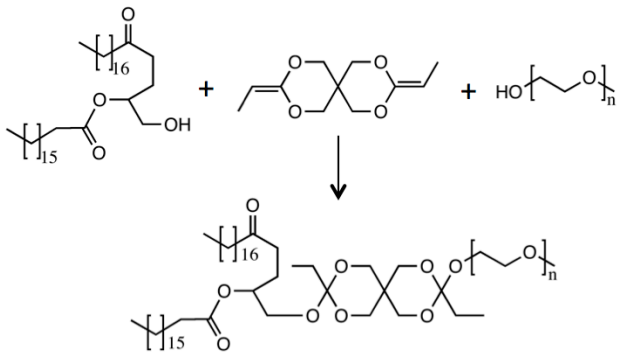

Figure 2.8. Synthetic scheme for preparation of a pH-sensitive PEGylated lipid. Consists of a distearoyl gylcerol hydrophobic tail conjugated to a PEG headgroup through a diortho ester linkage. Liposomes composed partially of this lipid demonstrated long circulation times and acid-triggerable content release. Especially useful is the diorthoester linkage, which leads to cleavage of the headgroup during the first step of hydrolysis, as opposed to an orthoester linkage.

This lipid was found to be stable in pH 7.4 buffer at 37^{o}C, but degraded in pH 5 within one hour. In a mild pH of 5.5, liposomes (10% lipid content were degradable) released most of their contents within 30 min.

2.2.3 Multi-functional polymeric drug delivery systems

In an effort to more closely mimic naturally occurring viruses and endosomal-disrupting toxins, researches have sought to design multifunction carriers which include three primary functions: targeting for endocytosis; disrupting the endosome by a triggered pH-responsive element; and delivering active therapeutic agents after trafficking into the cytoplasm.[66]

Murthy *et al*. developed one of the first designs of such multifunction polymeric carriers, termed “encrypted polymers”.[75, 76] In this approach (Figure 2.9), the polymer contains a membrane-disruptive backbone connected to the other molecular species via

acid labile acetal linkers. A disulfide bond connects the acid-degradable linker to either PEG grafts or therapeutic molecule. A targeting ligand for endocytosis can be attached to the PEG chains. In cases where the drug is not conjugated via a disulfide bond, ionic groups on the PEG terminus can complex with charged drugs.

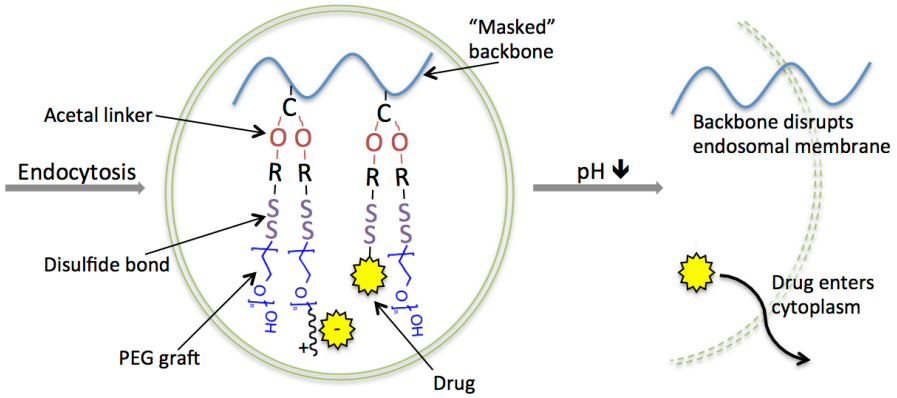

Figure 2.9. Cartoon depiction of internalization and endosomal disruption by encrypted polymer.

In the whole polymeric configuration, PEG chains "mask" the membrane disruptive potential of the backbone. However, once the pH of the maturing endosome drops, hydrolysis of the acid-degradable linker "unmasks" the backbone and allows it to disrupt the endosome, and the drug diffuses into the cytoplasm. Within the cytoplasm, disulfide bonds are reduced, and the active therapeutic molecule is free to perform its intracellular function.

Knorr *et al.* built on existing strategies and developed another approach for intracellular DNA delivery.[77] Historically, polyplexes of negatively charged DNA and positively charged polymers have been developed as a way to shield DNA from degradation in the endosome. Polyethylenimine (PEI) is a good choice due to its high proton buffering capacity. In order to achieve high gene transfer activity, an excess of

PEI is used, which abundance leads to a net positive charge of the polyplex. This can be detrimental due to interactions with negatively charged physiological compounds. It is possible to alleviate these side affects by neutralizing the polyplex surface by incorporating PEG chains in the formulation. The Knorr group used Buchwald-Hartig coupling to substitute a PEGylated aromatic bromine with piperazine (Figure 2.10). The remaining secondary amine of piperazine then reacted with an ester-maleimide compound, after which the exposed maleimide was free to react with a thiol-functionalized PEI.[77]

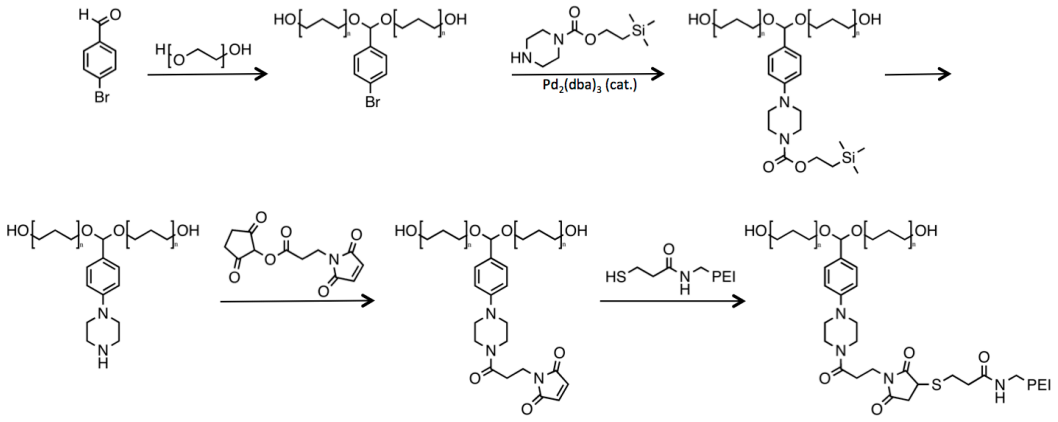

Figure 2.10. Scheme involving Buchwald-Hartig coupling for synthesis of a PEI polyplex. Substitution of a PEGylated aromatic bromine with a protected piperazine, followed by generation of an aniline-type acetal for acid-labile cleavage. PEI forms a polyplex with DNA, which surface is neutralized by the presence of PEG.

The acetal link between PEG and the compound has a purpose. Extensive PEGylation of polyplexes reduces the intracellular release of DNA from the endosome. Therefore, as the pH drops, the polyplex becomes less PEGylated and results indicate higher gene transfer efficiency from these de-PEGylated polyplexes than their non-acid labile counterparts.[77]

2.3 Peptide- and saccharide-conjugated dendrimers for targeted drug delivery

Dendrimers provide a unique scaffold for biological applications because of their size, multivalency, and well-defined chemical composition.[34] Dendrimeric conjugates containing multiples copies of saccharides or peptides may themselves exhibit therapeutic benefits and be developed as anti-prion, anti-microbial, and anti-viral agents. Positively charged dendrimers, due to either native PAMAM terminal amines or guanidine-modification, have shown the ability to prevent prion folding and even induce prion unfolding,[78] with decreased cytotoxicity due to dendrimer glycosylation.[79] For anti-microbial application, dendrimers modified with largely positive peptides show strong toxicity and selectivity for bacteria.[80] Glycodendrimers have demonstrated anti-viral properties by presenting saccharides to either directly bind to viruses or to saturate cell surface receptors;[81] both methods inhibit virus-cell interaction. In other applications, dendrimers can be used to modify other nanodevices, such as carbon nanotubes,[82-84] gold nanoparticles[85] and nanorods,[86] magnetic particles,[87, 88] and quantum dots.[89] Modification by dendrimers serves to improve biocompatibility, enhance solubility, and provide a mechanism for tissue- or cell-specific targeting.

As illustrated in Figure 2.11, there are in general three methods to load the dendrimer scaffolds with therapeutics. First, therapeutic compounds may associate with dendrimers through hydrophobic interactions, either by inclusion within the dendrimer or the hydrophobic pit of dendrimer-bound cyclodextrin. This method has provided for the solubilization of a huge range of hydrophobic small molecules involved in anti-cancer, -depressant, -inflammatory, and -microbial applications.[90-92] The second association is through electrostatic interaction: charged therapeutics can directly form complexes with dendrimers containing counter-charged groups. This method has been widely studied for nucleic acid-based therapeutics. The third approach is through covalent bonding, which method is convenient is convenient when the therapeutic contains functional groups that

are readily ligated. This can be beneficial to prevent hydrophilic molecules from leaching out of dendrimer and inducing side interactions. In the case where a therapeutic agent should be free from vehicle to be fully active, consideration should be taken for how the agent will be released, such as by conjugation via acid labile linkage that can be cleaved in the mature endosome. Covalently attaching molecules to dendrimers is also of use in the development of drug delivery vehicles, as bound fluorophores can elucidate vehicle biodistribution and localization.

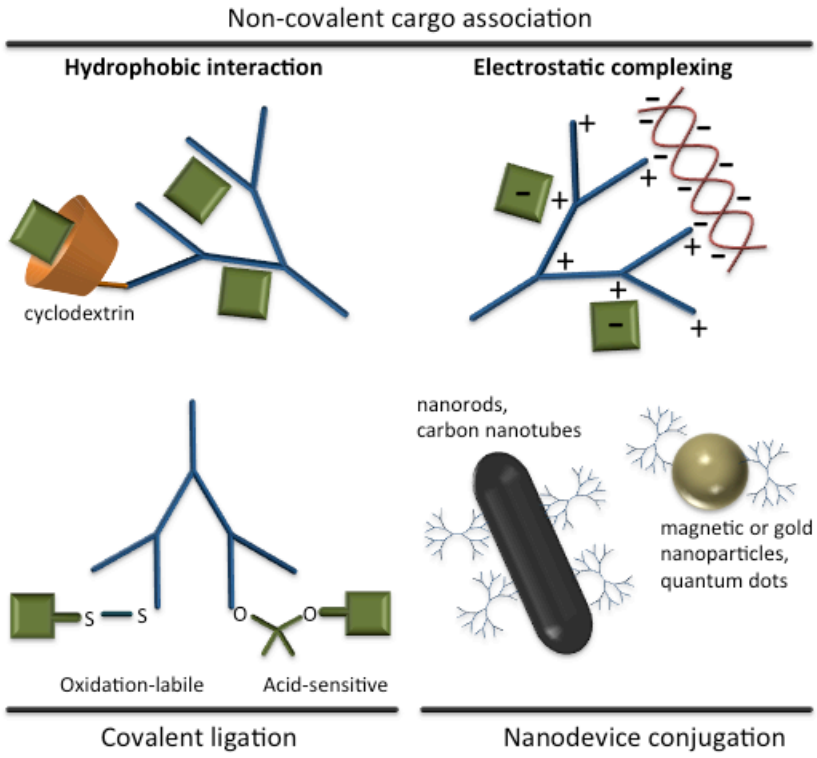

Figure 2.11. Different types of dendrimer–therapeutic cargo associations. (a) Hydrophobic interactions between drug molecules and dendrimer backbone or constituent. (b) Ionic binding. (c) Covalent ligation, including degradable linkages. (d) Dendrimers can also be used to functionalize and/or enhance the solubility and biocompatibility of other nanodevices.

2.3.1 Cell- and tissue-targeting of bioactive dendrimer conjugates

The short peptide RGD is known to bind to integrins,[93] and studies have indicated that cyclized RGD peptides bound with high affinity to cells expressing the a_Vb_3 integrin, such as angiogenic tumor endothelial cells. By decorating the surface of generation 5 PAMAM dendrimers with a double cyclized RGD peptide and Alexa Fluor 488, Baker's group showed preferential binding of the dendrimer to HUVECs, and some binding to Jurkat T lymphocyte cells *in vitro*.[94] In contrast, the dendrimers showed only moderate binding to KB cells and virtually no binding to L1210 mouse lymphocyte cells. This strategy for anti-tumor therapy would rely on targeting the tumor vasculature to inhibit neovascularization.

Other groups have applied cyclized RGD in dendrimeric delivery systems. Liskamp's group conjugated 1,4,7,10-tetraazacyclododecane-1,4,7,10-tetraacetic acid (DOTA) to a dendrimer featuring multivalent cyclic-RGD to develop a vehicle that could target and image tumors.[95] Following complexation of targeted vehicle with ^{111}In and *in vitro* validation of binding to a_Vb_3 integrin, the group injected the radiolabeled dendrimer into SK-RC-52 tumor-bearing mice and found enahanced uptake of the RGD-targeted vehicle in tumors. Their analysis on the effect of multivalency indicated that tetrameric RGD-dendrimer exhibited better tumor targeting than dendrimers decorated with two or fewer RGD peptides. Development of a targeted delivery vehicle that chelates radioisotopes could provide a pathway for tumor therapy by complexing DOTA-conjugated glycodendrimers with $^{90}Y^{3+}$. However in other studies, dendrimers conjugated to Gd(III)-chelating agents and cyclized RGD demonstrated effective binding to melanoma cells only *in vitro*, while *in vivo* tumor uptake was negligible.[96] The inability for vehicle to extravasate into tumor illustrates that RGD may be a ligand more suited for targeting tumor vasculature rather than tumor cells.

While most bioactive dendrimer conjugates rely on surface functionalization, Hammond's group ligated a clinically relevant anti-tumor peptide tryptophan-isoleucine-phenylalanine-tryptophan-isoleucine-glutamine-leucine (WIFPWIQL) for gene therapy.[97] This was accomplished by reducing the disulfide bond of a generation 4 cystamine-core PAMAM dendrimer, followed by conjugation to the peptide through a heterobifunctional linker. This vehicle showed propensity to condense plasmid DNA into small structures (<210 nm) and transfected prostate carcinoma cells *in vitro* to express luciferase. The group demonstrated up to 5x greater transfection with this asymmetrical vehicle than control groups, and even greater transfection than PEI, a transfection standard.

Liu *et al*. performed *in vivo* phage display to identify peptide sequences that targeted lung cancer xenografts in a mouse model.[98] After conjugating generation 4 PAMAM dendrimers with fluorescein isothiocyanate (FITC) and the phage display-identified targeting sequence arginine-cysteine-proline-leucine-serine-histadine-serine-leucine-isoleucine-cysteine-tyrosine (RCPLSHSLICY), the group found that the particles enriched three times more in NCI-460 than 293T cells in a time- and dose-dependent manner. *In vivo*, the group injected the same vehicles intravenously for biodistribution assay, and found that while the targeting and non-targeting vehicles were both found in other organs, animals treated with targeting vehicles exhibited 30% greater fluorescence intensity in the lung cancer xenograft than non-targeting vehicles.

Another research group investigated the use of a previously identified peptide cysteine-arginine-glutamic acid-lysine-alanine (CREKA) for use in a dendritic tumor-targeting vehicle.[99] *In vivo* phage display had demonstrated its ability to home to tumor extracellular matrix via recognition of blood clotting and in a separate study, was used for atherosclerotic plaque imaging. In addition to CREKA, the group also investigated the use of a cyclic nonapeptide, LyP-1 (cysteine-glycine-asparagine-lysine-arginine-threonine-arginine-glycine-cysteine) that recognizes tumor lymphatic cells. By tethering

these peptides and fluorescein to a pentavalent dendritic scaffold, the ability of these peptides to target tumors was elucidated: they found that CREKA-functionalized dendrimers localized in prostate cancer xenograft vasculature, thereby justifying the use of CREKA-functionalized dendrimers for the use of future cancer therapies through anti-vasculature means.

Besides phage display, another method for the development of a targeting dendrimer is through derivation of peptide sequences from known targeting proteins. Leptin is a 146 amino acide polypeptide that is secreted into the bloodstream by adipocytes and acts on leptin receptor-expressing cells in the brain, and Barrett *et al*. identified leptin30, a 30-amino acid derivative of the leptin polypeptide that localized in the parenchyma.[100] By conjugating a poly-L-lysine dendrimer with leptin30, Jiang's group demonstrated the ability of the dendrimer to traverse a brain capillary endothelial cell monolayer and then transfected brain cells with the targeting dendrimers.[101] This was followed by effective *in vitro* transfection of BV-2 microglial cells by luciferase plasmid DNA-loaded dendrimers and *in vivo* accumulation of the dendrimers in the brain of a mouse model. Luciferase activity in the brain was in 80% greater abundance in the targeting dendrimer group than the non-targeting dendrimer group, thus demonstrating the use of leptin30-decorated dendrimers for gene therapy to the brain.

Macrophages exhibit a receptor for mannose, so in an effort to develop a macrophage-targeting dendrimer, Benito, *et al*. conjugated mannose and b-cyclodextrin to dendrimers, followed by inclusion of fluorescent 6-*p*-toluidino-2-naphthalenesulfonic acid within the cyclodextran.[102] The group explored the multivalent effect of vehicle activity by varying level of decoration from one to six mannose molecules and found an amplification of lectin-binding strength for the dendrimers with higher valance, demonstrating the "cluster effect." Such a delivery vehicle could be useful in therapies to

target macrophages, such as rheumatoid arthritis and other macrophage-mediated disorders.

In addition to applicability of mannosylated dendrimers to macrophages, Uekama's group demonstrated gene transfer via these dendrimers in other cell types.[103] They found that mannosylated generation 3 dendrimers, complexed with luciferase pDNA, provided for high gene transfer activity in NR8383, NIH3T3, HepG2, and especially A549 cells. Interestingly, the group found that gene transfer activity of this glycodendrimer was not inhibited by the presence of serum in the treatment medium and described the ability of the vehicle to escape the endosome and localize to the nucleus. These results indicate that mannosylated dendrimer could provide for effective gene transfer therapy in various cell types.

Carbon nanotubes have great potential for biomedical applications, but can exhibit cytotoxicity. Bertozzi's group employed copper-mediated click chemistry to conjugate generation 3 glycodendrimers (mannose, lactose, galactose) to single-walled carbon nanotubes and found dramatically decreased cytotoxicity in HEK293 cells.[104] Furthermore, decoration of SWCNTs with glycodendrimers increased solubility up to a few months. *In vitro* studies with FITC-conjugated dendrimers demonstrated that these decorated SWCNTs showed selectivity in binding to lectins *Conavalia ensiformis* agglutinin, *Arachis hipogaea* agglutinin, and *Psophocarpus tetragonolobus* agglutinin.

Hepatic cells express asialoglycoprotein receptors that bind galactose and *N*-acetylgalactosamine (GalNAc), which receptors have been exploited for treatment of hepatic cancer with drug-loaded dendrimers. Medina, *et al*. GalNAc to generation 5 PAMAM dendrimers with a diaminobutane core[105] that had been shown to preferentially accumulate in the liver and extravasate through the leaky tumor vasculature.[106, 107] Through *in vitro* studies of HepG2 and MCF-7 cells, the group found selective uptake by hepatic cells, with nearly 100% of the HepG2 cells internalizing the dendrimers within a

short period of time. A benefit of this delivery system was that the vehicle required only 12 molecules of saccharide per dendrimer to trigger uptake. Nearly 90% of the terminal groups remain for conjugation to anti-tumor drugs or imaging moieties.

Asialoglycoprotein receptors on hepatic cells have been targeted for RNAi therapy with gene-loaded dendrimers. Following successful development of a charge neutral, hepatic cell-targeting delivery vehicle, Luo's group complexed anti-luciferase siRNA to hydrazide-terminated PAMAM at pH 5 via electrostatic interaction.[108] The remaining amines were crosslinked to retain encapsulated siRNA following pH neutralization. This loaded GalNAc-conjugated dendrimer successfully induced RNAi by reducing fluorescence in luciferase-expressing HepG2 cells *in vitro*. This demonstrated the potential for charge-neutral dendrimeric vehicles in drug-delivery applications where cytotoxic effects due to dendrimer cationic charge are detrimental.

2.3.2 Delivery of bioactive dendrimer conjugates carrying therapeutics

As a cell-penetrating peptide, glycine-arginine-lysine-lysine-arginine-arginine-glutamine-arginine-arginine-arginine-proline-glutamine (Tat)-decorated dendrimers have seen varied success as transfection agents. In an early paper by Juliano's group, generation 5 PAMAM dendrimers conjugated to Tat (15.9 peptides per dendrimer) showed no improvement in the delivery efficiency of siRNA oligonucleotides against the transmembrane protein p-glycoprotein MDR1 in 3T3 cells.[37] In a more recent paper, however, Chang's group found that Tat-functionalized dendrimers exhibited high transfection levels of anti- epidermal growth factor receptor (EGFR) psiRNA;[109] in fact, they demonstrated that the targeted dendrimer performed as well as the Lipofectamine 2000 treatment group. *In vitro*, EGFR knockdown in U251 glioma cells by the targeting dendrimer was slightly better than lipofectamine, whereas apoptosis was similar between the treatment groups. Furthermore, *in vitro* cell invasion was inhibited to a

greater degree by the targeted delivery vehicle than lipofectamine (66.0% versus 62.3%). In a U251 subcutaneous tumor mouse model, the group described significant apoptosis and depressed EGFR expression by the targeted vehicle, and that the tumor volume increased by only 15x whereas saline treated animals experience 89-fold increase. Following passive localization due to the enhanced permeability and retention effect of tumors, cell-penetrating peptides such as Tat can be used for anti-tumor therapies.

Another peptide derivative with great potential for targeting the brain is Agniopep-2. Part of the Kunitz domain of aprotinin, this 19-amino acid peptide accumulates in the parenchyma, binds to lipoprotein receptor-related protein 1, and exhibits a high propensity to transcytose across the blood-brain barrier.[110] Jiang's group conjugated Angiopep-2 to the terminal groups of generation 5 PAMAM and determined that the vehicle was internalized by brain capillary endothelial cells through clathrin and caveolae-mediated endocytosis, and to a small extent, macropinocytosis.[111] The group found in a mouse model that brain uptake of targeting vehicles loaded with fluorescent-labeled DNA was up to 8-fold greater than non-targeting vehicle, and determined a positive correlation between the level of dendrimer decoration and brain uptake. In a later study, the group found the biodistribution of the targeting vehicle in the brain—especially within the tumor—was greater than controls and demonstrated the ability of Angiopep-2 modified dendrimer to target glioma.[112] Furthermore, they loaded the dendrimers with tumor necrosis factor (TNF)-related apoptosis-inducing factor (TRAIL) and in a glial xenograft mouse model, found greater apoptosis in the tumors due to targeting dendrimer treatment groups than controls, including commercial Temozolomide. In survival studies, the targeting dendrimer increased mean survival time significantly: 61 days for Angiopep-2-modified dendrimer versus 49 and 25 days for Temozolomide and saline treatment groups. These results that the targeted delivery vehicle can perform

better than a clinical standard are promising for future applications in treating brain tumors.

Colchicine is a current standard treatment to treat gout, but has potential as an anti-cancer agent due to its inhibition of mitosis. In an attempt to develop a targeted vehicle for colchicine to cancer cells, Reymond's group conjugated the drug to dendrimers via a thioether bond and screened a small collection of attached glycans (glucose, galactose, GalNAc, and lactose) and amino acids (including serine, threonine, histidine, aspartic acid, glutamic acid, leucine, valine, and phenylalanine) for uptake by HeLa tumor cells.[113, 114] Although the decorated dendrimers reduced activity of the drug, the group found that all glycodendrimeric vehicles caused extensive in vitro HeLa cell death. Conversely, non-transformed mouse embryonic fibroblasts experienced extensive cell death only from treatment with highly GalNAc-decorated vehicles, and not other glycodendrimer treatments. These findings suggest that several saccharides may serve as effective ligands for selective anti-tumor dendrimeric delivery vehicles while not targeting other cell types; glucose-conjugated dendrimers demonstrated a high selectivity for HeLa cells by inducing cell death in 163-fold more HeLa cells than fibroblasts. It should be noted that, whereas many dendritic vehicles are based on branched polymers, the structure of Reynold's dendrimers consisted solely of amino acids. Their reasoning was based on the aspect that unless the vehicle is cleared from the body, dendritic drug carriers should undergo intracellular biodegradation after delivery, and that a dendrimer consisting of peptide building blocks could prove more biocompatible than other dendrimers.

One group used galactose-conjugated dendrimers as a delivery vehicle for anti-malarial therapy.[115, 116] Primaquine is a common anti-malarial medication, but in regular formulation can exhibit severe side effects, such as hemolysis. To target the drug to the site of metabolism in the liver and shield it from inducing side effects in side cell

populations, the researchers conjugated galactose to polypropyleneimine dendrimers and complexed primaquine within the carrier via the hydrophobic effect. Two hours after IV injection of the loaded vehicle, 50% of the initial dose was found in the liver, compared to 26% of the non-targeted vehicle, demonstrating the targeting ability of galactose. Besides targeting to the liver, coating of the dendrimer with galactose had three beneficial effects: prolonged drug release up to 6 days, compared to 2 days for uncoated dendrimer; 15-fold greater entrapment of primaquine; and drastically reduced hemolysis due to surface neutralization by glycosylation. In a later paper, the group loaded a related anti-malarial drug, chloroquine, into galactose-decorated poly-L-lysine dendrimers and found five-fold decreased uptake of the vehicle by macrophages than uncoated dendrimers.[115] This characteristic would allow for shielding of the delivery system from macrophages while targeting the liver. Similar to previous findings, coating of the lysine dendrimers with galactose reduced hemolytic toxicity and immunogenicity of the conjugates while extending the release of the anti-malarial drug.

Significant proof-of-principle research has been conducted with peptide- and glycodendrimer, i.e. the majority of research articles describe uptake of fluorophore-conjugated dendrimers, while relatively few articles demonstrate therapeutic effects of drug-loaded vehicles. Obviously, for proposed drug delivery vehicles to reach the clinic this next step of testing must be taken. It is difficult to directly compare peptide—versus saccharide—decorated dendrimers, but it is clear that if specificity in vehicle uptake is desired, then appropriate ligands for cell-material interactions must be identified. The ready availability of phage display allows for screening of a much larger number of potential peptidic ligands than the number of ligands generally screened in glyco-libraries. Considering the drastically greater number of permutations available in oligosaccharides than in peptides (20^6 versus $1.44*10^{15}$ in hexanucleotides and hexasaccharides, respectively),[117] potential exists for identification of more efficient

saccharide ligands. Glycan arrays exist that can identify glycans that bind to peptides[118, 119], but methods should be adapted for binding to cells. The *status quo* in the development of dendrimeric delivery vehicles relies heavily on phage display and screening of small saccharide libraries for ligand identification, and to a small extent, derivation of short peptidic ligands from much larger antibodies and other binding proteins. Future development could include these methods and screening of glycosylated peptides and larger saccharide libraries.

2.4 Therapeutic potential of exosomes

Exosomes are small membrane-bound vesicles (30 – 120 nm) of endocytic origin and are actively secreted from cells. They are derived from luminal membranes of multivesicular bodies and are constitutively released by fusion of multivesicular bodies with the cell membrane.[120] They are loaded with a variety of bio-active molecules—including mRNA, miR, and proteins—that may change based on normal or pathological conditions. Originally considered cell debris or to contain cell refuse, membrane-derived vesicles were more appropriately characterized in 1987,[121] and cell-cell information transfer via exosomes observed in 2002,[122, 123] but miR encapsulation by exosomes was not verified until 2007.[124, 125] Interestingly, the miR signatures are unique among the different carriers,[126] and even between carriers and parent cells, suggesting regulated export of miRs.[126-128] In the past few years, research results have suggested that exosomes can mediate cellular, tissue, and organ level communication under normal and pathological conditions.

2.4.1 Exosome-cell interactions

Once released, exosomes can interact with neighboring cells or enter the circulation, and have demonstrated the ability to cross the blood-brain barrier.[129, 130] Upon interaction with recipient cells, they may bind with plasma membrane via specific

receptors or be internalized by micropinocytosis to fuse with the plasma membrane, or be internalized by distinct endocytosis.[131, 132] Exosomes have been shown to mediate in a wide range of functions, including tumor progression by promoting angiogenesis, tumor metastasis, acting as antigen-presenting vesicles to stimulate the anti-tumoral response, disseminate Alzheimer pathology, and have been implicated in the activities of stem cells.[120]

2.4.2 Useful properties

Several properties of exosomes make them especially suitable for ex vivo study and manipulation, and potentially useful in cell-cell communication.[120] Exosomes have unique protein and miR signatures, which may differ from the parent cell. They exhibit specific biophysical properties, such as size and density that enable isolation/separation (such as by centrifugation).[133] Their rigid lipid membrane retains structural integrity through freezing and thawing, as well as rendering them insensitive to hypotonic bursting.[133, 134] Exosomes exhibit cell-specific signaling and targeting ligands. Finally, they are capable of acting as vehicles for drug delivery because of their ease of being isolated, and their potential for manipulation of RNA and protein content.[129]

2.4.3 Exosomes in the heart

Myocardial tissue secretes exosomes, which may be involved in heterocellular communication in the adult heart.[135] Telocytes have been observed to secrete them in the border zone of the post-infarct heart.[136] Barile *et al*. provided ultrastructural evidence that exosomes are secreted by cardiac progenitor in the normal adult mouse heart, and provided evidence of exosome uptake by CMs.[135] Furthermore, Losordo's group investigated exosome secretion from human and mouse hearts and provided electron microscopic images exosomes being formed within LV CMs from both healthy and heart failure patients.[137] Barile, *et al.* went on to show multivesicular bodies in CPCs,

suggesting that CPCs also generate exosomes.[135] Other researchers have observed exosomes in intracellular space between sarcomere, t-tubule, and nucleus after coronary artery.[138] While it is still unknown how cardiac cells internalize exosomes, evidence points to the active internalization, rather than nonspecific membrane fusion, of exosomes.[135, 139] Direct internalization and active transport of exosomes via the endocytic pathway to the perinuclear region has been shown, and Barile, *et al*. observed their uptake within small, cytoplasmic structures.[135] The therapeutic benefit of CPC exosomes have been briefly explored: they have been shown the enhance endothelial migration[140] and inhibit cell death in the MI heart.[141]

CHAPTER 3

GLCNAC-DECORATED PCADK NANOPARTICLES FOR POST-INFARCT HEALING

3.1 Introduction

Myocardial infarction affects 985,000 new patients in the U.S. annually and is the leading cause of global morbidity and mortality.[142] During ischemic injury and in subsequent reperfusion,[143] apoptotic signaling cascades in CMs are triggered, leading to localized death at the cellular level.[144] As adult CMs are terminally differentiated[145, 146] and relatively non-proliferative,[147] the ischemic insult leads to eventual dysfunction and failure at the organ level.[6, 148] Because the initial cell death is primarily regional,[7] localized therapy to target and reverse the damage to the injured myocardium is quite promising. Therefore, CM-specific rescue presents itself as a compelling therapeutic target following MI.

Apoptotic pathways are complex and include many molecules, including whose activation either promote or inhibit cell death. Several proteins in these pathways have demonstrated a cardioprotective role, such as Bcl-2,[8, 149] Bcl-xL,[10] and XIAP.[11] Other proteins outside of apoptotic pathways also improve cell survival, such as SOD and Catalase that attenuate oxidative stress produced during IR injury.[12, 150] Furthermore, expression and activity of these proteins are regulated by intracellular signaling molecules such as JNK,[151, 152] Akt[153] and p38.[154] Whereas many of these kinases have specific small molecule inhibitors, delivery and toxicity concerns due to the need for large systemic doses preclude their use.

While overexpressing anti-apoptotic proteins and antioxidants in CMs has shown functional improvements in animal models,[18, 19, 155-157] many delivery hurdles prevent clinical translation. The short circulation half-life of these proteins and small molecules[20] precludes systemic delivery due to the need for extended exposure to large amounts of therapeutic needed. To address this concern, many studies have been performed using biomaterials for sustained, local delivery.[21, 22, 30-32] Despite some successes, methods to deliver drugs to the infarct currently rely on passive release into the interstitium from delivery vehicles or internalization by phagocytic cells. As the majority of phagocyctic cells accumulate 24-72h following IR injury,[23] delivery vehicles that rely on passive macrophage-mediated release do not inhibit the excessive apoptosis that occurs in CMs during the initial 72h. Drug delivery vehicles that target CMs are virtually nonexistent, owing largely to the non-phagocytic nature of these cells. However, recent studies have implicated *N*-acetyl-D-glucosamine (GlcNAc) as a viable candidate for a drug delivery system targeted to CMs, demonstrating the ability of CMs to bind to and internalize GlcNAc-decorated liposomes.[24, 25] The use of liposomes as a drug delivery vehicle, however, may lead to challenges: leakage of water-soluble drugs during preparation and storage is a known disadvantage; and the destabilization of liposomes in the presence of high-density lipoproteins in blood plasma limits its use.[158]

Previously, we inhibited chronic cardiac dysfunction through the controlled release of the p38 inhibitor SB239063 from microparticles into the extracellular region of the post-infarcted heart.[32] Despite this improvement in chronic function, there was no change seen in early function, indicating release was not fast enough or the inhibitor was not taken up by the appropriate cell type. *In vitro*, macrophages readily phagocytosed the particles whereas other cell types did not, most likely due to lack of targeting agents. In this study, we developed a drug delivery system for enhanced CM uptake by decorating degradable, biocompatible polymeric nanoparticles (polyketals) with GlcNAc

(cartoon depiction in Figure 3.1) and demonstrated its ability to be internalized by CMs. Using these GlcNAc particles, we were able to reduce infarct size and improve acute cardiac function in strong contrast to our published data with unmodified polyketals.

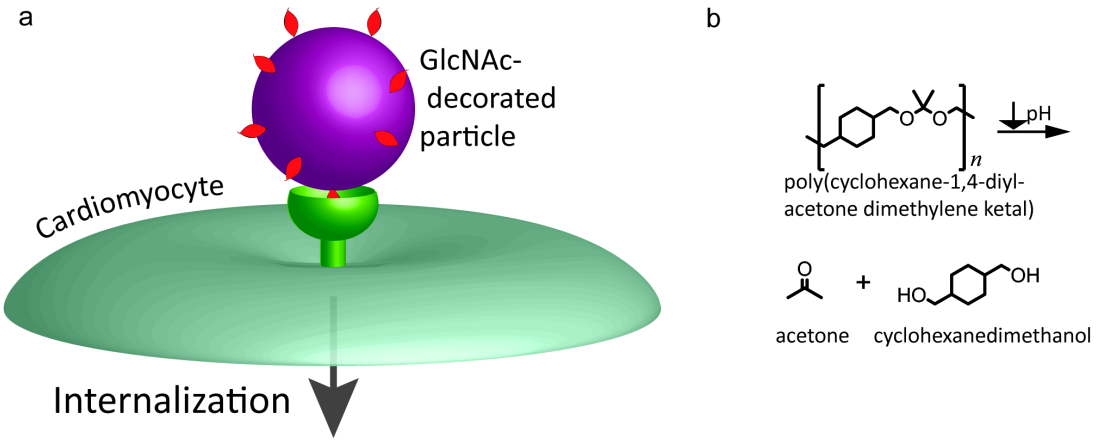

Figure 3.1. Overall scheme for proposed GlcNAc-mediated drug delivery system. A) Decoration of drug-loaded polymeric nanoparticle with GlcNAc should provide a mechanism whereby therapeutics may be delivered intracellularly to CMs. B) The particle will be composed of the acid-labile PCADK. Once internalized, the particle will degrade into the biocompatible products acetone and cyclohexanedimethanol.

3.2 Materials and methods

3.2.1 Synthesis of GlcNAc-alkyl

GlcNAc-alkyl (**1**) was synthesized by clicking an azide-modified GlcNAc (**6**) onto an alkyne-functionalized alkyl-hexaethylene glycol (**7**) (shown in Figure 3.2). The azide-modified GlcNAc (**6**) was synthesized by functionalizing the anomeric carbon of GlcNAc (**2**) in three steps. Briefly, the hydroxyl groups of GlcNAc were protected with acetic anhydride in pyridine, generating (**3**). The anomeric acetyl of (**3**) was activated with lewis acid to form the oxazoline donor, and then coupled with azido-propanol, using TMSOTf as the catalyst to afford the desired derivative (**6**). The final product GlcNAc-alkyl (**1**) was

synthesized by clicking the GlcNAc (**6**) onto the alkyl-hexaethylene glycol (**7**) in presence of catalyst copper(I) bromide, followed by deacetylation. The identities of final and intermediate species were confirmed by ^{1}H- and ^{13}C-nuclear magnetic resonance (NMR) and mass spectrometry. Compound (**1**) ^{1}H-NMR (400 MHz, CDCl3): δ (parts per million (ppm)) 7.57(s, 1H, triazole), 4.94 (t, 1H, J = 8.8 Hz), 4.56 (m, 2H), 4.48 (m, 1H), 4.36-4.33 (m, 2H), 4.14-4.12 (m, 2H), 3.77-3.57 (m, 26H), 3.25 (m, 2H), 3.30 (m, 2H), 2.07 (m, 2H), 1.98 (s, 3H), 1.40 (m, 2H), 1.22-1.13 (m, 31H). ^{13}C-NMR (100 MHz, CDCl3): δ (ppm) 173.8, 156.4, 145.1, 123.5, 101.2, 76.7, 75.7, 70.7, 70.5, 70.4, 70.3, 69.7, 65.2, 64.5, 63.6, 61.6, 56.6, 53.4, 46.6, 41.0, 31.9, 30.1, 29.9, 29.7, 29.6, 29.5, 29.3, 29.2, 26.7, 23.3, 22.7, 14.1. High resolution mass spectra (HRMS) fast atom bombardment (FAB): mass/charge (m/z) calculated for $C_{43}H_{81}N_5O_{14}$ $[M+Na]^+$: 914.6, found: 914.6.

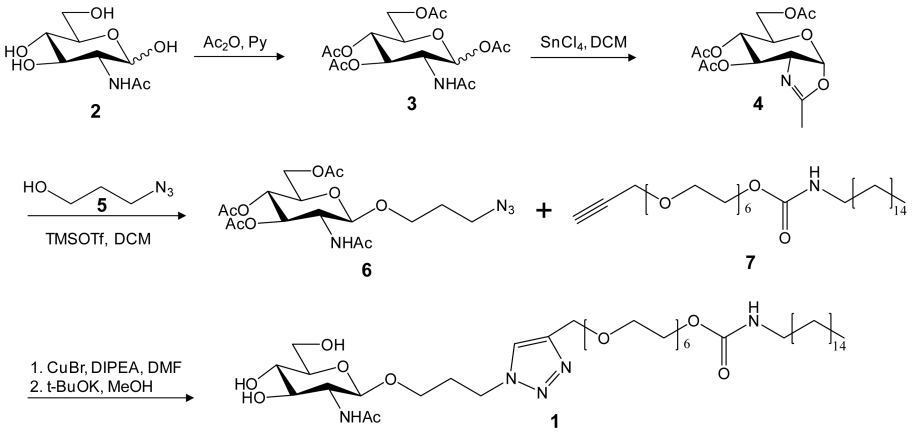

Figure 3.2. Synthetic scheme of GlcNAc-alkyl. A facile and scalable eight-step process is followed to produce the tethering and targeting compound GlcNAc-alkyl. During nanoparticle production, the hydrophobic alkyl chain associates with the polymeric particle and the hydrophilic carbohydrate headgroup is free to interact with CMs.

3.2.2 PCADK synthesis

PCADK was synthesized as previously described.[30] Briefly, 2,2-dimethoxypropane was reacted with 1,4-cyclohexanedimethanol in an acetal exchange reaction in distilled benzene at 100°C with p-toluenesulphonic acid as the polymerization catalyst. 2,2-dimethoxypropane was supplied to the reaction in an equimolar ratio to 1,4-cyclohexanedimethanol. To compensate for the loss of benzene and 2,2-dimethoxypropane through distillation, additional amounts were added every two hours. At 8 hr, a small amount of triethylamine was added to the reaction vessel to stop the reaction. Adding this reaction mixture dropwise to cold hexanes (-20°C) precipitated out the polymer, which was then removed by vacuum filtration and dried prior to particle formation.

3.2.3 Particle production

Polyketal particles loaded with rhodamine B (Sigma-Aldrich) (PK-GlcNAc-rhodamine) were prepared via a solvent displacement method. Briefly, a solution of 40 mg PCADK and 0.2 mg Rhodamine B in 8 mL tetrahydrofuran was added dropwise into a vigorously stirred aqueous solution of 1% GlcNAc-alkyl. The resulting stirred suspension was vented for 6h to allow for evaporation of solvent.

Polyketal particles loaded with 5-chloromethylfluorescein diacetate (CMFDA) (Invitrogen) (PK-GlcNAc-CMFDA), (9'-(4-(and 5)-chloromethyl-2-carboxyphenyl)-7'-chloro-6'-oxo-1,2,2,4-tetramethyl-1,2-dihydropyrido[2',3'-6]xanthene (Invitrogen) (PK-GlcNAc-CMRA), or SB239063 (Axxora) (PK-GlcNAC-SB) were generated using an emulsion-solvent evaporation technique. Fifty mg of PCADK and cargo (0.25 mg CMFDA, 100 µg CMRA, or 0.5 mg SB239063) were dissolved in 1 mL of dichloromethane. The polymer solution was then added to 7 mL of 5% polyvinyl alcohol (PVA) and 5 mg GlcNAc-alkyl (or 0.5 mg GlcNAc-alkyl for 1% decoration of PK-GlcNAc-

CMFDA particles), homogenized at high speed for 60s, and sonicated for 30s to produce nanoparticles. The resulting emulsion was transferred to 30 mL of 0.5% PVA and stirred at approximately 100 rpm for 4h to allow for evaporation of solvent. All of the particle suspensions were then centrifuged and washed with deionized water three times to remove residual PVA and GlcNAc-alkyl, as well as non-encapsulated cargo. The suspension was then snap frozen in liquid nitrogen and lyophilized to produce a free flowing powder.

3.2.4 Particle characterization

Particles were sized by a Wyatt DynaPro Nanostar dynamic light scattering (DLS) instrument (Wyatt Technology) and imaged by a Zeiss Ultra 60 scanning electron microscope (SEM). Nanoparticle circumferences were traced using ImageJ software to confirm DLS-determined sizes. Zeta potentials of particles in phosphate buffered saline (PBS) buffer (pH 7.4) were measured by a Malvern Instruments Zetasizer.

To determine cargo content, loaded and non-loaded particles were hydrolyzed overnight in 1 N HCl. Quadruplicates of 1 mg each of CMFDA-loaded nanoparticles (0%, 1%, and 10% decorated PK-GlcNAc-CMFDA particles) were hydrolyzed in 100 mL HCl at 80°C for 3h. To activate CMFDA fluorescence, 200 mL $Ba(OH)_2$ was added to each sample heated at 80°C for 3h. Following neutralization with 10x PBS, solutions were snap frozen in liquid N_2 and lyophilized to concentrate CMFDA. All readings were performed in 100 mL PBS, and fluorescence determined via plate reader (excitation/emission (exc/emi) = 492/517 nm) (BioTek Synergy 2) and loading amount calculated from a standard curve generated using free CMFDA (r^2=0.99). The absorbance of resultant solutions containing SB239063 was measured at 320 nm and loading efficiencies calculated from a standard curve generated using free SB239063 (r^2=0.99).

Degree of decoration was measured by first hydrolyzing 5 mg of PK-GlcNAc (with a theoretical decoration of 10% and 1%) and PK particles (in triplicate) in 1 N HCl, followed by neutralization with NaOH. The absorbance of the resulting solutions was measured at 278 nm in a plate reader and wt% decoration calculated from a standard curve generated from free GlcNAc-alkyl (r^2=0.99). GlcNac-alkyl decoration was orthogonally confirmed by analyzing molecular species by electrospray ionization mass spectrometry.

3.2.5 SB release characterization

2 mg of PK-GlcNAc-SB and PK-GlcNAc particles in triplicate were suspended 1 mL PBS (pH 7.4) and set on an inverting rotator (0.25 Hz) at 37°C. At specified timepoints, suspensions were spun at 13.3 rpm for 5 min to pellet particles and 100 µL supernatant removed for analysis. 100 µL fresh PBS was added to compensate and particles resuspended. The absorbance of the samples was measured at 320 nm and concentration calculated from a standard curve of free SB239063 (r^2=0.99). At the end of the experiment, the particles were hydrolyzed to determine the amount of remaining SB239063, and a release curve was generated accounting for amount of SB239063 released from and remaining in particles.

3.2.6 CM isolation

CMs were isolated from day-old Sprague Dawley rat pups as previously described [24, 31]. Briefly, excised rat hearts were washed with Hank's Balanced Salt Solution (HBSS) and minced, followed by extracellular matrix digestion in 1 mg/mL trypsin solution in a rotating shaker at 4°C for 6h. Following centrifugation, the supernatant was removed and pellet re-suspended in 0.8 mg/mL collagenase solution. The suspension was incubated at 37°C for 10 min and filtered through 70 mm syringe filter. To remove vascular smooth muscle cells and endothelial cells, the suspension was

plated for 1h in fibronectin-coated T75 flasks. The non-adherent cells were removed and plated in fibronectin-coated 6- or 12-well plates in antibiotic-supplemented Dulbecco's Modified Eagle Medium (DMEM) media (10% fetal bovine serum (FBS)). Twelve hours before treatment, cells were quiesced in serum-free media.

3.2.7 Imaging of rhodamine-loaded particles in cells

A 0.5 mg/ml particle suspension of rhodamine-loaded, GlcNAc-decorated particles in serum-free DMEM media was added to quiesced CMs. After incubation at 37°C for 12h, cells were washed three times with PBS and cells fixed in 4% paraformaldehyde (PFA). Following membrane permeabilization, immunostaining was performed with mouse anti-α-actinin (Sigma-Aldrich) and 4',6-diamidino-2-phenylindole (DAPI) to stain nuclei. Cells were imaged with a Zeiss 510 META confocal laser scanning microscope.

3.2.8 Determining uptake of CMFDA-loaded particles in cells

A 0.5 mg/ml suspension of CMFDA-loaded or non-loaded particles with varied levels of GlcNAc decoration was prepared in serum-free DMEM media and added to quiesced CMs. Following incubation at 37°C for 12h, fluorescence of cells was measured by plate reader (exc/emi = 492/517 nm).

3.2.9 Treatment of CMs with PK-GlcNAc-SB

Quiesced cells were incubated with 0.5 mg/mL of PK-GlcNAc-SB or PK-GlcNAc particles in serum-free DMEM at 37°C for 18h, followed by stimulation with TNF-α (10 mg/mL) 20 min. Cells were harvested in lysis buffer with protease and phosphatase inhibitors. Western analysis for p38 activation was performed on 35 μg of protein lysate. Following SDS-PAGE separation, proteins were transferred to a nitrocellulose

membrane and probed with antibodies against phosphorylated or total p38 (Cell Signaling).

3.2.10 Animal studies

Randomized and blinded studies were conducted using adult male Sprague-Dawley rats (obtained from Charles River) weighing 250 g. Rats were subjected to IR injury as described previously.[159] Briefly, under isoflurane anesthesia (1-3%), the left anterior descending coronary artery was occluded for 30 minutes using an 8-0 prolene suture. Following occlusion, reperfusion was initiated by removal of the suture and animals were divided into treatment groups. Particle suspension treatments were given in 100 mL of sterile saline into the perimeter of cyanotic ischemic zone (3 locations) through a 30-gauge needle immediately after reperfusion. The survival rate of animals during surgery was 80%, and 100% during recovery. All animal studies were approved by Emory University Institutional Animal Care and Use Committee.

To examine *in vivo* uptake of particles, rats were divided into three treatment groups: saline alone, PK-CMRA, and PK-GlcNAc-CMRA (*n*=3 for each group). Three days following IR and treatment, rats were sacrificed and hearts excised. After preservation in Optimal Cutting Temperature (OCT) compound (Tissue-Tek), hearts were sectioned into 7 μm thick slices and immunostaining performed with anti-α-actinin (Sigma-Aldrich) and DAPI to stain nuclei. Tissues were imaged with a Zeiss 510 META confocal laser scanning microscope (CMRA exc/emi = 548/576 nm).

In vivo reduction of apoptotic events was explored by dividing the rats into three treatment groups: saline alone, empty PK-GlcNAc, and PK-GlcNAc-SB (*n*=3 for each group). One day following IR and treatment, rats were sacrificed and hearts excised. After cryopreservation in OCT compound, hearts were sectioned and subject to immunostaining for α-actinin and DAPI. Tissues were subject to Terminal

deoxynucleotidyl transferase dUTP nick end labeling (TUNEL) *in situ* apoptosis detection, tetramethylrhodamine (TMR) red (Roche) to stain for apoptotic nuclei and imaged with a Zeiss Axioskop microscope. Using Image-Pro Plus software (MediaCybernetics), apoptotic and total nuclei were tallied and extent of apoptosis calculated for each treatment group.

For structural and functional experiments, rats were split into three groups: saline alone, PK-GlcNAc, and PK-GlcNAc-SB (n>7 for each group, N=29 total). Additionally, some animals received sham surgery. Echocardiography was performed three days following surgery. The animals were sacrificed and immediately perfused for infarct size measurements.

3.2.11 Echocardiography

Rats were anesthetized with inhaled isoflurane (1-3%; Piramal) and subjected to echocardiography 3 days after IR surgery. Short axis values of left ventricular end systolic and end diastolic dimension were obtained using a Vevo® 770 echocardiography workstation with a high frequency transducer. An average of 3 consecutive cardiac cycles was used for each measurement and was made 3 times in an investigator-blinded manner.

3.2.12 Infarct size

Three days following IR, animals were sacrificed and isolated hearts perfused at 37°C retrograde through the aorta with Krebs-Hepes buffer. The coronary artery was then re-occluded with the suture that was left in place at the time of reperfusion and the heart was perfused with filtered Evan's blue dye to define the LV area at risk. The LV was sliced into cross-sections followed by 2 min soaking in 1% 2,3,5-triphenyltetrazolium chloride (TTC) solution at 37°C to stain viable myocardium, followed by fixing in 4% PFA. Each section was photographed for analysis. Non-infarcted tissue (region outside the

ligated area) was identified by deep blue staining, ischemic but viable myocardium was identified by deep red staining (at-risk area), and non-viable LV tissue was identified by white coloration. ImageJ software was used to trace the three areas in all sections. The areas of the three regions from all slices were summed for each heart and data were expressed as infarct size/area-at-risk (IS/AAR).

3.2.13 Statistics

All statistics were performed using GraphPad Prism software.

3.3 Results

3.3.1 CM internalization of PK-GlcNAc-rhodamine nanoparticles

Cultured CMs harvested from day-old Sprague-Dawley rat pups were incubated with rhodamine-loaded, GlcNAc-decorated particles prepared by a solvent displacement method. Particles were imaged by SEM and analyzed by ImageJ software and had an average diameter of 320±156 nm (mean±SD; Figure 3.3 a). Cells were incubated with particles for 6h and analyzed by confocal microscopy to visualize particle uptake. To determine cell morphology, sections were counterstained with the cardiac-specific marker α-actinin (green) and images were merged to determine overlay. As demonstrated in the orthogonal images, rhodamine-loaded GlcNAc particles (red) were internalized by CMs (Figure 3.3 b).

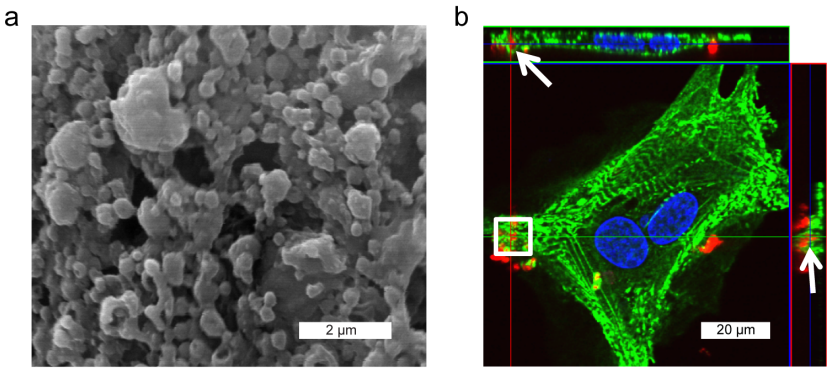

Figure 3.3. Incubation of CMs with PK-GlcNAc-rhodamine particles for internalization verification. A) Rhodamine-loaded particles (diameter = 320 ± 156 nm) were decorated with GlcNac-alkyl and imaged by SEM. B) Cultured CMs were treated with PK-GlcNAc-rhodamine particles for 12 h before fixation in PFA and immunostaining for CM-specific α-actinin (green) and DAPI for nuclei (blue). Confocal microscopy afforded orthogonal views of the cell, by which internalized nanoparticles (red) can be observed in the same plane as the α-actinin (arrows).

3.3.2 CM internalization of PK-GlcNAc-CMFDA nanoparticles in vitro

To further demonstrate particle internalization, GlcNAc-decorated (0%, 0.6%, 9% as determined experimentally) CMFDA-loaded nanoparticles were prepared via a single emulsion method. Following hydrolysis of particle samples and fluorescence activation, average CMFDA encapsulations were determined by plate reader to be 2.9, 5.1, and 4.3 nmol CMFDA/mg particle for 0%, 0.6%, and 9% sugar decoration, respectively (Figure 3.4 a).

The fluorescence of cultured CMs treated with CMFDA-loaded nanoparticles for 12h was determined by plate reader and normalized to the 0% GlcNAc particles and the respective particle CMFDA content. Cells treated with 0.6% GlcNAc decorated particles exhibited a 1.4±0.1-fold increase in fluorescence, whereas treatment with 9% GlcNAc particles resulted in a significant 2.8±0.1-fold increase in fluorescence over cells treated with CMFDA-loaded, non-decorated particles (mean±SEM; n=4; *p<0.01, ***p<0.001. analysis of variance (ANOVA); Figure 3.4 b).

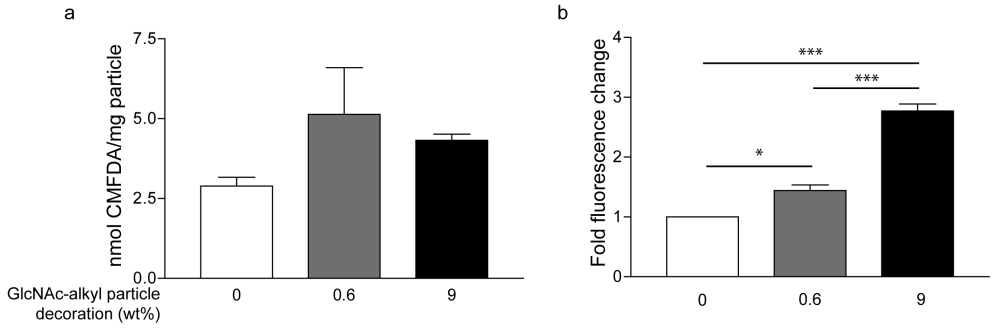

Figure 3.4. Measurement of particle internalization by CMFDA fluorescence demonstrating increased uptake. PK-GlcNAc-CMFDA nanoparticles were decorated with 0%, 0.6%, or 9% GlcNAc-alkyl by weight and loaded with the cell tracker dye, 5-CMFDA. A) Particles are closely load-matched for CMFDA content: 0%, 0.6%, and 9% decorated particles contained 2.9 ± 0.3, 5.1 ± 1.5, and 4.3 ± 0.2 nmol CMFDA/mg particle, respectively. Data are expressed as mean±SEM from three experiments. B) After incubation of CMs with particles, fluorescence of cell culture was obtained by a plate reader and normalized to 0% GlcNAc-alkyl decoration and respective particle CMFDA content. The positive correlation between fluorescence and degree of decoration indicates a dose response and confirms cell uptake of GlcNAc-decorated particles. Data are expressed as mean ± SEM from four separate experiments (*$p < 0.05$, ***$p < 0.001$; ANOVA followed by Newman–Keuls post test).

3.3.3 In vitro inhibition of p38 activation

PK-GlcNAc-SB and PK-GlcNAc particles were prepared by a single emulsion method and had a mean diameter of 370 nm by SEM image analysis and DLS (Figure 3.5 a&b). A cumulative release curve of SB239063 from PK-GlcNAc-SB particles was generated, with 24% released by day 5 in a 2 mg/mL suspension (Figure 3.5 c).

To evaluate *in vitro* particle internalization, CMs were pretreated with serum free media alone or particles for 18h and stimulated with TNF-α (10 mg/mL) for 20 minutes. Proteins were run on SDS-PAGE gel and membranes were stained for both phosphorylated and total p38 levels. Band densities were calculated by Carestream Health Imaging software. The amount of p38 phosphorylation (p-p38) was normalized to total p38 for each treatment (Figure 3.5 d). TNF-α stimulation significantly increased p-p38 over basal levels in PK-GlcNAc pretreated CMs (0.7±0.1 to 1.8±0.2), but not in the

PK-GlcNAc-SB pretreated cells. Additionally, the amount of TNF-a-stimulated p-p38 was significantly decreased in PK-GlcNAc-SB cells compared with PK-GlcNAc pretreatment (1.8±0.2 vs. 0.7±0.3; mean±SEM; n=3; p<0.05; ANOVA followed by Tukey post-test).

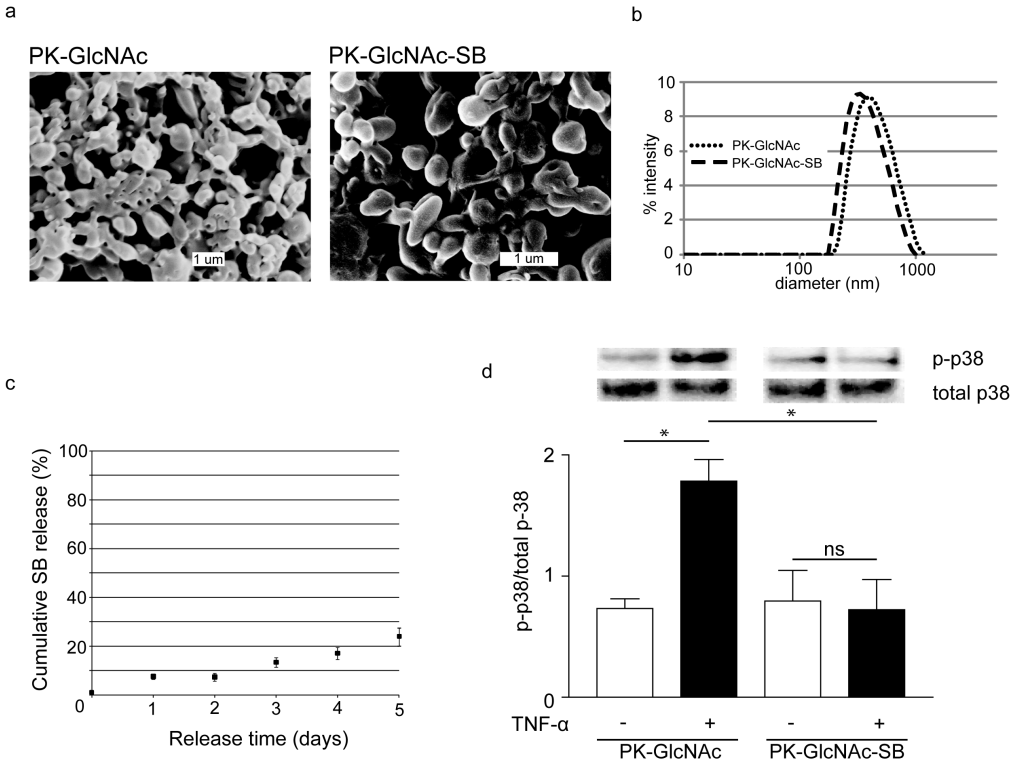

Figure 3.5. Treatment of CMs in vitro with p38 inhibitor-loaded nanoparticles reduces TNF-α-stimulated p38 activation. PK-GlcNAc and PK-GlcNAc-SB particles were imaged via a SEM (diameter = 407 ± 125 nm or diameter = 342 ± 165 nm, respectively) and b) analyzed by DLS (diameter = 465 ± 173 nm or diameter = 395 ± 145 nm, respectively). Data are mean ± SD. C) PK-GlcNAc-SB particles release cargo through diffusion at pH 7.4. D) PK-GlcNAc did not prevent p38 phosphorylation, as demonstrated by a 2.4-fold increase of p-p38 due to TNF-α treatment. However, PK-GlcNAc-SB treatment significantly inhibited p38 activation compared with empty particles. Data are mean ± SEM and are expressed as a ratio of phosphorylated to total p38 (n = 3; *p < 0.05; ANOVA followed by Tukey's post test).

3.3.4 In vivo uptake of PK-GlcNAc-CMRA particles and apoptotic inhibition by PK-GlcNAc-SB particles

To examine the ability of the GlcNac-decorated particles to be internalized *in vivo*, a blinded and randomized model of IR injury was used. Following 30 minutes of ischemia, the LV was reperfused and rats received injections of saline, PK-CMRA (average diameter=443 nm), or PK-GlcNAc-CMRA (average diameter=453 nm) particles in a randomized and blinded manner (*n*=3 for each group). Three days following IR, animals were sacrificed and hearts excised, snap frozen in OCT compound, and sectioned. Using immunohistochemistry, CMs were identifiable by α-sarcomeric actinin staining (green). CMRA-positive cells were identified by red fluorescence, and representative co-localization images are shown in Figure 3.6 a. Qualitative data from the images suggest efficient *in vivo* uptake of PK-GlcNAc-CMRA with little staining in PK-CMRA treated animals.

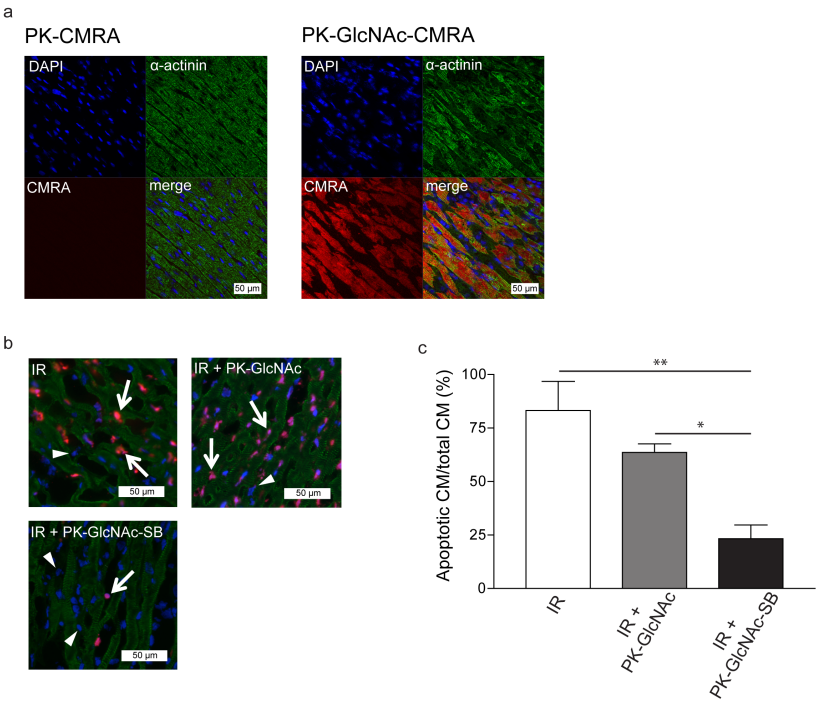

Figure 3.6. GlcNAc decoration enhances particle uptake in vivo following IR and reduces apoptotic events. A) Rats that received myocardial injection of (9'-(4-(and 5)-chloromethyl-2-carboxyphenyl)-7'-chloro-6'-oxo-1,2,2,4-tetramethyl-1,2-dihydropyrido[2',3'-6]xanthene) (CMRA)-loaded GlcNAc-decorated particles (PK-GlcNAc-CMRA) immediately following IR exhibited a greater CMRA fluorescence 3 days post-IR than animals that had received PK-CMRA particles, indicating enhanced in vivo uptake due to GlcNAc decoration. B), C) Immediately following IR, particles were injected intramyocardially and hearts removed 1 day post-IR. TUNEL staining indicated apoptotic nuclei (b) (apoptotic nuclei [purple] indicated by arrow, non-apoptotic nuclei [blue] indicated by triangle), and comparison against total CM nuclei indicated that animals that received PK-GlcNAc-SB particle injections achieved 3.6-fold fewer apoptotic events in the injured myocardium compared to IR and 2.7-fold fewer than the PK-GlcNAc group (c) (n = 3 for each group). Data are mean ± SEM. **p < 0.05, *p < 0.01. ANOVA followed by Newman–Keuls post test.

After establishing that GlcNAc-decorated particles are internalized by CMs *in vivo*, we sought to evaluate the anti-apoptotic effect of PK-GlcNAc-SB particles *in vivo* in a randomized and blinded manner. Using the IR rat model, we injected saline, PK-GlcNac, and PK-GlcNAc-SB particles (*n*=3 for each group) into the border zones of the LV as described in the methods. Twenty-four hours following IR, the rats were sacrificed, and TUNEL staining was performed for identification of the apoptotic nuclei (purple color;

Figure 3.6 b) of a-sarcomeric actinin-positive cells (green). The number of apoptotic CMs for each treatment group was determined and expressed as a percent of total CMs counted. We found that delivery of PK-GlcNAc-SB particles to the heart significantly reduced the percentage of apoptotic myocytes in the infarcted area as identified by TUNEL staining (Figure 3.6 b). In saline-only and PK-GlcNAc treated rats, 83%±14% and 64%±4% of CMs counted were TUNEL-positive (Figure 3.6 c). However, a significantly lower number of apoptotic CMs were counted in hearts treated with PK-GlcNAc-SB particles (23%±6%) (*p<0.05 and **p<0.01; ANOVA followed by Newman-Keuls post-test). Taken together, these data suggest that GlcNAc decoration of particles enhanced CM uptake *in vivo*, and delivered anti-apoptotic signals following IR.

3.3.5 In vivo cardiac function

We next sought to determine the ability of the SB-loaded particles to rescue rats from acute cardiac dysfunction. Following 30 minutes of ischemia, the LV was reperfused and rats received injections of saline, PK-GlcNAc, or PK-GlcNAc-SB particles in a randomized and blinded manner. Three days following IR, rats were subjected to small animal echocardiography (n=4 for sham, n>7), prior to determination of infarct size using TTC staining. Saline treated rats had an infarct size/area-at-risk (IS/AAR) of 43.7%±5.6% (Figure 3.7 a). While no significant difference was seen in rats that received PK-GlcNAc particle injection post-IR (IS/AAR = 49.4%±3.1%), rats that received PK-GlcNAc-SB particles had a significant reduction in IS/AAR (28.4%±3.2%; p<0.05 vs. IR and p<0.01 vs. PK-GlcNAc; ANOVA).

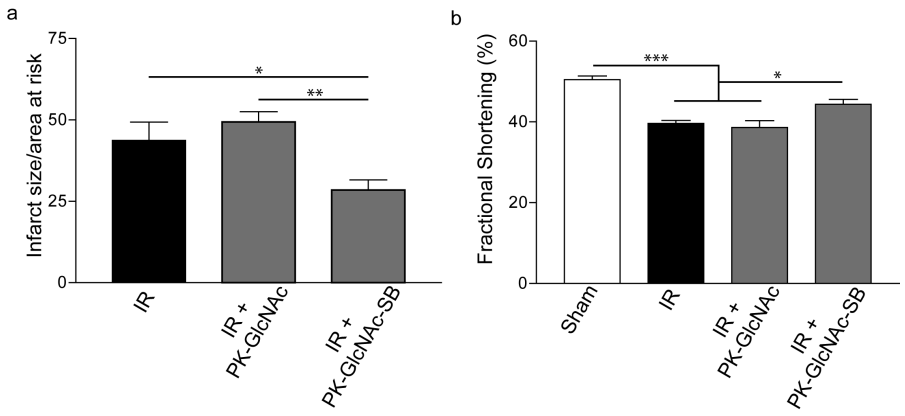

Figure 3.7. Infarct size reduction and functional improvements seen in PK-GlcNAc-SB treatment following ischemia–reperfusion injury. Immediately following IR, particles were injected directly into the injured myocardium. Three days following surgery, echocardiography was performed and heart cross sections analyzed for infarct size. A) The ratio of infarct size to area at risk was calculated for the treatment groups. PK-GlcNAc treatment had no significant effect, but PK-GlcNAc-SB treatment significantly decreased infarct size compared to both treatment groups (mean ± SEM, n = 5; *p < 0.05, **p < 0.01; ANOVA followed by Newman–Keuls multiple comparison post test). B) Fractional shortening calculated from echocardiographic measurements demonstrated a significant decrease in function in IR animals compared to sham. There was no significant improvement seen with PK-GlcNAc, though PK-GlcNAc-SB treatment improved function compared with other IR groups (n = 4 for sham n > 7 for IR groups). Data are mean ± SEM. *p < 0.05, ***p < 0.001. ANOVA followed by Tukey's post test.

To determine functional changes, left ventricular diameters were measured at peak systole and diastole to determine fractional area of shortening (*n*=5). Sham-operated rats had a fractional shortening (FS) of 50.5%±0.9% that was significantly lower in IR animals (39.6%±0.7%; *p*<0.05; ANOVA) (Figure 3.7 b). While no significant increase was seen in PK-GlcNAc treated rats (38.6%±1.7%), treatment with PK-GlcNAc-SB significantly improved FS (44.4%±1.2%; *p*<0.05 vs. IR, *p*<0.05 vs. PK-GlcNAc; ANOVA). Taken together, these data demonstrate a positive effect of PK-GlcNAc-SB on cardiac function following IR.

3.4 Discussion

Apoptosis of CMs following IR is suggested to be the dominant cause of chronic heart failure,[6, 148] but despite the existence of molecules with the potential to inhibit

apoptotic pathways, development of vehicles for intracellular drug delivery into CMs remains a large challenge for post-MI healing. Systems exist for sustained extracellular release of therapeutic molecules or that act through phagocytic cells, such as macrophages. However, potential therapeutics that act intracellularly are precluded from existing systems due to their inability to transmigrate cell membranes. Previous studies discovered that CMs bind to and internalize GlcNAc, providing a compelling targeting agent in CM-targeting drug delivery systems.[24] The researchers delivered pravastatin (a 3-hydroxy-3-methylglutaryl-CoA reductase inhibitor)-loaded GlcNAc-decorated liposomes to CMs and following stimulation with interleukin-1β, showed enhanced nitric oxide production and inducible nitric oxide synthase expression. However, the studies were limited to *in vitro* experiments and relied on liposomal vehicles, which are known to be unstable and leak water-soluble contents.[158] In our approach, we decorated acid-sensitive nanoparticles with GlcNAc and validated our delivery system both *in vitro* and *in vivo*. *O*ur preliminary findings implicate GlcNAc-decorated nanoparticles as a novel method of delivering therapeutic molecules to CMs to heal the post-infarct heart.

In our studies, we synthesized a targeting molecule consisting of GlcNAc tethered to an alkyl chain via a PEG linker. This was completed in a facile 8-step process with inexpensive materials. The reactions were conducted at the gram scale, but are scalable to kilogram quantities, allowing for larger production applications. Through hydrophobic interactions, the hydrophobic tail associated with the polymeric particle, allowing for the more hydrophilic sugar head group to partition into the aqueous phase to interact with CMs. In fact, this proposed particle-GlcNAc-alkyl interaction proved effective in decorating particles: in initial formulations of 10% and 1% by weight GlcNAc-alkyl to PCADK, the actual degree of decoration was 9 wt% and 0.6 wt%, respectively. This decoration of hydrophobic polymeric particles with hydrophilic GlcNAc increased the zeta potential from -8.97 mV (0% decoration) to -3.39 mV (9% decoration).

We have used this strategy in prior studies to bind large proteins to the outside of microparticles. Additionally, this strategy is not all that uncommon and is used to surface modify hydrophobic polymers with hydrophilic molecules.[31, 160] The polymer was composed of the polyketal PCADK that degrades in acidic environments, such as in the developing endosome. The byproducts are biocompatible (acetone is on the generally regarded as safe (GRAS) list and 1,4-cyclohexanedimethanol is Food & Drug Administration (FDA) approved as an indirect food additive and has an excellent animal toxicity profile[30]) and PCADK particles have been shown to neither incite the inflammatory response nor induce cell death.[32] We are able to routinely produce nanoparticles ranging in size from 200 to 800 nm, which is small enough to allow for cell internalization and large enough to avoid being flushed from the injured myocardium.

To initially demonstrate enhanced cellular uptake due to GlcNAc-decoration, particles were loaded with rhodamine B and incubated with CMs. Confocal images taken 12 hr later presented evidence of particle internalization wherein red nanoparticles were positioned within cells, visible within orthogonal frames. However, to more quantifiably determine internalization, we produced size- and load-matched particles with 0%, 1%, or 10% GlcNAc-alkyl decoration that contained the cell tracker dye CMFDA. The dye is non-fluorescent until activated by intracellular esterases and becomes cell impermeant by reaction with glutathione, thus fluorescence should only been seen when the CMFDA is released from the particles into the cell. To account for any CMFDA release from non-internalized particles, we normalized fluorescent readings to non-GlcNAc decorated CMFDA-loaded particle treatment. This approach allowed us to attribute fluorescence increase only with internalized particles. By comparing against the 0% decoration control, we saw a significant increase in fluorescence at 10% GlcNAc decoration, which confirmed that increasing GlcNAc decoration enhanced cellular uptake. While particle hydrolysis is possible outside the cell, which would allow release of the cell permeable

CMFDA in the media, our published studies would argue against that. The hydrolysis half-life of PCADK polymer at pH 7.4 was four years in serum-free media,[30] and thus it was unlikely that significant amounts of the hydrophobic CMFDA were released into the media. Furthermore, we examined release of CMFDA over 12 hr in cell free conditions and found no differences between the different particle preparations. The positive trend between degree of GlcNAc decoration and fluorescence increase implicates varying GlcNAc decoration to tune internalization kinetics, though more data points are needed. Moreover, it was suggested in prior studies that oligosaccharide decoration may also enhance uptake, setting the stage for a multi-sugar decorated particle to alter cell specificity.[25] We did not explore the mechanism for GlcNAc internalization, but findings from a recent study indicate that the intermediate filaments vimentin and desmin possess lectin-like domains on the cell surface that bind to and internalize GlcNAc.[25] Although vimentin and desmin are not unique to CMs, they are enriched in muscle cells[161] and gene knockouts demonstrate negative cardiac phenotypes.[162]

The MAPK p38 is known to be a key regulator of apoptotic pathways and is triggered by IR.[163-165] While our prior studies confirmed that PCADK was able to deliver therapeutics to macrophages, significant activation of p38 in CMs leads to apoptosis, activation of inflammatory genes, and stimulation of pro-fibrotic factors. Previously, we incubated CMs with SB239063-loaded non-decorated PCADK particles and analyzed TNF-stimulated p38 activation at several time points. We found no significant decrease in activated p38 when comparing inhibitor loaded and empty PCADK particles up to 6 hr, indicating that CMs internalized little non-sugar decorated particle, correlating with our current study using CMFDA. As our CMFDA data demonstrated significant uptake at 18 hr, we used this time point to determine efficacy of our inhibitor-loaded GlcNAc particles. After 18 hr of incubation with PK-GlcNAc or PK-GlcNAc-SB, we examined kinase activity by measuring TNF-a-stimulated p38 phosphorylation. We found that while PK-GlcNAc

(empty particle) treatment did not prevent p38 activation by TNF-a, treatment with PK-GlcNAc-SB did prevent this activation, suggesting internalization of particles and release of the inhibitor. Additionally, p38 activation was verified through a no particle control treatment, with a 1.8-fold increase in p-p38 due to TNF-a treatment. The delivery of SB239063 to cells via non-internalization means (i.e. extracellular release) in the acute phase is relatively low; our release curve indicates that only up to 13% of SB239063 may be released outside cells at pH 7.4 within three days. Though the current study only examined a small molecule p38 inhibitor, we have demonstrated the ability of PCADK particles to encapsulate a broad range of compounds from siRNA to proteins, and future work will determine whether these cell impermeant factors can also be delivered intracellularly to CMs.

To evaluate the applicability of our GlcNAc-decorated nanoparticle as a drug delivery system to CMs *in vivo*, we first examined the enhanced uptake of GlcNAc-decorated particles and then the anti-apoptotic effect of PK-GlcNAc-SB particles before assessing functional responses. We injected a saline particle suspension into the myocardium immediately following IR and evaluated cardiac function and structure in the acute temporal window. Although injection of small molecule therapeutics would be possible in a clinical setting, small molecules are cleared quickly from the well-perfused heart. We examined direct particle injection to the myocardium as intramyocardial injections in humans has been performed for cell therapy applications and is considered safe.[166-168] Although signaling cascades persist for weeks following MI and therapeutic treatments would benefit from sustained delivery, acute therapies are also needed. Our published data demonstrated that sustained inhibition of p38 by particles *in vivo* had a chronic—but little acute—benefit. Therefore we hypothesized that delivery of particles with enhanced CM uptake would improve acute myocyte survival. We qualitatively found that more CMs internalized CMRA-loaded particles due to GlcNAc decoration, validating

in vivo applicability of this delivery system. Furthermore, the anti-apoptotic effect of PK-GlcNAc-SB particles was successfully demonstrated *in vivo* following IR through the use of TUNEL staining: a 3.6-fold decrease in apoptotic CMs was observed due to PK-GlcNAc-SB treatment from the saline-only treatment. While the levels of TUNEL-positive cells in our studies seem rather high, it is important to note that much of our measurement comes from the border zones as that is where therapy was introduced. A more thorough study of apoptosis is underway.

In the structural response of rat model, no significant reduction in infarct size was seen between IR and PK-GlcNAc treatments, indicating no benefit of the empty sugar particle. However, delivering PK-GlcNAc-SB particles to the injured myocardium significantly decreased infarct by 35% from IR animals, indicating improved myocyte survival. While CM survival was not directly measured via cellular markers, infarct size is a well-known indicator of CM damage. This protective effect of PK-GlcNAc-SB was not only seen on infarct size, but cardiac function as well. Our data demonstrated significant decreases in FS in IR and PK-GlcNAc groups as compared with sham-operated animals. However, PK-GlcNAc-SB particle treatment restored nearly 50% of lost function over IR levels. While this was not restored to sham levels, the improvement was significant and indicates a functional benefit of GlcNAc-decorated particles loaded with a p38 inhibitor.

We did not directly compare with non-decorated, inhibitor-loaded particles in our current study because it was unnecessary to duplicate negative data we previously produced utilizing animal studies.[32] In that study, rats that received the p38-loaded inhibitor in PCADK particles had FS values similar to empty GlcNAc particle- and saline-treated IR rats (below 40%). Statistical comparison indicated no significant differences between those treatments, and PK-GlcNAc-SB was significantly improved over PCADK-SB particles, despite it being a separate study. It is important to note that we did not examine long-term function in this study, and the effect of sugar decoration on particle

efficacy in the chronic phase is unknown. As our prior barrier was lack of efficacy during the acute phase, we only examined this time point. One would hypothesize that increasing CM uptake would lead to a rapid depletion of drug-loaded nanoparticles available in the myocardium. While some studies suggest that inhibiting early apoptosis is critical for long-term function,[169, 170] our prior studies with encapsulated SOD suggest that inhibition of apoptosis alone may not be sufficient for long-term improvements.[159] Thus, the optimal therapy may involve a mixture of decorated and non-decorated nanoparticles to target both phases of post-MI cardiac dysfunction. In future studies, we will determine the long-term benefit of PK-GlcNAc-SB treatment and determine whether this early rescue of function leads to long-term improvements; or if combination with PCADK-SB particles that chronically inhibited p38 in macrophages gives a synergistic effect. Finally, despite the fact that GlcNAc glycosylation of proteins improves function of CMs and may play a role in the response following infarction,[171] we saw no beneficial effect of empty PK-GlcNAc particles. The studies demonstrating a critical role for this sugar did so by altering the activity or expression of the enzyme O-GlcNAc transferase (OGT). Thus the potential exists for the empty PK-GlcNAc particles to possess bioactivity in the setting of altered OGT activity. While not explored in our studies, encapsulation of OGT within PK-GlcNAc nanoparticles could have therapeutic potential.

In summary, our work[172] demonstrates that GlcNAc-decorated nanoparticles can be effective vehicles for intracellular delivery of therapeutic molecules to CMs. As verified by confocal microscopy and fluorescent plate readouts, CMs effectively internalized dye-loaded GlcNAc-decorated particles. Additionally, we demonstrated *in vitro* therapeutic delivery of the p38 inhibitor, SB239063, to CMs and validated GlcNAc-decorated nanoparticles as *in vivo* delivery vehicles by decreasing infarct size and restoring cardiac function. The lack of uptake of some molecules by non-phagocytic CMs, toxic doses required of others, and sustained temporal availability preclude systemic

delivery of most therapeutics as a method of treatment following MI. With the large scalability and non-toxic nature of the nanoparticles, as well as the ability to encapsulate a variety of compounds, the clinical potential is quite compelling. The proposed delivery system described in this study demonstrates a potential means to enrich intracellular therapeutics within CMs, providing a novel vehicle for treatment for acute myocardial function and possible prevention of heart failure resulting from massive CM death.

CHAPTER 4

DENDRIMERIC BOWTIES FEATURING HEMISPHERIC-SELECTIVE DECORATION OF LIGANDS FOR MICRORNA-BASED THERAPY

4.1 Introduction

The development of miR-based therapies holds exciting promise for improving the *status quo* of medicine.[13] Delivery of traditional pharmaceuticals has faced significant limitations: protein-based therapeutics are generally restricted to extracellular receptors; and small-molecule drugs modulate only certain functions of their targeted protein and are limited in specificity. In contrast, by exploiting endogenous post-transcriptional mechanism by delivering synthetic miR mimics, genetic pathways can be regulated selectively.[14] The range of miR-based pharmaceuticals is wide, with potential applications ranging from cancer to diabetes and heart failure.

However, challenges exist in the development of such therapies such as protecting the miR molecules from ribonucleases (RNases),[14] and difficulty inducing cellular uptake by the target cell population. RNases that are present in bodily fluids readily degrade miR, requiring protective measures, such as encapsulation of the miR[26] or the use of chemically modified RNA.[27] The highly charged backbone and size of nucleic acids precludes passive cell penetration,[14, 173] necessitating incorporation of a mechanism for cellular uptake in most cell types. Additionally, specificity in targeting certain cell types is generally desired in order to reduce miR uptake in unintended cells.

Dendrimers, a class of radially symmetric, regularly branched polymers, have been extensively studied as delivery agents for a variety of drugs.[174-176] One well studied dendrimer is PAMAM, which generally consists of an ethylenediamine core that is

reacted alternatively with methyl acrylate and ethylenediamine to form a size-tuned dendrimer that features amino termini.[177] Traditional strategies have largely consisted of physical entrapment of drugs within the relatively hydrophobic dendrimer core, with conjugated targeting moieties distributed among the dendrimer terminal groups. As such, dendrimers are attractive multi-functional nanomaterials despite some side effects, such as cytotoxicity.[36] Recent studies have extended dendrimer applications to siRNA- and miR-based therapeutics.[37, 38, 40, 65, 176, 178, 179] The suitability of a dendrimer-based RNAi therapeutic lies in part with the amino groups present at the termini and within the dendrimer that afford electrostatic interactions with—and thereby encapsulation and protection of—anionic miR mimics.[37] The interior amines can also provide "proton sponge" mechanisms for the endosomal escape of the trapped nucleic acids.[179] Another compelling reason for dendrimer-based therapeutics is that the terminal amines can be readily conjugated with biomolecular ligands, which "decorate" the dendrimer with signals to potentially enhance cell targeting and uptake. Studies have indicated that varying the number of ligands on the vehicle surface elicits different binding and internalization kinetics, and dendrimeric materials can handily exert these "multivalent effects" by presenting an increased number, density, and arrangement of ligands.[38-40, 180-182]

However, previous studies in dendrimer delivery systems where ligands were conjugated to surface groups may have had a significant design shortcoming: greater ligand density may result in enhanced delivery, but as PAMAM dendrimers present a defined number of terminal amines, an increase in the number of terminal amines conjugated to ligands necessitates a decrease in the number and density of PAMAM terminal amines available for RNA binding. These competing uses of terminal groups may create an impasse in dendrimer vehicle design if the need for decorated termini allocates insufficient numbers of terminal groups for RNA binding, or vice versa. Thus,

the need exists for a new dendrimeric structure with a higher degree of spatial control over the surface functional regions for effective delivery of RNAi therapeutics.

We present here the design and application of a novel multi-functional dendrimeric vehicle with two discrete regions: one that retains a high density of cations for RNA binding with the other region simultaneously presenting locally concentrated ligands that enhance cellular uptake. In this study, we prepared our “bowtie” dendrimer by coupling the cores of functionally unique reduced cystamine core PAMAM dendrimers. To promote binding of miR mimics, one side of the resulting dendrimeric bowtie consisted of one half of a generation 4 PAMAM (g4P) dendrimer, and the other side of the bowtie was one half of a generation 2 PAMAM dendrimer (g2P). The g2P presented either poly(arginine)$_9$ (polyR)—a cell-penetrating peptide—or the peptide RGD, a component of the integrin-binding matrix that facilitates the cellular uptake of RGD-bound particles.

To demonstrate the suitability of our dendrimeric bowtie as a transfection vehicle, we loaded the bowties with miR-126 mimic—an important modulator of vascular integrity, endothelial cell proliferation, and neovascularization—and incubated the resulting complexes with HUVECs. Treatment with our bowties significantly enhanced cell proliferation and tube formation of HUVECs, and knocked down SPRED1 mRNA levels, a target of miR-126.

4.2 Materials and Methods

4.2.1 Materials

Water was distilled and deionized at 18 MΩ resistance (Gelante Pure Water, Shijiazhuang, China). Peptides composed of sequences cysteine-glycine-glycine-arginine-glycine-aspartic acid-serine (CGGRGD) and cysteine-(arginine)$_9$ (polyR) were obtained from GL Biochem (Shanghai, China). GeneFinder nucleic acid dye was

purchased from Bio-V (Xiamen, China). 1,4-bis(maleimido)butane (BMB) coupler was purchased from Thermo Scientific. A HUVEC line was obtained from ScienCell, and daughter cells from passages under passage seven were used in *in vitro* experiments. Cells were cultured in endothelial cell medium (ECM, Cat. No. 1001, ScienCell) supplemented with 5% FBS (Cat. No. 0025, ScienCell), endothelial cell growth supplement (Cat. No. 1052, ScienCell), and penicillin/streptomycin (Cat. No. 0503, ScienCell). Opti-MEM reduced serum medium and Dulbecco's phosphate buffered saline (DPBS) were purchased from Invitrogen. Double-stranded miR-126, non-mammalian mRNA targeting negative control miR #22 (*C. elegans* miR cel-miR-239b-59), and cy3-labeled control miR #22 mimics were synthesized by RiboBio (Guangzhou, China). The sequences for miR-126 mimic were 5'-UCG UAC CGU GAG UAA UAA UGC G dTdT-3' (sense) and 3'-dTdT AGC ATG GCA CTC ATT ACG CAA-5' (antisense). The sequences for control miR #22 were 5'-UUU GUA CUA CAC AAA AGU ACU G dTdT-3' (sense) and 3'-dTdT AAA CAT GAT GTG TTT TCA TGA C-5' (antisense).

4.2.2 Synthesis

Generation 4 and hydrazide-terminated generation 2 cystamine core PAMAM dendrimers (g4P and g2P, respectively) were prepared as previously described.[180] Peptide decoration of g2P was accomplished via the bifunctional coupler, succinimidyl-([*N*-maleimido propionamido]-diethylene glycol) ester ($SM(PEG)_2$, Thermo Scientific), which featured amine- and thiol-reactive termini (Figure 4.1 A). In DPBS, 0.93 mM g2P dendrimer and 30 mM $SM(PEG)_2$ were reacted for 1 hour at room temperature. Following extensive washing in DPBS by centrifugal filtration (molecular weight cut off (MWCO) 3000, Millipore) to remove unreacted $SM(PEG)_2$, RGD or polyR peptides (18 mM final) were dissolved into reaction mixtures at a 1.2-fold excess to terminal groups. The reaction proceeded overnight at room temperature, followed by centrifugal filtration.

The modification levels of polyR or RGD on g2P was evaluated by analysis of ^{1}H-NMR spectra (ARX400, Bruker, Switzerland).

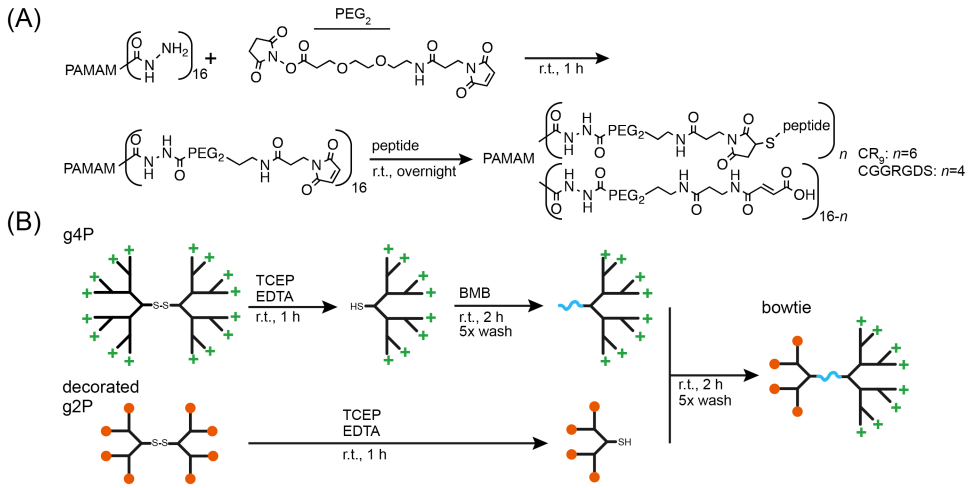

Figure 4.1. Synthesis and coupling of bowtie dendrimer. (A) Synthetic scheme for modification of g2P with RGD or polyR. (B) Cartoon of a synthetic scheme illustrating the coupling of cleaved g4P dendrons with cleaved, decorated g2P dendrons to generate dendrimeric bowties.

To generate dendrimeric bowtie conjugates (Figure 4.1 B), the reducing agent *tris*(2-carboxyethyl) phosphine (TCEP, 15 mM) was added to a solution of cystamine-core g4P (0.15 mM) in DPBS to reduce the disulfide bond within the core of the dendrimer. The reaction solution contained 10 mM ethylenediaminetetraacetic acid (EDTA) to prevent disulfide re-formation. A 10-fold molar excess BMB dissolved in dimethyl sulfoxide (DMSO) was then added to react with the newly generated thiols of the resulting dendron. The reaction was carried out for 2 hours at room temperature. The resulting g4P-BMB intermediate conjugate was washed by extensive centrifuge filtration (MWCO 3000, Millipore) to remove excess BMB. In a parallel reaction (Figure 4.1 B), the disulfide cores of polyR-, RGD-, and non-modified g2P were reduced with TCEP, and added in 20% molar excess to the activated g4P-BMB conjugate. This final coupling

reaction was carried out overnight. Non-reacted g2P dendron species were removed by extensive centrifuge filtration (MWCO 10000, Millipore). Bowtie conjugates were subjected to ^{1}H-NMR analysis, and bowtie spectra were compared to the polyR- and RGD-g2P spectra to verify coupling. Final dendrimeric bowtie species consisted of a non-modified g4P dendron coupled with a g2P dendron. Specifically, “non-dec-bowtie” consisted of no additional modifications, but polyR- and RGD-bowties presented either polyR or RGD peptides on the periphery of the g2P dendron.

4.2.3 Evaluation of reaction progression

Reaction completion status during bowtie generation was evaluated with Ellman’s reagent (*5*,*5*’-dithio-*bis*-(2-nitrobenzoic acid), DTNB). Briefly, g4P and unmodified g2P were reduced with 15mM TCEP and 10 mM EDTA in DPBS to give rise to thiol-containing hemispheric dendrons, which were then coupled with BMB as described above. To monitor the coupling reaction, 2 mL samples of dendrimer reagents or reaction mixtures were added at prescribed time points to 198 mL of an assay solution composed of 0.1 mM DTNB, 2.5 mM sodium acetate, and 50 mM tris(hydroxymethyl)aminomethane for a final volume of 200 mL in a 96-well plate well. Solutions were incubated for 5 min at room temperature, after which absorbance at 412 nm was measured by SpectraMax M2 plate reader (Molecular Devices). Free thiol concentration was calculated from absorbance values and used to evaluate reaction status.

4.2.4 Particle sizing and zeta-potential measurement

The sizes of complexed miR-bowtie particles were determined using DLS. Complexes were prepared at an N/P ratio of 2. The selected dendrimer (500 μM in diethylpyrocarbonate (DEPC)-treated water) and miRNA (20 μM in DEPC water) were mixed at 1:12.5 volume ratio (1:25 for g4P), sonicated for 5 min, and incubated at room

temperature for 15 min. Then complexes were diluted to 0.175 μM (miRNA concentration) in water. The aqueous solutions were filtered through 0.20 μm filters (Sartorius stedim Biotech, Goettingen, Germany) to remove the dust. All the vials used during the experiment were carefully washed and sterilized.

A commercialized spectrometer from Brookhaven Instruments Corporation (BI-200SM Goniometer) was used to perform both static light scattering (SLS) and DLS over a scattering angular range of 20-120°. A vertically polarized, 33 mW solid-state laser (Brookhaven Instruments Corporation) operating at 635 nm was used as the light source, and a BI-TurboCo Digital Correlator (Brookhaven Instruments Corporation) was used to collect and process data. For a very dilute solution, the weight-averaged molar mass and the root mean-square radius of gyration (Rg) can be obtained from SLS data. By using a Laplace inversion program, CONTIN, the normalized distribution function of the characteristic line width was obtained which could be further converted into the hydrodynamic radius Rh by using the Stokes-Einstein equation $D=k_BT/(6\pi\eta Rg)$, where D, kB, T, η are the translational diffusive coefficient, the Boltzmann constant, the absolute temperature, and the viscosity of the solvent, respectively.

The zeta-potentials of miR-bowtie complexes were measured through electrophoretic light scattering experiments, which were performed by a ZetaPALS zeta potential analyzer (Brookhaven Instruments) with the samples described above.

4.2.5 Gel retardation analysis

To estimate the minimum of amount of dendrimeric bowties that can form complexes with certain amount of miRNA, gel retardation assay was carried out to visually analyze the unbound miRNA. Complex solutions were prepared as described above, with volume ratio of dendrimers and miRNA adjusted to the corresponding N/P ratio varied from 0 to 1.31. The solutions were diluted to 2 μM (miRNA concentration) in

DEPC water, and loading buffer was added to the solutions at 1:5 ratio. Samples containing miR-bowtie complexes were loaded in 3% agarose gel containing 1/10000 GeneFinder™ nucleic acid dye prepared in 0.5x tris-borate-ethylenediaminetetraacetic acid (TBE), and electrophoresis was carried out at 110 V in 0.5x TBE buffer (pH 8.5). Bands were imaged by a Tanon-1600 Gel Documentation System (Tanon, Shanghai, China).

4.2.6 Fluorescent dye exclusion assay

To quantitatively evaluate the ratio of dendrimer to miR for complete oligonucleotide encapsulation, miR was complexed with varying molar ratios of dendrimeric bowties in DEPC-treated water for 2 min. Then GeneFinder nucleic acid dye was added in DPBS to a final volume of 50 mL for a GeneFinder dilution of 1:10000 and 0.2 mM miR concentration. After 5 min incubation, GeneFinder-dyed Dendrimer-miR solutions were transferred in triplicate to a 96-well plate. The fluorescent signals (excitation: 489 nm, emission: 517 nm) resulting from GeneFinder binding non-encapsulated miR were measured by a SpectraMax M2 plate reader (Molecular Devices).

4.2.7 Transfection

For the *in vitro* studies, HUVECs were subjected to reverse transfection before any further experiments. Cells were starved for at least 6 hours in no-serum ECM, then seeded in collagen-coated 24-well plates together with miR-bowtie complex solution in Opti-MEM with 2% FBS. After incubation for 8 hours at 37°C with 5% CO_2, transfection media was replaced by 2% FBS Opti-MEM. Complexes (N/P ratio of 1.5) were prepared as above, and diluted to 0.175 μM (miR concentration) in 2% FBS Opti-MEM.

4.2.8 qRT-PCR primer design

The primers for quantitative real-time polymerase chain reaction (qRT-PCR) assay were designed by online National Center for Biotechnology Information (NCBI) primer designing tool (http://www.ncbi.nlm.nih.gov/tools/primer-blast/), the product length is set between 100-250bp. The primers for SPRED1 and glyceraldehyde-3-phosphate dehydrogenase (GAPDH) were: SPRED1 forward, 5'-GCG ACT CAG GGA CAA AAT GGT GGT-3'; SPRED1 reverse, 5'-TCA AAA GCC CTA GCA TCA GCA GGA C-3'; GAPDH forward, 5'-GGT CGT ATT GGG CGC CTG GT-3'; GAPDH reverse, 5'-TAC TCA GCG CCA GCA TCG CC-3'.

4.2.9 mRNA knockdown assay

Twenty-four hours after transfection initiation (treatment groups included g4P, non-dec-bowtie, polyR-bowtie, and RGD-bowtie carrying either negative control miR or miR-126), total RNA of treated HUVECs was extracted using TRIzol (Invitrogen). Total isolated RNA (500-1000 ng) was reverse transcribed with TransScript First-Strand cDNA Synthesis SuperMix (Transgene, China, Beijing). The gene expression levels were analyzed using the SYBR Green real-time PCR method and quantified with the Bio-Rad CFX96 Real time PCR System (Bio-Rad). Primers for SPRED1 and GAPDH were all obtained from Sangon (China, Shanghai). SPRED1 gene expression values were normalized to GAPDH levels, followed by comparison of knockdown due to transfection of miR-126 or negative control miR within each transfection vehicle. Relative expression was calculated using the comparative CT method. The mean minimal cycle threshold values were calculated from triplicate reactions.

4.2.10 Toxicity and proliferation

After 40 hours incubation in 2% FBS Opti-MEM, media was removed, and the cells were fixed in 2% PFA and stained with 0.5 μg/mL DAPI for 10 min. Fluorescence

images were captured by an IX71 fluorescence microscope (Olympus, Japan), and the number of cells in each well was counted.

4.2.11 Tube formation

Forty hours after transfection media replacement with fresh media, cells were detached and counted. Ten thousand cells from each treatment group were re-suspended in ECM supplemented with 5% FBS and plated onto Matrigel films in 96-well plates. Cells were incubated for 6 hours and imaged under bright-field microscopy. Tube length was quantified by ImageJ software analysis.[183] Tube formation experiments were performed three times.

4.2.12 Statistics

Quantitative results were presented as means ± standard error of measurements. Where appropriate, statistical comparisons were performed with one-way ANOVA followed by Fisher's least significant difference post-hoc test. All statistical tests were conducted using IBM SPSS 20.0.0 statistical software. The level of significance was denoted by *, **, and ***, denoting p values of <0.05, <0.01, and <0.001, respectively.

4.3 Results

4.3.1 Synthesis of dendrimeric bowtie conjugates

After decoration of g2P dendrimers with ligands (Figure 4.1 A), the dendrimers were cleaved with TCEP and coupled with similarly cleaved g4P dendrons (Figure 4.1 B), giving rise to a bowtie structure containing two distinct hemispheric regions. The conjugates were termed "non-dec-bowtie", "polyR-bowtie", and "RGD-bowtie".

We monitored the dendron coupling process by evaluating the reduction of g2P and g4P with TCEP, and the coupling of the thiol-containing dendrons with BMB. Ellman's reagent, DTNB, was employed to relatively quantify the remaining free thiol

groups such as those generated and consumed in our bowtie conjugation scheme (Figure 4.2). By sampling our reaction mixture at various stages, we confirmed with statistical significance the cleavage and coupling of dendrimers of dendrimeric bowties. Specifically, only 3.7 ± 0.6% of the cleaved g4P dendrons remained unmodified after 30 min, whereas the free thiols from the second infusion of cleaved dendrons remained unmodified for a longer period: 54.5 ± 5.1% after 30 min and 1.3 ± 0.6% overnight. The modification of cleaved g4P dendrons with BMB proceeded at a faster overall rate than the coupling of BMB-g4P conjugates with cleaved dendrons: whereas 96% of g4P sulfydryl groups conjugated to BMB within 30 min, only 46% of free thiols from the second infusion of cleaved dendrimers converted within a matched time frame. This was likely due to differences in the ratios between sulfydryl and maleimide groups; our reaction mixture between cleaved g4P dendrons contained a free thiol:maleimide ratio of 1:20, whereas the subsequent BMB-g4P reaction with cleaved dendrons contained a stoichiometric ratio of 1:1.2. Also, the relatively small size of free BMB (248.23 Da) may have contributed to an increased reaction rate compared to the larger BMB-g4P dendrons (>7.4 kDa).

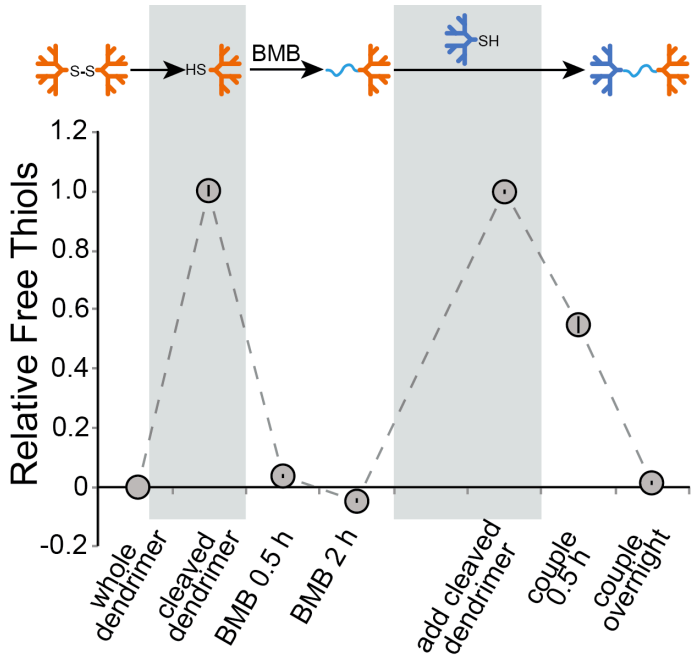

Figure 4.2. Progression of coupling reaction. Indicated by the generation and consumption of unreacted free thiols.

Further confirmation of the coupling between cleaved g4P and g2P dendrons was conducted by examining the ^{1}H-NMR spectra of g4P, decorated g2P dendrimers, and final bowtie conjugates (Figure 4.3). The representative PAMAM peaks occur in the 2.6 to 2.9 ppm range and the polyR and RGD peaks occur in the 1.5 to 2.0 ppm range (in both cases due to the alkene protons present in the arginine side chain). Qualitative comparison between the g2P conjugate and the bowtie spectra indicate a decrease in the area of the arginine peaks, correlated with an increase in the area of the PAMAM peaks. This analysis confirms the coupling between the thiols of the cleaved g4P and g2P dendrons.

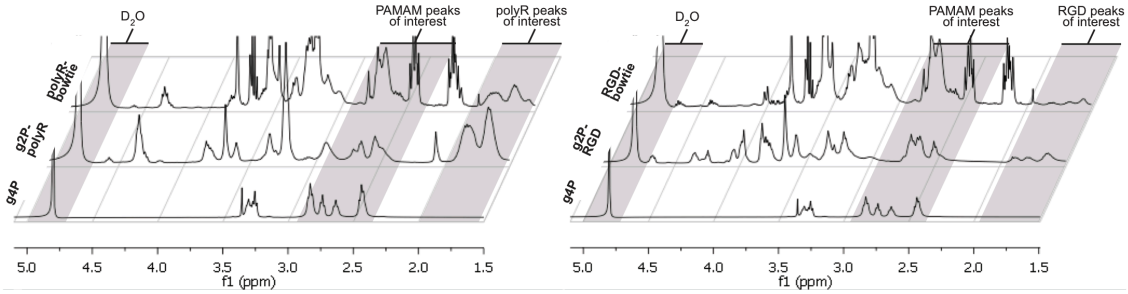

Figure 4.3. Comparison among g4P, decorated g2P, and bowtie NMR spectra. The decrease in peptide peaks and concurrent increase in PAMAM peaks indicate coupling.

4.3.2 Encapsulation of miR by dendrimeric bowtie

We characterized the complexation capacity of miR by dendrimers to determine the maximum payload. We first evaluated this by dye exclusion assay, as measured by fluorescent plate reader (Figure 4.4 A). As the N/P ratio increased from 0 to 0.33, the amount of non-encapsulated miR decreased as evidenced by the decreased fluorescence intensity. When N/P ratios were greater than 0.33, the change in fluorescence intensity decreased, indicating that the maximum loading capacity of dendrimeric bowties with miR corresponded with an N/P ratio of approximately 0.66.

To corroborate these findings, we performed gel electrophoresis experiments with similar N/P ratios (Figure 4.4 B). For ratios less than 0.33, bands present in the gel indicated that the amounts of dendrimer in the systems were insufficient for complete miR encapsulation. In contrast, the lack of bands in lanes where the N/P ratio was greater than or equal to 0.33 signified the total encapsulation of miR. This trend was similar to that observed in the fluorescent dye exclusion assay. Loading capacity of miR was conserved among the vehicle types.

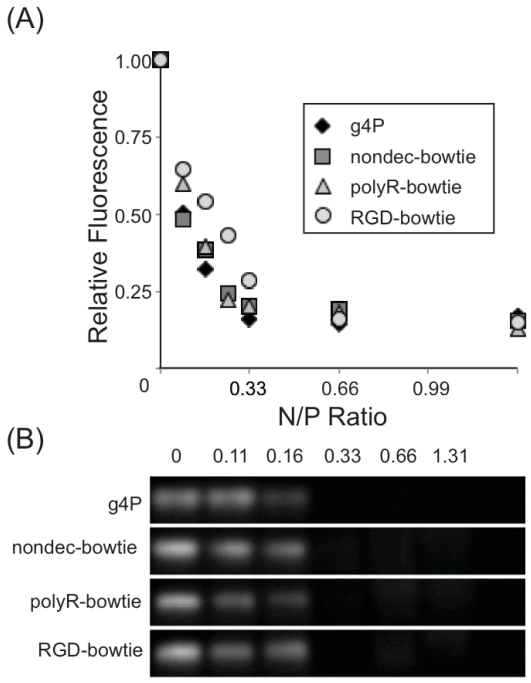

Figure 4.4. Evaluation of the dendrimeric vehicle encapsulation capacity. Measured by (A) fluorescent dye exclusion and (B) gel retardation. The N/P ratio that maximized payload and minimized non-encapsulated miR was 0.66.

4.3.3 Physical characterization of dendrimer conjugates

The particle sizing spectra as measured by SLS at 90^{o} is displayed in Figure 4.5 A. Average radii (radius of gyration) and zeta potentials of particles formed by miR-encapsulated dendrimers are presented in Figure 4.5 B. Particle radii ranged from 96 to 108 nm, indicating the occurrence of dendrimer aggregation. Zeta potentials ranged from -21 to +2 mV.

(A)

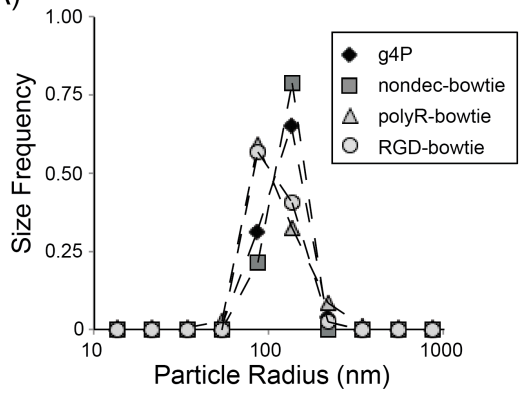

(B)

dendrimer/bowtie	average particle radius (nm)	zeta potential (mV)
g4P	108	2.1 ± 1.0
nondec-bowtie	117	-21.8 ± 0.8
polyR-bowtie	97	1.5 ± 1.2
RGD-bowtie	96	-8.6 ± 0.3

Figure 4.5. Dendrimer sizes. (A) DLS particle size spectra. (B) Summary of particle radius and zeta potential measurements.

4.3.4 Dendrimer conjugate type affects cell viability and transfection efficacy

Cells were treated with dendrimeric bowties and g4P loaded with non-targeting miR to evaluate toxic effects of the delivery systems. We found that compared to non-treated cells, g4P and non-dec-bowties significantly reduced HUVEC cell number by 76.2 ± 3.3% (p=0.032) and 74.7 ± 4.2% (p=0.024) of non-treated group size, respectively (Figure 4.6 A). In contrast, treatment of cells with bowties polyR- or RGD-bowties loaded with non-targeting miR mimic exhibited no statistically significant detrimental effect on cell number.

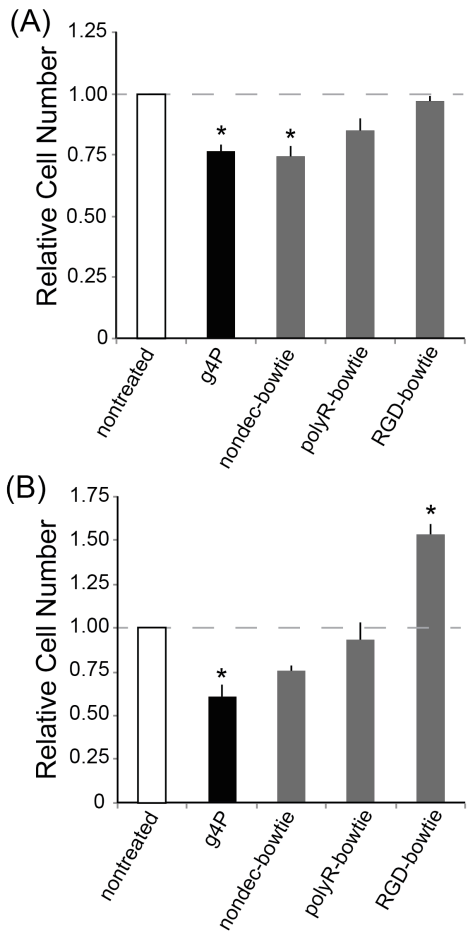

Figure 4.6. Cytotoxic and proliferative effects of dendrimers. (A) Cytotoxicity effects of dendrimeric vehicles on HUVECs. G4P and nondec-bowties were both toxic, whereas neither polyR-bowtie and RGD-bowtie affected cell population. (B) Proliferative effects of miR-126-loaded vehicles. RGD-bowtie was the only group to increase proliferation, whereas g4P decreased cell number. Asterisks denote comparison to nontreated control groups.

We then treated cells with miR-126-loaded dendrimers for 8 hours followed by 40 hours incubation and measured proliferation by cell counting. Only transfection mediated by RGD-bowtie demonstrated a significant proliferative effect (Figure 4.6 B). Compared to non-treated cells, transfection by loaded g4P caused a statistically significant loss in cell numbers of 60.8 ± 7.1 % (p=0.050). This result is consistent with the g4P loaded with non-targeting miR. Transfection by non-dec- and polyR-bowties demonstrated no significant negative or beneficial effect on cell number: just 75.1 ± 3.7 % (p=0.187) and

93.0 ± 9.8 % (p=0.698), respectively, compared to non-treated groups. In contrast, miR-126 transfection mediated by RGD-bowties resulted in a statistically significant increase of 153.8 ± 5.8% (p=0.012) in cell number.

4.3.3 HUVEC tube formation as a function of dendrimer type

We evaluated the ability of miR-126-loaded dendrimers to induce tube formation in HUVECs (Figure 4.7). When plated on matrigel films, tubes formed by cells treated with miR-126-loaded g4P were statistically shorter: only 59.9 ± 1.6 % (p=0.036) as long as tubes formed by non-treated cells. Likewise, treatment with miR-loaded non-dec-bowties failed to show an increase in tube length. However, both polyR- and RGD-bowties loaded with miR-126 significantly increased tube formation: compared to non-treated cells, polyR-bowtie-treated cells formed 160.5 ± 8.4 % (p=0.004) tube length and RGD-bowtie-treated cells almost doubled tube length to 191.5 ± 9.6 % (p=0.0003) of non-treated cells.

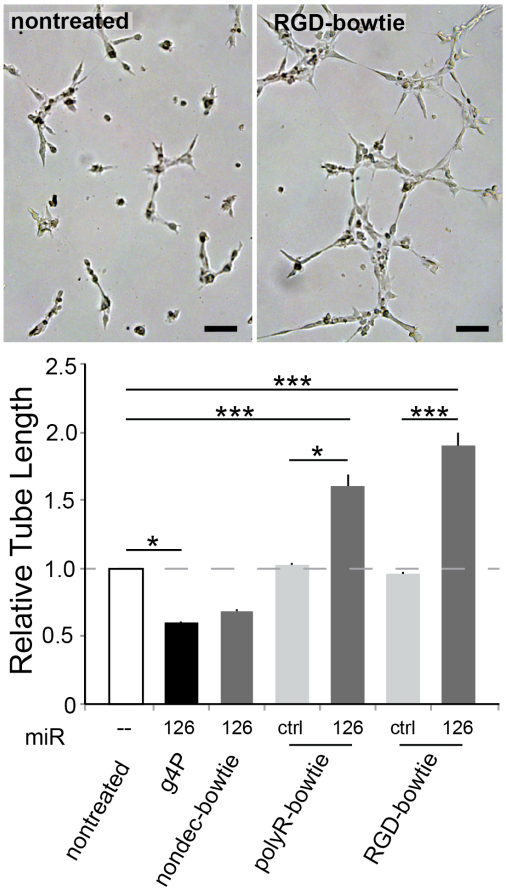

Figure 4.7. Tube formation analysis as a result from transfection of miR-126 or negative control miR with dendrimeric vehicles. G4P-mediated transfection failed to induce tube formation of HUVECs, whereas both polyR- and RGD-bowtie enhanced tube formation when delivering miR-126. Neither polyR- nor RGD-bowtie loaded with negative control miR induced tube formation. Scale bars = 100 μm.

To evaluate if the increase in tube formation was elicited by cell-material interactions from polyR- or RGD-bowtie, or if it were due to miR-126 transfection, we transfected HUVECs with negative control miR. We found that neither treatment groups exhibited a significant change in tube formation compared to non-treated cells (Figure 4.7).

4.3.6 Molecular analysis of dendrimer-mediated knockdown

To further evaluate transfection efficacy of miR-loaded dendrimers, we measured the presence of SPRED1-encoding mRNA, the target of miR-126, in treated and non-treated cells (Figure 4.8). Of note was that polyR-bowtie- and g4P-mediated transfection showed significant decreases in SPRED1 mRNA: g4P and polyR-bowtie dropped SPRED1 mRNA levels to 50.4 ± 10.7% (p=0.046) and 49.7.0 ± 3.0% (p=0.044) compared to non-treated cells. Our experiments suggested a trend for RGD-bowtie-mediated transfection to knock down SPRED1 mRNA (67.1 ± 6.6%, p=0.162), and non-dec-bowtie dendrimers did not knock down the presence of SPRED1 mRNA. However, decoration of dendrimeric bowties enhanced knockdown of SPRED1 mRNA: compared to cells treated with non-dec-bowties, dendrimeric RGD-bowties and polyR-bowties showed significant knockdown of SPRED1 mRNA of 40.3% (p=0.007) and 54.5% (p=0.028), respectively.

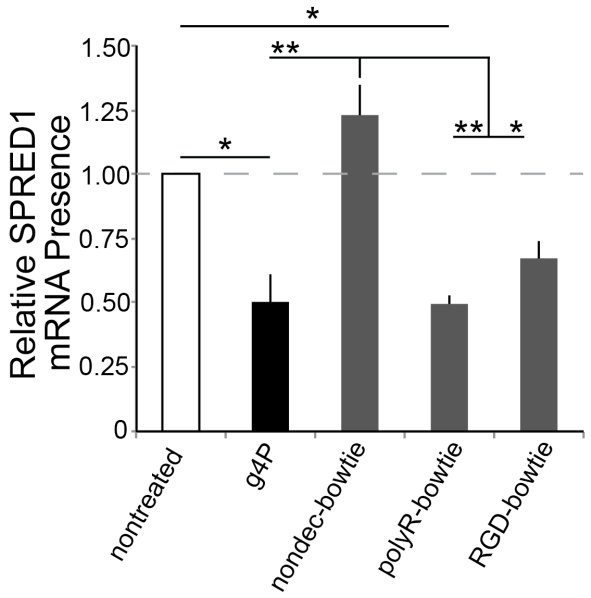

Figure 4.8. Efficiency of dendrimeric vehicle-mediated transfection of miR-126. Compared to nontreated control groups, only g4P and polyR-bowtie downregulated SPRED1, a target of

miR-126. Compared to no-dec-bowtie, the other vehicles—including RGD-bowtie—decreased the presence of SPRED1.

4.4 Discussion

Dendrimers have been explored as drug delivery agents because they present a stable, well-defined nanoscale architecture with a tunable number of reactive terminal groups.[174-176] The efficacy of "naked" siRNA therapy has been due to circulating RNase A-type nucleases and rapid renal clearance.[184, 185] Dendrimers have proven protective against degradation by RNase,[37] which—coupled with their functionalizable surface groups—intimates their application for RNAi therapeutics. However, the traditional dendrimer design potentially faces limited application: although altering ligand density is a feasible way to tune particle uptake, hemispheric selectivity of ligand conjugation to simultaneously spatially control both the density and number of ligands or RNA-binding sites is virtually non-existent. To address this insufficiency, we proposed a bowtie design that features two regions of either locally dense ligands or RNA-binding amines.

Synthetic schemes for generating dendrimeric bowties can be divergent[186, 187] or convergent, i.e. grown from a "seed" dendrimer that features *ab initio* orthogonally reactive terminal groups or generating a final molecule from unique dendrimers developed *a priori*. Convergent synthesis can feature either the coupling of dendrons featuring unique reactive groups at the core, such as that rely on click chemistry,[188] or the cleaving and coupling of identical functional groups, such as dendrimers with reducible disulfide cores.[189, 190] Divergent synthesis can be problematic in that not all terminal groups may be modified at each synthetic step. However, cystamine-core PAMAM dendrimers of several generations are commercially available and feature readily functionalizable reactive terminal amines. One other advantage of these

dendrimers is the availability of thiol-reactive coupling agents that minimize the reaction incidences of non-unique dendrons (as opposed to re-oxidation in the presence of air); by reacting the coupler with one dendron type before adding the second species, the synthesis of homogenous bowties is avoided. The method presented here generates disulfide-core dendrimers decorated with desired terminal groups before reduction of the disulfide bond and convergent bowtie synthesis by bismaleimido coupling.

It is seen that the RGD-bowtie and non-decorated bowtie (but not polyR-bowtie or PAMAM) showed reduced zeta potential but were still in the negative range. These results are considered reasonable for the following reasons. First, we chose to use minimum amounts of dendrimeric carrier to complex with RNA to test the carrier under high loading capacity. Second, this result actually matches with the structure of the carrier, as aspartic acid (in RGD)—which is speculated to be on the surface of the nanocomplex—is negatively charged, as are the hydrolyzed maleimide groups (which converted to carboxylic acids) on the peptide-modified dendrimeric bowties. PolyR may provide more positively charged groups that balanced the negative charges on bowtie surface.

Our studies[191] demonstrated the superiority of bioactive ligand-decorated dendrimeric bowties compared with both non-decorated bowties and g4P in preventing cell toxicity under experimental conditions of 0.175 mM miR and N/P ratio of 1.5. Whereas both g4P and non-dec-bowtie were detrimental to cell number, neither polyR-bowtie nor RGD-bowtie materials exerted cytotoxicity. The toxic effects that dendrimers exhibit are generally attributed to the cationic charges of the terminal amines, which can contribute to membrane destabilization[192] and apoptotic pathway activation.[193] Therefore, it is important to consider such electrostatic interactions when evaluating vehicle performance, and in our dendrimeric bowties were structurally different from g4P: each bowtie bore half of the charged amines as compared to g4P, which featured higher local

charge density. But despite containing half of the positive surface charges as g4P, it was apparent that the existing charges on non-dec-bowtie were sufficient to induce similar toxic effects. In contrast, the lack of cytotoxicity exerted by either polyR- or RGD-bowtie indicated the beneficial consequence of surface peptide decoration-mitigated toxicity. By conjugating peptides to an otherwise cytotoxic backbone, the overall concentration of PAMAM terminal amine charges within one vehicle is decreased, which may ameliorate toxic interactions such as membrane destabilization. Furthermore, peptides on dendrimer surfaces may activate internalization mechanisms different from those elicited by PAMAM surface charges.

Characterizing the effects of vehicle type on cell viability provided preliminary information on the suitability of dendrimeric bowties for transfection, but we were interested in examining the further pro-angiogenic effects of the decorated bowtie-mediated delivery versus delivery mediated by g4P and non-dec-bowtie. Both g4P and non-dec-bowtie were unable to induce cell proliferation or tube formation, perhaps due to their relatively high cytotoxicity that may have counteracted any proliferative effects. On the other hand, PolyR-bowtie knocked down SPRED1 by half and successfully induced tube formation despite having no effect on proliferation. Considering that the polyR-bowtie exerted no detrimental effects on cell viability, a proliferative/tubulogenic-decoupled interaction may be taking place between the material and signaling or translational pathways that remains to be explored. The possibility of distinctive effector pathways was further demonstrated by miR-126-loaded RGD-bowtie, which both induced cell proliferation and tube formation. Although RGD-bowtie lacked statistical significance in its knockdown of SPRED1 by a third compared to non-treated cells, we did find that RGD decoration enhanced SPRED1 knockdown significantly compared to non-dec-bowtie. As others have demonstrated that RGD induces cellular internalization,[40, 178, 194-196] it is entirely possible that in our studies, the RGD-bowtie

mediated uptake of miR-126 improved proliferation and tube formation through an independent non-SPRED1 pathway. The mRNA targets of miR-126 include CRK,[197] CXCL12,[198] HOXA9,[199] PIK3R2,[200] TOM1,[201] and SPRED1.[200] The last is a negative regulator of MAPK and PI3K signaling, and served as a surrogate for ascertaining transfection efficacy in our study. We also failed to find significant regulation of PIK3R2 mRNA in any treatment groups. Another possible mechanism for the angiogenic effects of RGD-bowtie is that, as RGD is part of the recognition sequence that binds integrin,[202] extracellular interactions from the tethered RGD may have contributed to downstream results through differential gene expression.[203] However, neither polyR- nor RGD-bowtie materials alone were found to increase tube length, indicating that tube formation was dependent on at least miR-126 internalization, though vehicle type may compound angiogenic effects. The ability of g4P to downregulate SPRED1 mRNA while exerting deleterious downstream effects was a striking demonstration of its unsuitability as a transfection agent in pro-angiogenic applications.

There has been a burgeoning field of miR discoveries in the last several years, and research toward application is in close suit. The miRs 27b,[204] 92a,[205] 126,[200] 130a,[206] 132,[207] and 210[200] among others have been reported to regulate angiogenesis.[208] Additionally, miRs associated with cardiac development, endothelial cell proliferation, vascular integrity, and CM and vascular smooth muscle cell differentiation have been identified.[15-17, 209] The promise of therapeutic applications exists in exploiting the endogenous RNAi machinery by delivery of effective levels of miRs or antagomirs to the intended cell types. The field of delivery nanovehicles for miRs, however, is largely undeveloped. Future *in vivo* studies are warranted to investigate treatment with miR-loaded bowties to rescue the heart in a rat MI model.

Taken together, RGD-bowtie functioned as a potential miR-delivery agent for angiogenic application by significantly enhancing cell proliferation and tube formation of

endothelial cells without contributing to cytotoxicity. Our study could have wide-ranging implications for developing new transfection reagents for primary cells as well as for promoting angiogenesis by enhancing endothelial proliferation and tube formation, which would be considered a significant and applicable accomplishment. As a cardiology lab, we are especially interested in these functions as a potential therapeutic system to treat the infarcted heart.

Multi-functional dendrimeric bowties are substantially versatile in regards to size, shape, and regio-selectivity of terminal chemical groups. In the field of RNAi therapeutics, they may prove to be superior transfection agents due to the high concentration of miR- and siRNA-binding groups and targeting groups that they simultaneously offer. Our overall objective in this study was to present the design and functionality of a novel bi-functional dendrimeric conjugate, one half consisting of a cationic PAMAM dendron capable of binding miR, and the other half decorated with cell-targeting peptide ligands. We presented a facile synthetic scheme for generating our bowtie construct and demonstrated successful knockdown of a targeted SPRED1 mRNA with miR-126. As it stands, these dendrimeric bowties were substantially more effective in inducing downstream effects than conventional g4P while exhibiting much greater biocompatibility. Our study demonstrates the paradigm to synthesize ligand-decorated dendrimeric bowties with defined spatial structures and this model system could lay the groundwork for development of a miR-based therapy for myocardial and peripheral ischemic diseases by promoting angiogenesis and subsequent blood flow to the diseased regions.

CHAPTER 5

THERAPEUTIC EFFECTS OF EXOSOMES FROM HYPOXIC CARDIAC PROGENITOR CELLS

5.1 Introduction

Cardiovascular disease is the leading cause of morbidity and mortality in developed nations, and acute MI is the major subgroup, with an estimated 1.1 million Americans suffering MI alone.[49] Beyond the acute treatment of restoring blood flow to the infarct, subsequent measures focus on improving the contractility of the remaining tissue. The damaged, relatively non-regenerative myocardium undergoes a degenerative process leading to heart failure. Consequently, the annual financial cost of cardiovascular totaled $315.4 billion in 2010, and costs are expected to grow to $918 billion annually by 2030 when 43.9% of the population is expected to suffer from CVD.[49]

Cell-based therapies to treat the heart—including injection of stem cells from various sources—have yielded mixed results in several species.[41-44] Cardiac progenitor cells, a small population of stem-like cells residing in the heart, are of interest as they only differentiate in to cardiac lineages and can be isolated by tissue biopsy. Researchers have induced differentiation of stem cells into various cardiac cell types, and observed that cell secretion changes in response to alterations in extracellular conditions.[210-215] However, whether stem cells contribute to the cardiac response through differentiation or paracrine signaling—or a combination of the two—is still unknown. Despite the moderate benefit in stem cell therapy, major hurdles remain, including immunogenicity, toxic engraftment environment, and temporal constraints in patient-specific cell expansion.

MicroRNAs have been known to function in intracellular gene regulation, but in the past decade have been discovered to circulate in mammals.[216, 217] Since then, stable miRs have also been discovered in urine, saliva, semen, breast milk, and cerebrospinal fluid.[217-220] Differential miR profiles were found in biofluids based on pathology, leading to interest in the development of disease biomarkers.[120, 130, 221] These profiles have already been explored for a range of conditions, including cancer, diabetes, and CVDs.[120, 222, 223]

The discovery of stable circulating miR was met with some surprise, as circulating nucleases would be expected to degrade extracellular miR.[126] However, various protective carriers for extracellular miR have been observed: membrane-derived vesicles (apoptotic bodies, microvesicles, and exosomes), high-density and low-density lipoproteins, and proteins (especially from ribonucleoprotein complexes).[126, 209, 217, 222] Recent efforts have been made to explore the endogenous function of circulating miRs, especially in intercellular gene regulation.[217, 224] Originally considered cell debris, membrane-derived vesicles were more appropriately characterized in 1987,[121] and cell-cell transfer of exosomes observed in 2002,[122, 123] but miR encapsulation by exosomes was not verified until 2007.[124, 125] Interestingly, the miR signatures are unique among the different carriers,[126] and even between carriers and parent cells, suggesting regulated export of miRs.[15, 126, 128] Most cells secrete exosomes; those verified include platelets,[222, 225] lymphocytes,[224] and adipocytes,[226] and, muscle,[120, 135, 227] tumor,[228, 229] glial,[230] and stem cells.[48, 138, 140, 141, 231]

In this report, we generated exosomes from CPCs exposed to hypoxic and normoxic conditions for 3 hr or 12 hr and explored the effects of these exosomes on cardiac cells in vitro. We found that exosomes from CPCs subjected to hypoxia for 12 hourr induced significantly more tube formation and reduced fibrotic gene expression as compared to exosomes from normoxic CPCs. We also analyzed secreted miR via array and identified several miRs upregulated by hypoxia 12 hr exosomes. Using empirical data and statistical transformation processes, we

developed a computational model of miR content to predict the effects of 3 hr exosomes from hypoxic and normoxic CPCs. Finally, we identified co-varying miR clusters that may lead to future bio-inspired therapeutics.

5.2 Materials and Methods

5.2.1 Media components

The media that was used for the fibroblasts consisted for 10% FBS, 1% L-glutamine, 1% penecillin, and 1% streptavidin, and DMEM basal media. For DMEM quiescent media, FBS was reduced to 2%. The culture media that was used for the cardiac microvascular endothelial cells (CECs) consisted of animal cardiac endothelial cell basal media, 2% FBS, 1% L-glutamine and 1% antibiotic/amniotic and 0.1% endothelial cell growth supplement. For CEC quiescent media, FBS was reduced to 0.04%. The CPC culture media, Ham's F-12 basal media was used along with 10% FBS, 1% penecillin, 1% streptavidin, 1% L-glutamine, 0.1% Leukemia Inhibitory Factor (LIF), and 10% fetal bovine growth factor. For CPC quiescent media, no FBS was used and 1% ITS was added. For CPC treatment media, no FBS or LIF was used and 1% insulin-transferrin-selenium (ITS) was added.

5.2.2 Exosome generation

Cardiac progenitor cells were grown to 90% confluence and quiesced for 12 hr. Plated cells were subjected to normoxic or hypoxic conditions for 3 hours or 12 hours. To generate hypoxic conditions, cells were transferred to an incubator chamber (Billups-Rothenberg MIC-101) and flushed with hypoxic gas mixture (95% N_2, 5% CO_2). After conditioning, the media was subjected to sequential centrifugation (Optima XPN-100 ultracentrifuge; Beckman Coulter SW 41 Ti rotor) at 10,000 x *g* for 35 min to remove cell debris and 100,000 x *g* for 70 min., followed by two washings in PBS (100,000 x *g*, 70

min.). The exosome pellet was isolated and the protein content of the exosome suspension was analyzed by Micro BCA Protein Assay kit (Thermo Scientific Pierce 23235) according to manufacturer's instructions.

5.2.3 Secreted miR analysis

miR was isolated from conditioned media with the miRVANA PARIS kit (Invitrogen AM1556M) according to manufacturer's protocol. The miR solutions were then analyzed (Agilent 2100 Bioanalyzer) for size, quality, and quantity of miR. Following characterization, miR was subjected to analysis via Affymetrix MultiSpecies MicroRNA GeneChip array. Data were analyzed in Affymetrix Expression Console to determine levels of miR upregulation.

To evaluate levels of upregulated miR in exosomes, exosomal miR was isolated with the miRVANA PARIS kit and cDNA generated via NCode miRNA First-Strand cDNA Synthesis Kit (Invitrogen MIRC-50) according to manufacturer's protocol. cDNA samples were then subjected to qRT-PCR and relative mRNA levels ascertained by comparative CT method. The primers for CTGF and GAPDH GAPDH were: CTGF forward, 5'- AAT GCT GTG AGG AGT GGG TG-3'; CTGF reverse, 5'- TGG CTC GCA TCA TAG TTG GG-3'; GAPDH forward, 5'- CCA GCC CAG CAA GGA TAC TG-3'; GAPDH reverse, 5'- GGC CCC TCC TGT TGT TAT GG-3'.

5.2.4 Flow cytometry on exosomes

Pooled exosomes were incubated with 1 uL sulfate-aldehyde latex beads (Invitrogen A37304) for 2.5 hr at 37 C, after which 100 mM glycine in 10% goat serum was added to quench the reactive groups and block. Exosome-bead complexes were centrifuged (4,000 x *g*, 5 min) and washed with 1% bovine serum albumin (BSA) in PBS. Complexes were resuspended and incubated with mouse anti-rat CD 1° antibody (BD Biosciences 551808) for 12 hr at 4 °C. Complexes were washed in 1% BSA/PBS and

incubated in Alexa Fluor 488 goat anti-mouse IgG (H+L) antibody (Invitrogen A-11001). After incubation (2 hr at 37 °C), complexes were washed twice and subjected to flow cytometry (BD Biosciences BD LSR II), where at least 50,000 events were collected.

5.2.5 Transmission electron microscopy

Exosome pellets were isolated. The samples were prepared by a negative staining method using 1% phosphotungstic acid. 5 µl of the sample was deposited onto carbon-coated 200 mesh cooper grids that have been treated by glow discharge. After 5 minutes, the grid was dragged on a peiece of filter paper to remove excess liquid on grid. 5 µl of 1% aqueous phosphotungstic acid (PTS, ph6.5) was deposited onto the grid before sample on grid was dried. After 30 seconds, the grid wad dragged on a piece of filter paper to remove the PTA on the grid. In the end, the grid was left to air-dry. The samples were then imaged using the JEOL JEM-140 0 transmission electron microscope.

5.2.6 Cellular uptake of exosomes

Exosomes were stained with calcein (2 uM final concentration) for 30 min at room temperature, followed by two washes in PBS (100,000 x *g*, 70 min). Pellets were then passed through 0.20 um filters. Rat cardiac fibroblasts and endothelial cells were treated with the stained exosomes (1 mg/mL) for 12 hr and washed before being trypsonized and subjected to flow cytometry (Imagestream X Mark II), where 10,000 events were collected. Images were analyzed by Amnis IDEAS image analysis software using spot count and channel intensity wizards.

5.2.7 Tube formation

Rat primary CECs (CellBiologics R2111) were plated on gelatin-coated 12 well plates. Following quiescence for 12 hr, cells were then treated with 0.01, 0.1 and 1

mg/ml hypoxic or normoxic exosomes for 24 hours. The cells were then lifted and counted so that 10,000 cells from each treatment group were plated onto 30 ul Geltrex (Invitrogen A1413202) thick gels in 96-well plates. The cells were then incubated for 6 hours and stained with 2 μM calcein in PBS. Cell groups were imaged with a fluorescent microscope (Olympus IX71) and the tube length was quantified using ImageJ software analysis.

5.2.8 Rat cardiac fibroblast isolation

Excised hearts from adult male Sprague-Dawley rats were minced and subjected to trypsin digestion (1 mg/mL in HBSS-, 4 C, 6 hr), followed by collagenase digestion (0.8 mg/ml in HBSS-, 37 C, 15 min). Digestion solutions were quenched with culture media and cell suspension passed through a 100 um filter. Cells were pelleted and plated for 3 hr to allow adherence of fibroblasts before washing plates to remove non-fibroblasts.

5.2.9 TGF-β stimulation

Fibroblasts were quiesced for 12 hr and treated with 0.1 mg/ml exosome for 12 hr before the addition of TGF-β (2 ng/ml final concentration) for 12 hr. Cell mRNA was isolated via Trizol reagent (Invitrogen 15596-026) according to manufacturer's instructions. cDNA was generated via M-MLV Reverse Transcriptase (Invitrogen 28025-013) and qRT-PCR (Power SYBR Green, Invitrogen 4368708) was performed to evaluate CT levels. Relative expression was calculated using the comparative CT method. The mean minimal cycle threshold values were calculated from triplicate reactions.

5.2.10 Principle component and partial least squares regression analysis

Principle component analysis was applied to normalized miR array data (3 hr or 12 hr generation duration; normoxic or hypoxic conditions) to evaluate data along three principle components. Then Simca-P (UMetrics) software was used to establish relationships between miR levels (signals) responding to cues (exosome generation conditions) and responses (tube formation and connective tissue growth factor (CTGF) mRNA levels). Variable Importance of Projection (VIP) were calculated to determine which signals have the greatest projection/contribution towards a phenotypic outcome. By identifying the VIPs, the number of miRs needed to evaluate was reduced from 378 to 100. A new model was produced by iteration using the same response matrix values. Finally, another PLSR model was created trained on the 7 miRs confirmed by qRT-PCR. Goodness of prediction was tested using a bootstrapping approach; cross-validation was performed by omitting an observation, then using the calculated weighted coefficient matrix to predict response values without those removed observations. This procedure was repeated until every observation had been excluded exactly once. Then predictability was determined using root mean square error between predicted and experimentally observed values.

5.2.11 Statistics

All statistics were prepared with Graphpad Prism software. Results are reported as average±SEM.

5.3 Results

5.3.1 Characterization of isolated exosomes

To verify that hyopoxic and normoxic CPCs release exosomes media was subjected to high-speed centrifugation and exosome fraction was collected. We bound

exosomes to reactive sulfate-aldehyde latex beads and incubated the complexes with antibody against CD9, an exosomal surface marker. Flow cytometry revealed the exosome-bead complexes as CD9+, whereas the negative controls—beads alone and antibody-incubated beads—were negative for CD9 (Figure 5.1 A). Transmission electron microscopy confirmed exosome isolation, with visual confirmation of vesicles with average diameter of 102.0±3.1 nm and 96.1±6.1 nm for exosomes from normoxic or hypoxic exosomes, respectively (Figure 5.1 B). We measured total small RNA and protein levels in exosomes from both hypoxic and normoxic CPCs, and confirmed that total small RNA and protein levels were not different between exosome type (Figure 5.1 C, D).

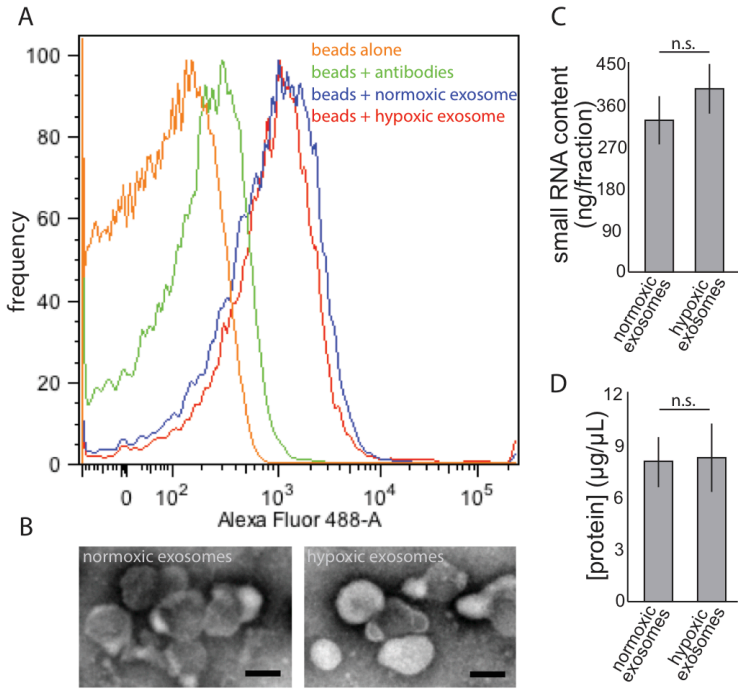

Figure 5.1. Characterization of isolated exosomes. A) Flow cytometry validated presence of CD9+ exosomes. B) Transmission electron microscopy imaged exosomes generated in normoxic and hypoxic conditions (scale bar = 100 nm). No difference was observed in (C) small RNA or (D) protein concentration between exosomes generated in normoxic or hypoxic conditions.

5.3.2 Evaluation of cellular uptake of exosomes

We next determined whether cardiac cell types of interest could internalize exosomes. To test this, we treated cardiac endothelial cells and cardiac fibroblasts with fluorescent calcein-stained exosomes for 12 hr, and imaged cells quantitatively with ImageStream flow cytometry (Figure 5.2 A, B). Internalization of exosomes was confirmed visually by the presence of intracellular punctate fluorescence. In addition, we evaluated if rates of internalization were dependent on exosome type. Analysis of number of spots per cell revealed no difference in uptake between exosomes from hypoxic or normoxic CPCs in either cell type (Figure 5.2 C, D). Furthermore, no difference was observed in average fluorescence intensity per cell between exosome type (Figure 5.2 E, F).

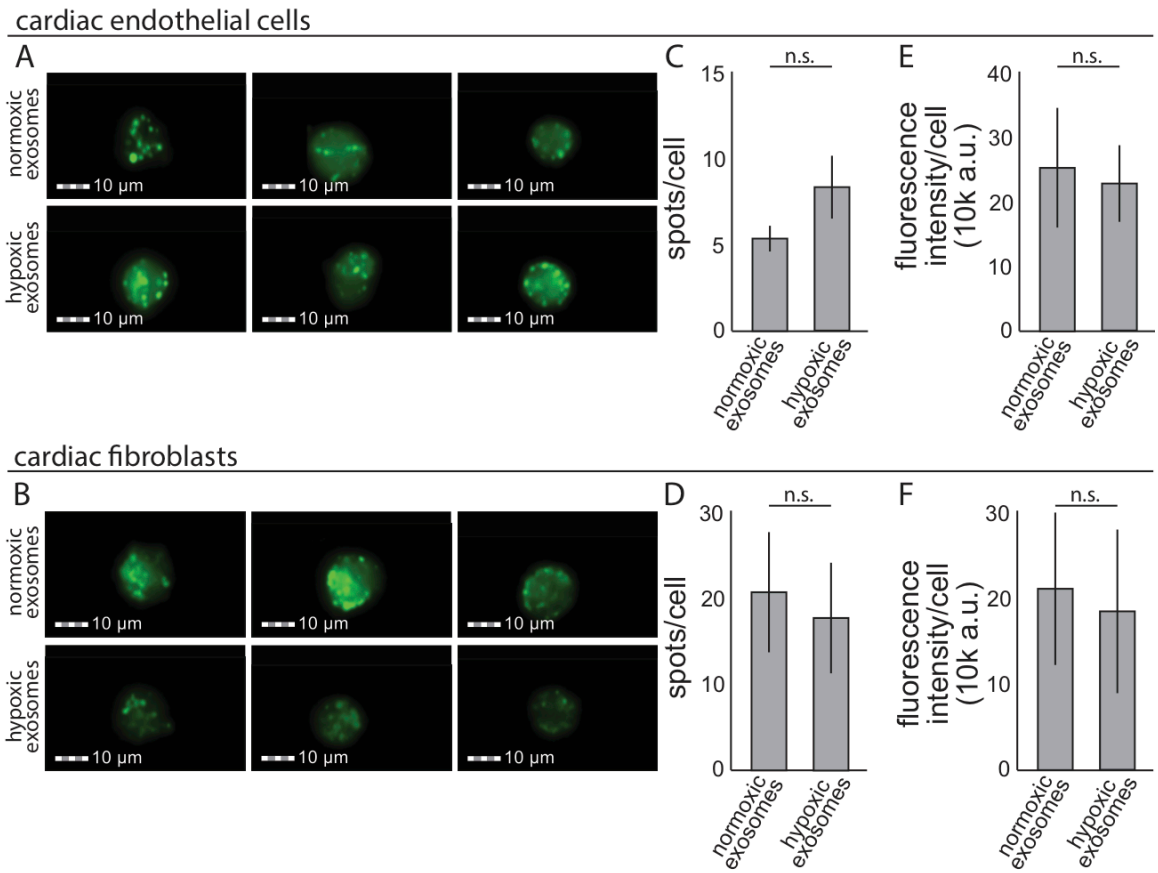

Figure 5.2. Cardiac cells internalize exosomes. Calcein-stained exosomes were internalized by both CECs (A) and fibroblasts (B). There was no difference in uptake of exosomes by either cell type when spots per cell (C, D) or fluorescence intensity per cell (E, F) were analyzed.

5.3.3 Effects of exosomes on endothelial tube formation

We sought to evaluate whether internalization of exosomes could induce endothelial tube formation. Cardiac endothelial cells were treated for 24 hrs with exosomes from hypoxic or normoxic CPCs and then plated on Geltrex prior to imaging (Figure 5.3 A). While exosomes from normoxic CPCs had no significant effect on tube formation, exosomes from hypoxic CPCs significantly enhanced formation of tube-like structures (Figure 5.3 B). This response was dependent on exosome dose, plateauing

at 0.1 mg/mL with a 2.24±0.24-fold increase in tube formation. Disruption of exosomes from hypoxic CPCs via sonication abrogated the effect.

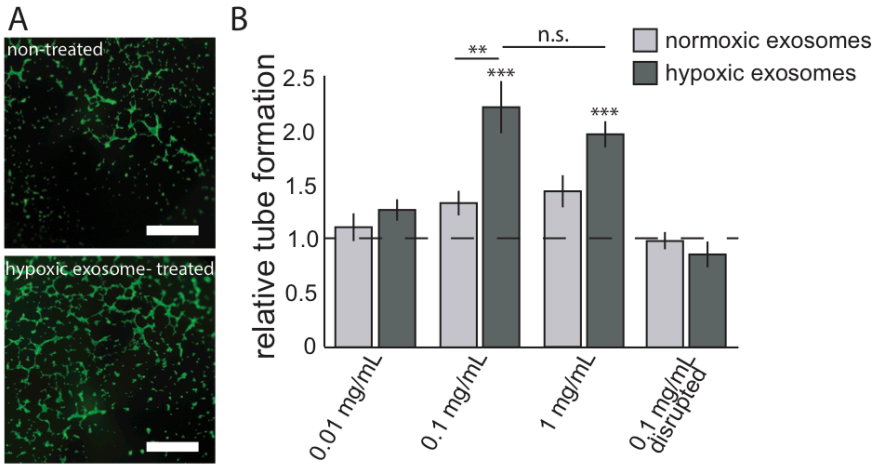

Figure 5.3. Exosomes from hypoxic CPCs enhance endothelial tube formation. Tube-like structures were imaged (A) and quantified (B). While exosomes from normoxic CPCs did not significantly influence tube formation, exosomes caused up to 2.4-fold greater tube formation.

5.3.4 Mitigation of fibroblast stimulation by exosomes

To investigate the potential effects of exosomes on fibrosis, we treated rat cardiac fibroblasts with either exosomes derived from normoxic or hypoxic CPCs prior to stimulation with the TGF-β. Levels of mRNA encoding connective tissue growth factor (CTGF) were determined by qRT-PCR (Figure 5.4). As expected, CTGF mRNA levels increased 3.6±0.28-fold upon TGF-β stimulation. We observed no significant decrease in CTGF mRNA levels in response to treatment with exosomes from normoxic CPCs, but detected a significant decrease in cells treated with hypoxic exosomes to only 2.1±0.14-fold compared to non-treated cells.

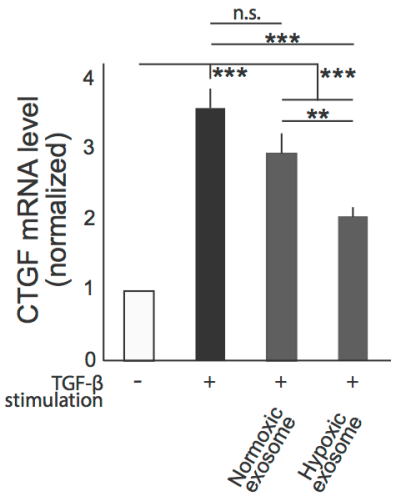

Figure 5.4. Exosomes from hypoxic exosomes mitigated fibroblast stimulation.TGF-β stimulated CTGF mRNA levels, but only hypoxic exosomes decreased CTGF levels.

5.3.5 Evaluation of miR exosome contents

We next evaluated the change in the miR secretome of CPCs in response to hypoxic conditions. We isolated the small RNA fraction of CPC conditioned media (3 and 12 hour, normoxic and hypoxic) and performed Affymetrix GeneChip miR array. We found 11 miRs upregulated 2-fold or more due to hypoxic conditions at the 12 hour time point. Conducting qRT-PCR on the small RNA isolated from pooled exosomes, we validated the upregulation in hypoxic exosomes of seven of the 11 miRs upregulated in hypoxic conditioned media (Figure 5.5 A). Conducting a literature review for these seven miRs and their reported functions revealed correlative and relationships between the miRs and cardiac functions of interest (Figure 5.5 B).

Figure 5.5. Identification and review of upregulated exosomal miRs. A) qRT-PCR identified seven miRs upregulated in exosomes generated by hypoxic CPCs. B) The miRs have been identified to regulate functions of interest, except for miR-292 that has not been explored.

5.3.6 Statistical modeling of exosomal miRs and physiological responses

Principle component analysis was applied to normalized data from the microarray to help group miR that co-vary based on the treatment condition. Exosomes treated with normoxia or hypoxia were examined and their miR levels and fold changes were input into PCA. The first PC clearly separated the fold change differences from the other signals. PC2 was the normoxia/hypoxia axis. However, 4 distinct clusters of miRs were co-variant as shown in Figure 5.6 A.

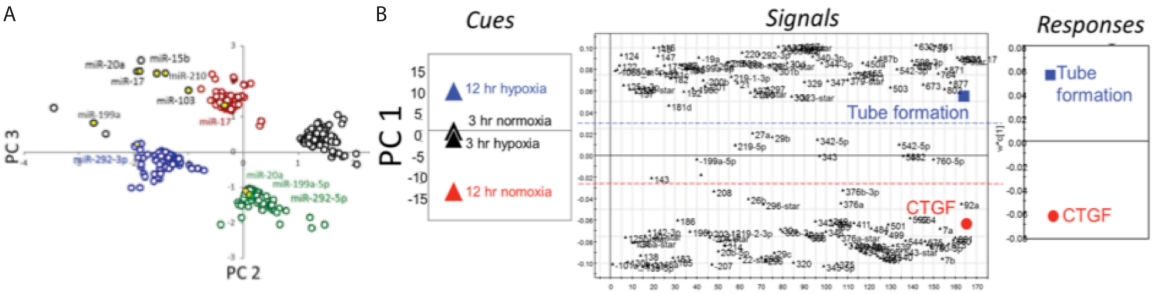

Figure 5.6. PC and PLSR analysis of upregulate miRs and physiological functions. A) PC analysis discovered 4 unique clusters of miR that associate with either hypoxia or normoxia. B) PLSR of 3 or 12 hour hypoxia matched with outputs of tube formation (angiogenesis) and CTGF (fibrosis). Top 100 VIPs were used to make the new model to determine which miRs contributing to one outcome or the other. Clear covariance of 12 hr hypoxia with tube formation and 12 hr normoxia with CTGF.

Using the software Simca-P (UMetrics), PLSR first considered the entire dataset and established a relationship between miR levels as signals responding to the cues of 3 or 12 hr normoxia or hypoxia treatment, and the responses of tube formation, as a surrogate for angiogenesis, and CTGF levels, as a surrogate for fibrosis. Then the VIP (Variable Importance of Projection) were calculated to determine which signals (miRs) have greatest projection/contribution towards a phenotypic outcome. PLSR analysis also can identify the most important miR signals for a response outcome by calculating VIP using a weighted sum of squares of the coefficients calculated for a signal, such that those signals projecting strongly either positively or negatively with either CTGF or tube formation response, are highly ranked. By identifying these VIPs, the amount of data needed to capture and predict a specific response can be reduced from the 378 miR down to the top 100 VIPs, and a new model was made using same response matrix values. Scores plot shows 12 hr hypoxia and 12 hr normoxia plotted on only one principle component (PC) that was calculated (Figure 5.6 B); this was due to these top signals, again projecting most towards the key driving cue, hypoxia vs. normoxia. Clear separation of normoxia and hypoxia in the scores plot match the separation of tube formation and CTGF in the response loadings plot. More, fibrosis (CTGF) co-varies with normoxia cues and tube formation co-varies with hypoxia cues.

A new PLSR model was created trained on the 11 miR confirmed by qRT-PCR from preliminary data discussed in Aim 1 that were matched to physiologically relevant outcomes for cardiac function post-MI (Figure 5.7). Goodness of prediction was tested using a bootstrapping approach; cross-validation was performed by omitting an observation, then using the calculated weighted coefficient matrix to predict response values without those removed observations. This procedure was repeated until every

observation had been excluded exactly once. Then predictability was determined using root mean square error between predicted and experimentally observed values (Figure 5.7 C). For the preliminary dataset, only four outcomes were tested, 12 hr norm CTGF or tube formation and 12 hr hypoxic CTGF or tube formation.

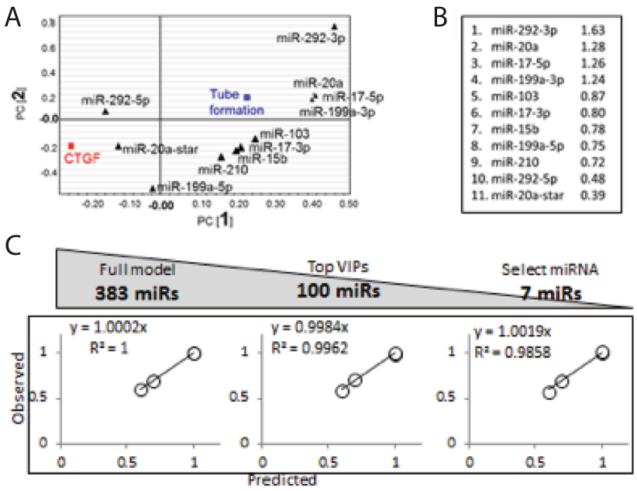

Figure 5.7. Refined PLSR analysis. A) Shows miRs that cluster with a certain function which can then be scored (B) for potential involvement, leading to regression analysis to determine predictability of response based on miR levels.

5.4.7 Validation of statistical modeling

To test the principle component analysis that 3 hr exosomes would have a diminished influence on cellular responses, we treated cardiac endothelial cells with 3 hr normoxic and hypoxic exosomes tested for tube formation (Figure 5.8). We found that, whereas tube formation was significantly increased by hypoxic 12 hr exosomes and not 12 hr normoxic exosomes, the vasculogenic effects were removed in treatment with either 3 hr normoxic or hypoxic exosomes.

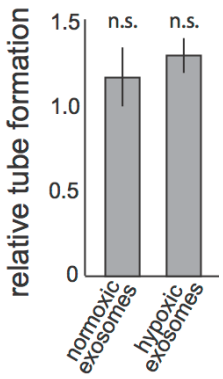

Figure 5.8. Validation of statistical modeling by tube formation. Whereas exosomes generated by hypoxic CPCs in 12 hr improved tube formation, treatment with exosomes generated by either normoxic or hypoxic exosomes in 3 hr yielded no difference.

5.4 Discussion

Myocardial infarction can trigger death in billions of cardiac myocytes, but myocytes are largely non-proliferative and thus the local environment compensates by replacing the cells with non-contractile scar tissue.[120] While this non-contractile tissue provides structural integrity, cardiac function suffers. No definitive treatments exist for MI, and a third of patients will progress toward heart failure.[120] Cell-based therapies in the last decade have demonstrated the benefit of injected stem cells on LV function post-MI.[232-234] However, several major hurdles exist including cell retention, toxic engraftment environment, immunogenicity of transplanted cells, and temporal limitations in expanding autologous cells. Cardiac progenitor cells reside in the heart that may exert a beneficial influence, but their population is too small to substantially protect or repair the heart. Although injected stem and progenitor cells alike may differentiate into functional tissue, many researchers believe that the benefits are due to production of growth factors, cytokines, and other paracrine signals.[138, 235-237] We postulated that substantially amplifying this signal would leverage endogenous reparative mechanisms, while side-stepping hurdles involved with cell-based therapies.

Because CPCs are specialized to function in the heart, CPC-generated exosomes may be well-suited to treat cardiac pathologies. Very few studies have investigated the therapeutic potential of CPC exosomes. In one, the exosomes enhanced endothelial migration, indicating angiogenic effects.[140] In another, CPC exosomes reduced myoblast apoptosis *in vitro* and decreased myocyte cell death in an animal MI model.[141] However, exosomes were generated in normoxic conditions in both of these studies, not hypoxic conditions that may better reflect post-infarct tissue. Hypoxic preconditioning enhanced the benefit of CPC therapy for in an animal MI model,[238] and as such, we hypothesized that CPC exosomes generated in hypoxic conditions would exert greater beneficial effects on cardiac cells (CECs and fibroblasts) than normoxic exosomes. Our findings indicate that hypoxic exosomes indeed benefitted the cells more so than normoxic exosomes, providing foundation for their development as a post-MI therapeutic. Additionally, statistical analysis of the miR exosome components may aid in the development of future bio-inspired therapeutics.

In comparing normoxic and hypoxic exosomes, it was important to evaluate vesicle size, total miR or protein levels, or cell internalization rate as contributing factors in different downstream effects we might observe. All these being similar between the two groups, we ruled out differences in loaded amounts or uptake as causes of physiological response. While we did not evaluate mechanism of uptake, it could be different between the two groups as surface markers may change during hypoxia. We found punctate fluorescence in the cells which is interesting as there is debate whether exosomes deposit their contents by cell membrane fusion or active internalization.[120] Observation of ~1 um spots lent support to the latter and may agree with what other groups have been found, that exosomes are internalized via endocytic pathways and transported to the perinuclear region by the cytoskeleton.[120, 135]

We found that although normoxic exosomes had no effect on tube formation, there was a positive effect of hypoxic exosomes a low treatment levels, but that it plateaued after 0.1 mg/mL. These effects could be due to the increased intra-exosomal levels of pro-angiogenic miR-17[239-241] and -210[242-244]. In fact, miR-210 has been explored as a potential therapeutic for the post-MI heart.[244] Disruption of exosomes by means of sonication abrogated the effect of hypoxic exosomes on tube formation, indicating the need for intact exosomes and not just surface binding of membranes. Exosomes from other cell types and tissues have also been found to induce angiogenesis, though sometimes resulting in pathological states, such as in tumor growth.[130, 138, 245, 246] Additionally, relating to CPC exosomes, one study found that treatment with exosomes enhanced endothelial cell migration in a scratch wound assay.[140] While not measured in the study, our data, along with these supporting data provide support for the angiogenic potential of CPC hypoxic exosomes.

Fibroblasts respond to the remodeling environment during post-period by forming non-contractile scar tissue,[247] and this paired with the extensive cardiomyocyte death and non-proliferation,[120] leads to long-term dysfunction. Further, stimulation of fibroblasts with cytokines such as TGF-b in the damaged myocardium increases production of CTGF, and other factors.[248] We found that our exosomes from hypoxic CPCs significantly decreased CTGF mRNA levels 42% from stimulated levels, while there was no effect of exosomes from normoxic CPCs. Aberrant CTGF expression is associated with cardiovascular disease and involved in fibrotic pathology, exacerbating extracellular matrix production.[249] Studies have shown that deletion of CTGF reduces fibrosis.[250] This decrease could potentially translate to reduced scar formation in vivo, which if combined with improved angiogenesis could lead to replacement of the lost tissue or enhanced survival of the host tissue. The benefit of hypoxia-derived CPC exosomes could be due

to the increased levels of miR-17,[251-253], -199a,[254] -210,[244] and -292,[254] all of which have been demonstrated or predicted to regulate fibrosis.

Cells have been shown to alter the secretion of bioactive molecules in varying conditions, including hypoxia.[214] We examined extracellular miR release following 3 or 12 hours by microarray. Of those upregulated at least 2-fold by hypoxia at the 12 hour time point, we found that of the 11 miRs upregulated, seven were encapsulated by exosomes as confirmed by qRT-PCR. When we conducted a literature search on the upregulated miRs, we found most to regulate cardiac functions. We found that none of our eleven upregulated miRs have been previously discovered to regulate cardiac functions, though the human analog of miR-15b is upregulated in the circulation of patients with critical limb ischemia.[255] These novel findings are therefore extremely useful to the scientific community, as a major development needed in the nascent cardiac exosome field is the characterization of exosomal contents. This will lead to better biomarkers for pathology and more effective therapeutics.

Our array studies generated lots of data that may be difficult to attribute to a specific function. Indeed, we measured over 750 mature miRs and found changes at the 3 and 12 hour time point. To understand these data and potentially identify miR clusters that may regulate function, we employed principle component and partial least squares regression analyses and compared the effects of treatment conditions for exosome generation (cues) on specific miR levels (signals) and eventual physiological responses (tube formation, CTGF mRNA levels). This method served as a statistical instrument to generate a theoretical hypothesis based on empirical data. Whereas the exosomes initially explored for function were produced following 12 hours of normoxia or hypoxia, to generate and validate our model we also produced and examined the secreted miRnome of exosomes generated during 3 hours of hypoxia and normoxia.

We first examined the principle component analysis on the normalized data from the microarray to identify miR clusters that co-vary based on treatment condition. We were surprised to find that the majority of miRs clearly grouped into four major clusters. The black cluster is pro-hypoxic and blue is the opposite. Red and green clusters do not respond to hypoxia (zero projection onto PC2, the hypoxia axis), but are the effects due to another currently unknown mechanism. More interestingly, three of the 11 miRs secreted by CPCs and cluster with three of the groups miR-292 with the blue group, miR-20a with the green group, and mir-17 with the red group, but the others contribute to both oxygen treatment and time component induced cellular responses. This is denoted by the magnitude of their distance from axes of PC2 and PC3.

Our PLSR analysis first evaluated the total miR array results to establish a relationship between signals (individual miR levels) responding to the cues of exosome-generating conditions and the downstream responses. Then the VIP (Variable Importance of Projection) were calculated to determine which signals have greatest projection/contribution towards a phenotypic outcome. We were surprised to observe such clear separation of 12 hr normoxic and hypoxic exosomes in the cues plot, and the clear separation of the tube formation and fibrosis in the response plot as well. More, CTGF mRNA levels co-vary with 12 hr normoxic exosome cues and tube formation co-varies with 12 hr hypoxic exosome cues. Of these top 100 miRs, it can be seen which miRs co-vary with CTGF mRNA and which co-vary with tube formation, that identify which miRs may be targeted for further investigation into these outcomes.

To validate our computational model, we performed tube formation experiments with exosomes from CPCs exposed to hypoxia or normoxia for 3 hours. Whereas the separation of the 12 hour normoxic and hypoxic exosomes in the cues plot was profound, 3 hour exosomes were hardly separated, predicting little difference in their effect on tube formation. When we performed our tube formation experiments with the 3 hour

exosomes, we saw no difference in their effects, validating the PLSR model. Interestingly, the model predicted that had any significant difference been observed, 3 hour normoxic exosomes might have enhanced tube formation, albeit very minor. This is in contrast to the 12 hour exosomes, indicating that CPCs alter the exosome miR load not only as a function of oxygen levels, but also how long the CPCs are subjected to the conditions.

A new PLSR model was created trained on the 11 upregulated miRs identified by microRNA array. This is the benefit of PLSR, in that it allows the reduction of large datasets to smaller, more informative datasets, reducing experimental burden while maintaining integrity and predictability of a dataset. Figure 5.7 reflects that the 11 miRs actually maintain 98% predictability for the outcomes of tube formation and CTGF expression, while the full set of 383 miRs has closer to 100% predictability. Of note is the high scoring of miR-292, predicting its role as highly influential on tube formation and fibrosis. Studies are underway to determine the effects of miR-292 on tube formation and CTGF expression.

In this report we show that CPCs release a beneficial signal in response to hypoxia, but that the population in vivo is likely too small to exert a substantial effect. We confirmed that CPCs secrete exosomes under both normoxic and hypoxic conditions, and that miR content is dynamically regulated based on time as well. Exosomes generated under hypoxic conditions for 12 hours enhanced endothelial tube formation and attenuated CTGF mRNA levels in stimulated fibroblasts, supporting the potential of hypoxia-derived exosomes as a potential therapeutic agent. Based on our results, we developed an empirically derived computational model to determine how exosome-generating conditions, miRs, and physiological responses co-vary. Our findings support the development of hypoxic CPC-derived exosomes as naturally derived therapeutics and lay the groundwork for statistical models that—by characterizing the relationship

among exosome generating conditions, miR regulation, and physiological responses—can lead to bio-inspired therapeutics of rational design.

CHAPTER 6

PERSPECTIVES AND FUTURE DIRECTIONS

6.1 GlcNAc and PCADK particles

Since their development in our collaborating lab in 2006, the pH-sensitive polyketal polymers—of which PCADK is a member—have been explored in a range of therapeutic settings, with the biocompatibility of their degradation products being a key benefit. The polymer has been used to form non-water soluble micro- and nanoparticles and shown to encapsulate small molecules and proteins. However, our study was the first to decorate the surface with ligands to trigger uptake by non-phagocytic cells. Cardiomyocytes internalized the particles for the intracellular delivery of an anti-apoptotic molecule, and we found decreased myocyte death and improved cardiac function in a rat IR model.

Our *in vivo* findings were crucial, as our delivery system addressed the acute phase wherein apoptotic pathways are triggered immediately during and after MI. However, long-term effects of our novel system would be important to explore. We may find that decreased myocyte death leads to a reduced pressure overload and less fibrotic scarring. Additionally, an influx of the phagocytic macrophages presents another opportunity; that a combination of delivery of these PK-GlcNAc-SB particles to both moycytes and macrophages could create a synergestic effect to attenuate cardiac dysregulation. Another application of PK-GlcNAc particles worth exploring is the delivery of cell-impermeant proteins to CMs, as this would open delivery of a large class of protective proteins to ischemic myocytes.

Recent findings out of a research lab at University of Louisville has demonstrated the cardioprotective effects of GlcNAc on CMs[256] and CPCs[257], potentially enhancing the therapeutic effects of GlcNAc-presenting delivery systems. In fact, one of our collaborators has been evaluating the regenerative potential of empty PK-GlcNAc particles. Since the completion of our work as it currently stands, nine research articles have been published on polyketal particles,[258-265] indicating the increasing interest in the scientific community on these particles as delivery vehicles.

6.2 Regio-selectively decorated dendrimers

We found that our RGD-bowtie effectively transfected cells with miR by enhancing angiogenesis, increasing cell proliferation. Importantly, our dendrimeric vehicle did not exhibit cytotoxicity, an effect that many dendrimers elicit. Depending on application, cellular toxicity may be a benefit or undesirable, but as we aim to create a pro-regenerative environment, toxicity would be deleterious.

Our finding that different materials elicit different responses is not entirely surprising; the processes between internalization of miR-loaded vehicles and cell proliferation or tube formation is complex and may be perturbed by various material features. In addition to tuning vehicle design for desired extracellular interactions and uptake, investigation of the intracellular interactions and subsequent effects are essential in the development of effective transfection vehicles. The bowtie template affords a wide range of possibilities for tuning parameters and properties, such as ligand and charge densities, dendron size, and incorporation of other specialized bioactive groups (e.g., aptamers, saccharides, and antibodies).[14] In turn, these design alterations may influence binding avidity and specificity, multivalent interactions, cargo capacity, cytotoxicity, endosomal escape, immunogenicity, and stability. Keeping these research considerations in mind, we plan on further developing our bowtie structure in the near

term by increasing RGD peptide density on RGD-bowtie and N/P ratio to further enhance transfection. In the long term, we will characterize uptake kinetics in relation to ligand density and dendrimer size, examine the electrostatic binding and loading of miR to the cationic region of the bowtie, and investigate bowtie modification with other ligands to enhance uptake and cell specificity.

In *in vivo* application, a single dose of the dendrimer bowtie may transfect the cells in the acute phase. However, should the infarct become reperfused, the small size and solubility of these dendrimers may allow their clearance. A strategy for prolonged treatment may be loading the bowties into a hydrogel for sustained delivery and regional retention.

6.3 Exosomes and the heart

Previous findings have shown the benefit of the secretome of CPCs in treating the MI heart, but ours was the first to study how exosomes generated in hypoxic conditions—that mimic ischemia—might affect the physiology of cardiac cells. We found them to improve the tube formation of cardiac endothelial cells and reduce fibrotic mRNA in cardiac fibroblasts. This may have the effects of enhancing blood flow to the infarct and reducing non-contractile scar formation. Additionally, we found several miRs to be upregulated in hypoxic exosomes. While we correlated upregulated exosomal miRs with beneficial cellular effects, we have yet to show causation. To do so, our plans in the near future include inhibiting the ribonucleic acid-induced silencing complex (RISC) and observing reducing impact of hypoxic exosomes. Additionally, as our study postulated a role of miR-292 (that has heretofore been unexplored), we will repeat our cell experiments with co-transfection of anti-mir-292.

Our statistical modeling has provided insight into future bio-inspired therapeutics. With the knowledge that CPCs produce exosomes that may be internalized by cardiac

cells, engineering of these exosomes with miR cocktails may allow for tuned therapies. PC analysis identified miRs that co-varied and predicted their function. Creating a CPC line that overexpressed a desired miR cassette, and generating exosomes from the line may be one route for future therapies.

The field of cardiac exosomes is in its infancy, and several broad questions remain to be answered, some of which we have attempted to address in part. Namely, how does the myocardium initiate the local repair process? Are exosomes shuttles for unwanted material, or cell-cell communicators? Do secreted exosomes from the heart have any physiological function? Do secreted cardiac exosomes function in autocrine, paracrine, or endocrine signaling, or a combination? If one of their roles is endocrine, then could they be recruiting cells, such as bone marrow, to the infarct and conditioning them en route? Research efforts to answer these questions will yield a greater understanding of the heart and provide for development of naturally derived therapies that leverage endogenous mechanisms.

REFERENCES

1. Morbidity & mortality: 2012 chart book on cardiovascular, lung, and blood diseases. Health NIo. 2012.

2. Maulik N, Yoshida T, Das D. Oxidative stress developed during the reperfusion of ischemic myocardium induces apoptosis. *Free Radical Biology and Medicine*. 1998;24:869-875

3. Bialik S, Geenen D, Sasson I, Cheng R, Horner J, Evans S, Lord E, Koch C, Kitsis R. Myocyte apoptosis during acute myocardial infarction in the mouse localizes to hypoxic regions but occurs independently of p53. *Journal of Clinical Investigation*. 1997;100:1363

4. McGill CJ, Brooks G. Cell cycle control mechanisms and their role in cardiac growth. *Cardiovascular research*. 1995;30:557-569

5. Kajstura J, Leri A, Finato N, Di Loreto C, Beltrami C, Anversa P. Myocyte proliferation in end-stage cardiac failure in humans. *Proceedings of the National Academy of Sciences of the United States of America*. 1998;95:8801

6. Garg S, Narula J, Chandrashekhar Y. Apoptosis and heart failure: Clinical relevance and therapeutic target. *Journal of Molecular and Cellular Cardiology*. 2005;38:73-79

7. Buja LM, Vela D. Cardiomyocyte death and renewal in the normal and diseased heart. *Cardiovascular Pathology*. 2008:1-26

8. Hockenbery DM, Oltvai ZN, Yin XM, Milliman CL, Korsmeyer SJ. Bcl-2 functions in an antioxidant pathway to prevent apoptosis. *Cell*. 1993;75:241-251

9. Maulik N, Yoshida T, Das DK. Oxidative stress developed during the reperfusion of ischemic myocardium induces apoptosis. *Free radical biology & medicine*. 1998;24:869-875

10. Huang J, Ito Y, Morikawa M, Uchida H, Kobune M, Sasaki K, Abe T, Hamada H. Bcl-xl gene transfer protects the heart against ischemia/reperfusion injury. *Biochemical and Biophysical Research Communications*. 2003;311:64-70

11. Potts MB. Reduced apaf-1 levels in cardiomyocytes engage strict regulation of apoptosis by endogenous xiap. *The Journal of Cell Biology*. 2005;171:925-930

12. Khaper N, Kaur K, Li T, Farahmand F, Singal P. Antioxidant enzyme gene expression in congestive heart failure following mycardial infarction. *Molecular and Cellular Biochemistry*. 2003;251:9-15

13. Broderick JA, Zamore PD. Microrna therapeutics. *Gene Therapy*. 2011;18:1104-1110

14. Peer D, Lieberman J. Special delivery: Targeted therapy with small rnas. *Gene Therapy*. 2011;18:1127-1133

15. Fichtlscherer S, Zeiher AM, Dimmeler S. Circulating microrna: Biomarkers or mediators of cardiovascular diseases? *Arteriosclerosis, Thrombosis, and Vascular Biology*. 2011;31:2383-2390

16. Liu N, Olson E. Microrna regulatory networks in cardiovascular development. *Developmental Cell*. 2010;18:510-525

17. Yue J. Mirna and vascular cell movement. *Advanced Drug Delivery Reviews*. 2011;63:616-622

18. Chen Z, Chua CC, Ho YS, Hamdy RC, Chua BHL. Overexpression of bcl-2 attenuates apoptosis and protects against myocardial i/r injury in transgenic mice. *American Journal of Physiology-Heart and Circulatory Physiology*. 2001;280:H2313

19. Chen Z, Siu B, Ho YS, Vincent R, Chua CC, Hamdy RC, Chua BHL. Overexpression of mnsod protects against myocardial ischemia/reperfusion injury in transgenic mice. *Journal of Molecular and Cellular Cardiology*. 1998;30:2281-2289

20. Harris JM, Chess RB. Effect of pegylation on pharmaceuticals. *Nature Reviews Drug Discovery*. 2003;2:214-221

21. Hsieh PCH, Davis ME, Gannon J, MacGillivray C, Lee RT. Controlled delivery of pdgf-bb for myocardial protection using injectable self-assembling peptide nanofibers. *Journal of Clinical Investigation*. 2006;116:237-248

22. Lee S, Murthy N. Targeted delivery of catalase and superoxide dismutase to macrophages using folate. *Biochemical and Biophysical Research Communications*. 2007;360:275-279

23. Sutton MG, Sharpe N. Left ventricular remodeling after myocardial infarction: Pathophysiology and therapy. *Circulation*. 2000;101:2981

24. Aso S, Ise H, Takahashi M, Kobayashi S, Morimoto H, Izawa A, Goto M, Ikeda U. Effective uptake of n-acetylglucosamine-conjugated liposomes by cardiomyocytes in vitro. *Journal of Controlled Release*. 2007;122:189-198

25. Ise H, Kobayashi S, Goto M, Sato T, Kawakubo M, Takahashi M, Ikeda U, Akaike T. Vimentin and desmin possess glcnac-binding lectin-like properties on cell surfaces. *Glycobiology*. 2010;20:843

26. Nam HY, Nam K, Lee M, Kim SW, Bull DA. Dendrimer type bio-reducible polymer for efficient gene delivery. *Journal of Controlled Release*. 2012;160:592-600

27. Behlke MA. Chemical modification of sirnas for in vivo use. *Oligonucleotides*. 2008;18:305-319

28. Yan Y, Such GK, Johnston AP, Best JP, Caruso F. Engineering particles for therapeutic delivery: Prospects and challenges. *ACS nano*. 2012;6:3663-3669

29. Shive MS, Anderson JM. Biodegradation and biocompatibility of pla and plga microspheres. *Advanced drug delivery reviews*. 1997;28:5-24

30. Lee S, Yang SC, Heffernan MJ, Taylor WR, Murthy N. Polyketal microparticles: A new delivery vehicle for superoxide dismutase. *Bioconjugate Chemistry*. 2007;18:4-7

31. Sy J, Phelps E, García A, Murthy N, Davis M. Surface functionalization of polyketal microparticles with nitrilotriacetic acid-nickel complexes for efficient protein capture and delivery. *Biomaterials*. 2010;31:4987-4994

32. Sy J, Seshadri G, Yang S, Brown M, Oh T, Dikalov S, Murthy N, Davis M. Sustained release of a p38 inhibitor from non-inflammatory microspheres inhibits cardiac dysfunction. *Nature Materials*. 2008;7:863-868

33. Astruc D, Boisselier E, Ornelas C. Dendrimers designed for functions: From physical, photophysical, and supramolecular properties to applications in sensing, catalysis, molecular electronics, photonics, and nanomedicine. *Chemical Reviews (Washington, DC, United States)*. 2010;110:1857-1959

34. Liu J, Gray WD, Davis ME, Luo Y. Peptide- and saccharide-conjugated dendrimers for targeted drug delivery: A concise review. *Interface focus*. 2012;2:307-324

35. Soliman G, Sharma A, Maysinger D, Kakkar A. Dendrimers and miktoarm polymers based multivalent nanocarriers for efficient and targeted drug delivery. *Chemical Communications (Cambridge, United Kingdom)*. 2011;47:9572-9587

36. Jain K, Kesharwani P, Gupta U, Jain N. Dendrimer toxicity: Let's meet the challenge. *International Journal of Pharmaceutics*. 2010;394:122-142

37. Kang H, DeLong R, Fisher M, Juliano R. Tat-conjugated pamam dendrimers as delivery agents for antisense and sirna oligonucleotides. *Pharmaceutical Research*. 2005;22:2099-2106

38. Liu J, Zhou J, Luo Y. Sirna delivery systems based on neutral cross-linked dendrimers. *Bioconjugate Chemistry*. 2012;23:174-183

39. Hong S, Leroueil PR, Majoros IJ, Orr BG, Baker JR, Banaszak Holl MM. The binding avidity of a nanoparticle-based multivalent targeted drug delivery platform. *Chemistry & Biology (Cambridge, MA, United States)*. 2007;14:107-115

40. Waite CL, Roth CM. Binding and transport of pamam-rgd in a tumor spheroid model: The effect of rgd targeting ligand density. *Biotechnology and bioengineering*. 2011;108:2999-3008

41. Beltrami AP, Barlucchi L, Torella D, Baker M, Limana F, Chimenti S, Kasahara H, Rota M, Musso E, Urbanek K, Leri A, Kajstura J, Nadal-Ginard B, Anversa P.

Adult cardiac stem cells are multipotent and support myocardial regeneration. *Cell*. 2003;114:763-776

42. Kattman SJ, Huber TL, Keller GM. Multipotent flk-1+ cardiovascular progenitor cells give rise to the cardiomyocyte, endothelial, and vascular smooth muscle lineages. *Dev Cell*. 2006;11:723-732

43. Linke A, Muller P, Nurzynska D, Casarsa C, Torella D, Nascimbene A, Castaldo C, Cascapera S, Bohm M, Quaini F, Urbanek K, Leri A, Hintze TH, Kajstura J, Anversa P. Stem cells in the dog heart are self-renewing, clonogenic, and multipotent and regenerate infarcted myocardium, improving cardiac function. *Proceedings of the National Academy of Sciences of the United States of America*. 2005;102:8966-8971

44. Assmus B, Schachinger V, Teupe C, Britten M, Lehmann R, Dobert N, Grunwald F, Aicher A, Urbich C, Martin H, Hoelzer D, Dimmeler S, Zeiher AM. Transplantation of progenitor cells and regeneration enhancement in acute myocardial infarction (topcare-ami). *Circulation*. 2002;106:3009-3017

45. Wollert KC, Meyer GP, Lotz J, Ringes-Lichtenberg S, Lippolt P, Breidenbach C, Fichtner S, Korte T, Hornig B, Messinger D, Arseniev L, Hertenstein B, Ganser A, Drexler H. Intracoronary autologous bone-marrow cell transfer after myocardial infarction: The boost randomised controlled clinical trial. *Lancet*. 2004;364:141-148

46. Timmers L, Lim SK, Arslan F, Armstrong JS, Hoefer IE, Doevendans PA, Piek JJ, El Oakley RM, Choo A, Lee CN, Pasterkamp G, de Kleijn DP. Reduction of myocardial infarct size by human mesenchymal stem cell conditioned medium. *Stem cell research*. 2007;1:129-137

47. Timmers L, Lim SK, Hoefer IE, Arslan F, Lai RC, van Oorschot AA, Goumans MJ, Strijder C, Sze SK, Choo A, Piek JJ, Doevendans PA, Pasterkamp G, de Kleijn DP. Human mesenchymal stem cell-conditioned medium improves cardiac function following myocardial infarction. *Stem cell research*. 2011;6:206-214

48. Lai RC, Arslan F, Lee MM, Sze NS, Choo A, Chen TS, Salto-Tellez M, Timmers L, Lee CN, El Oakley RM, Pasterkamp G, de Kleijn DP, Lim SK. Exosome secreted by msc reduces myocardial ischemia/reperfusion injury. *Stem cell research*. 2010;4:214-222

49. Go AS, Mozaffarian D, Roger VL, Benjamin EJ, Berry JD, Blaha MJ, Dai S, Ford ES, Fox CS, Franco S, Fullerton HJ, Gillespie C, Hailpern SM, Heit JA, Howard VJ, Huffman MD, Judd SE, Kissela BM, Kittner SJ, Lackland DT, Lichtman JH, Lisabeth LD, Mackey RH, Magid DJ, Marcus GM, Marelli A, Matchar DB, McGuire DK, Mohler ER, 3rd, Moy CS, Mussolino ME, Neumar RW, Nichol G, Pandey DK, Paynter NP, Reeves MJ, Sorlie PD, Stein J, Towfighi A, Turan TN, Virani SS, Wong ND, Woo D, Turner MB. Heart disease and stroke statistics--2014 update: A report from the american heart association. *Circ*. 2014;129:e28-e292

50. Woollard KJ, Geissmann F. Monocytes in atherosclerosis: Subsets and functions. *Nature reviews. Cardiology*. 2010;7:77-86

51. Thygesen K, Alpert JS, White HD. Universal definition of myocardial infarction. *Journal of the American College of Cardiology*. 2007;50:2173-2195

52. Alpert JS, Thygesen K, Antman E, Bassand JP. Myocardial infarction redefined--a consensus document of the joint european society of cardiology/american college of cardiology committee for the redefinition of myocardial infarction. *Journal of the American College of Cardiology*. 2000;36:959-969

53. French JK, White HD. Clinical implications of the new definition of myocardial infarction. *Heart*. 2004;90:99-106

54. Jaffe AS, Babuin L, Apple FS. Biomarkers in acute cardiac disease: The present and the future. *Journal of the American College of Cardiology*. 2006;48:1-11

55. Jaffe AS, Ravkilde J, Roberts R, Naslund U, Apple FS, Galvani M, Katus H. It's time for a change to a troponin standard. *Circulation*. 2000;102:1216-1220

56. Muller JE, Stone PH, Turi ZG, Rutherford JD, Czeisler CA, Parker C, Poole WK, Passamani E, Roberts R, Robertson T, et al. Circadian variation in the frequency of onset of acute myocardial infarction. *The New England journal of medicine*. 1985;313:1315-1322

57. Moe KT, Wong P. Current trends in diagnostic biomarkers of acute coronary syndrome. *Annals of the Academy of Medicine, Singapore*. 2010;39:210-215

58. Isbell DC, Kramer CM. Cardiovascular magnetic resonance: Structure, function, perfusion, and viability. *Journal of nuclear cardiology : official publication of the American Society of Nuclear Cardiology*. 2005;12:324-336

59. Krijnen PA, Nijmeijer R, Meijer CJ, Visser CA, Hack CE, Niessen HW. Apoptosis in myocardial ischaemia and infarction. *Journal of clinical pathology*. 2002;55:801-811

60. Pearson TA, Mensah GA, Alexander RW, Anderson JL, Cannon RO, 3rd, Criqui M, Fadl YY, Fortmann SP, Hong Y, Myers GL, Rifai N, Smith SC, Jr., Taubert K, Tracy RP, Vinicor F. Markers of inflammation and cardiovascular disease: Application to clinical and public health practice: A statement for healthcare professionals from the centers for disease control and prevention and the american heart association. *Circulation*. 2003;107:499-511

61. Pack D, Putnam D, Langer R. Design of imidazole-containing endosomolytic biopolymers for gene delivery. *Biotechnology and Bioengineering*. 2000;67:217-223

62. Murthy N, Robichaud J, Tirrell D, Stayton P, Hoffman A. The design and synthesis of polymers for eukaryotic membrane disruption. *Journal of Controlled Release*. 1999;61:137-143

63. Stayton P, Hoffman A, Murthy N, Lackey C, Cheung C, Tan P, Klumb L, Chilkoti A, Wilbur F, Press O. Molecular engineering of proteins and polymers for targeting and intracellular delivery of therapeutics. *Journal of Controlled Release*. 2000;65:203-220

64. Kyriakides T, Cheung C, Murthy N, Bornstein P, Stayton P, Hoffman A. Ph-sensitive polymers that enhance intracellular drug delivery in vivo. *Journal of Controlled Release*. 2002;78:295-303

65. Pack D, Hoffman A, Pun S, Stayton P. Design and development of polymers for gene delivery. *Nature Reviews Drug Discovery*. 2005;4:581-593

66. Murthy N, Campbell J, Fausto N, Hoffman AS, Stayton PS. Design and synthesis of ph-responsive polymeric carriers that target uptake and enhance the intracellular delivery of oligonucleotides. *J Control Release*. 2003;89:365-374

67. Gillies E, Goodwin A, Fréchet J. Acetals as ph-sensitive linkages for drug delivery. *Bioconjugate Chem*. 2004;15:1254-1263

68. Chu C, Szoka F. Ph-sensitive liposomes. *Journal of Liposome Research*. 1994;4:361-395

69. Guo X, Szoka Jr F. Chemical approaches to triggerable lipid vesicles for drug and gene delivery. *Acc. Chem. Res*. 2003;36:335-341

70. Song J, Hollingsworth R. Synthesis, conformational analysis, and phase characterization of a versatile self-assembling monoglucosyl diacylglycerol analog. *J. Am. Chem. Soc*. 1999;121:1851-1861

71. Wong JB, Grosse S, Tabor AB, Hart SL, Hailes HC. Acid cleavable peg-lipids for applications in a ternary gene delivery vector. *Mol Biosyst*. 2008;4:532-541

72. Gopferich A. Mechanisms of polymer degradation and erosion. *Biomaterials*. 1996;17:103-114

73. Zhu J, Munn R, Nantz M. Self-cleaving ortho ester lipids: A new class of ph-vulnerable amphiphiles. *J. Am. Chem. Soc*. 2000;122:2645-2646

74. Guo X, Szoka FC, Jr. Steric stabilization of fusogenic liposomes by a low-ph sensitive peg--diortho ester--lipid conjugate. *Bioconjug Chem*. 2001;12:291-300

75. Murthy N, Campbell J, Fausto N, Hoffman AS, Stayton PS. Bioinspired ph-responsive polymers for the intracellular delivery of biomolecular drugs. *Bioconjug Chem*. 2003;14:412-419

76. Murthy N, Thng Y, Schuck S, Xu M, Frechet J. A novel strategy for encapsulation and release of proteins: Hydrogels and microgels with acid-labile acetal cross-linkers. *J. Am. Chem. Soc*. 2002;124:12398-12399

77. Knorr V, Allmendinger L, Walker GF, Paintner FF, Wagner E. An acetal-based pegylation reagent for ph-sensitive shielding of DNA polyplexes. *Bioconjug Chem*. 2007;18:1218-1225

78. Supattapone S, Nguyen HO, Cohen FE, Prusiner SB, Scott MR. Elimination of prions by branched polyamines and implications for therapeutics. *Proceedings of the National Academy of Sciences of the United States of America*. 1999;96:14529-14534

79. Soto C, Kascsak RJ, Saborio GP, Aucouturier P, Wisniewski T, Prelli F, Kascsak R, Mendez E, Harris DA, Ironside J, Tagliavini F, Carp RI, Frangione B. Reversion of prion protein conformational changes by synthetic beta-sheet breaker peptides. *Lancet*. 2000;355:192-197

80. Pini A, Giuliani A, Falciani C, Runci Y, Ricci C, Lelli B, Malossi M, Neri P, Rossolini GM, Bracci L. Antimicrobial activity of novel dendrimeric peptides obtained by phage display selection and rational modification. *Antimicrobial agents and chemotherapy*. 2005;49:2665-2672

81. Bourne N, Stanberry LR, Kern ER, Holan G, Matthews B, Bernstein DI. Dendrimers, a new class of candidate topical microbicides with activity against herpes simplex virus infection. *Antimicrobial agents and chemotherapy*. 2000;44:2471-2474

82. Chen X, Tam UC, Czlapinski JL, Lee GS, Rabuka D, Zettl A, Bertozzi CR. Interfacing carbon nanotubes with living cells. *Journal of the American Chemical Society*. 2006;128:6292-6293

83. Chen X, Wu P, Rousseas M, Okawa D, Gartner Z, Zettl A, Bertozzi CR. Boron nitride nanotubes are noncytotoxic and can be functionalized for interaction with proteins and cells. *Journal of the American Chemical Society*. 2009;131:890-891

84. Liu Z, Sun X, Nakayama-Ratchford N, Dai H. Supramolecular chemistry on water-soluble carbon nanotubes for drug loading and delivery. *ACS nano*. 2007;1:50-56

85. Sakai T, Alexandridis P. Mechanism of gold metal ion reduction, nanoparticle growth and size control in aqueous amphiphilic block copolymer solutions at ambient conditions. *The journal of physical chemistry. B*. 2005;109:7766-7777

86. Li Z, Huang P, Zhang X, Lin J, Yang S, Liu B, Gao F, Xi P, Ren Q, Cui D. Rgd-conjugated dendrimer-modified gold nanorods for in vivo tumor targeting and photothermal therapy. *Mol Pharm*. 2010;7:94-104

87. Martin AL, Li B, Gillies ER. Surface functionalization of nanomaterials with dendritic groups: Toward enhanced binding to biological targets. *Journal of the American Chemical Society*. 2009;131:734-741

88. Pan B, Cui D, Sheng Y, Ozkan C, Gao F, He R, Li Q, Xu P, Huang T. Dendrimer-modified magnetic nanoparticles enhance efficiency of gene delivery system. *Cancer research*. 2007;67:8156-8163

89. Ghosh S, Saha A. Synthesis and spectral studies of cdte-dendrimer conjugates. *Nanoscale research letters*. 2009;4:937-941

90. Svenson S. Dendrimers as versatile platform in drug delivery applications. *European journal of pharmaceutics and biopharmaceutics : official journal of Arbeitsgemeinschaft fur Pharmazeutische Verfahrenstechnik e.V*. 2009;71:445-462

91. Zhou Y, Guo Z, Zhang Y, Huang W, Zhou Y, Yan D. Hyperbranched polyamidoamines containing beta-cyclodextrin for controlled release of chlorambucil. *Macromolecular bioscience*. 2009;9:1090-1097

92. Kihara F, Arima H, Tsutsumi T, Hirayama F, Uekama K. In vitro and in vivo gene transfer by an optimized alpha-cyclodextrin conjugate with polyamidoamine dendrimer. *Bioconjug Chem*. 2003;14:342-350

93. Pasqualini R, Koivunen E, Ruoslahti E. Alpha v integrins as receptors for tumor targeting by circulating ligands. *Nat Biotechnol*. 1997;15:542-546

94. Shukla R, Thomas TP, Peters J, Kotlyar A, Myc A, Baker Jr JR. Tumor angiogenic vasculature targeting with pamam dendrimer-rgd conjugates. *Chem Commun (Camb)*. 2005:5739-5741

95. Dijkgraaf I, Rijnders AY, Soede A, Dechesne AC, van Esse GW, Brouwer AJ, Corstens FH, Boerman OC, Rijkers DT, Liskamp RM. Synthesis of dota-conjugated multivalent cyclic-rgd peptide dendrimers via 1,3-dipolar cycloaddition and their biological evaluation: Implications for tumor targeting and tumor imaging purposes. *Organic & biomolecular chemistry*. 2007;5:935-944

96. Boswell CA, Eck PK, Regino CA, Bernardo M, Wong KJ, Milenic DE, Choyke PL, Brechbiel MW. Synthesis, characterization, and biological evaluation of integrin alphavbeta3-targeted pamam dendrimers. *Molecular pharmaceutics*. 2008;5:527-539

97. Wood KC, Azarin SM, Arap W, Pasqualini R, Langer R, Hammond PT. Tumor-targeted gene delivery using molecularly engineered hybrid polymers functionalized with a tumor-homing peptide. *Bioconjug Chem*. 2008;19:403-405

98. Liu J, Liu J, Chu L, Wang Y, Duan Y, Feng L, Yang C, Wang L, Kong D. Novel peptide-dendrimer conjugates as drug carriers for targeting nonsmall cell lung cancer. *International journal of nanomedicine*. 2011;6:59-69

99. Lempens EH, Merkx M, Tirrell M, Meijer EW. Dendrimer display of tumor-homing peptides. *Bioconjugate Chemistry*. 2011;22:397-405

100. Barrett GL, Trieu J, Naim T. The identification of leptin-derived peptides that are taken up by the brain. *Regul Pept*. 2009;155:55-61

101. Liu HL, Hua MY, Yang HW, Huang CY, Chu PC, Wu JS, Tseng IC, Wang JJ, Yen TC, Chen PY, Wei KC. Magnetic resonance monitoring of focused ultrasound/magnetic nanoparticle targeting delivery of therapeutic agents to the

brain. *Proceedings of the National Academy of Sciences of the United States of America*. 2010;107:15205-15210

102. Benito JM, Gomez-Garcia M, Ortiz Mellet C, Baussanne I, Defaye J, Garcia Fernandez JM. Optimizing saccharide-directed molecular delivery to biological receptors: Design, synthesis, and biological evaluation of glycodendrimer-cyclodextrin conjugates. *Journal of the American Chemical Society*. 2004;126:10355-10363

103. Arima H, Chihara Y, Arizono M, Yamashita S, Wada K, Hirayama F, Uekama K. Enhancement of gene transfer activity mediated by mannosylated dendrimer/alpha-cyclodextrin conjugate (generation 3, g3). *J Control Release*. 2006;116:64-74

104. Wu P, Chen X, Hu N, Tam UC, Blixt O, Zettl A, Bertozzi CR. Biocompatible carbon nanotubes generated by functionalization with glycodendrimers. *Angew Chem Int Ed Engl*. 2008;47:5022-5025

105. Medina SH, Tekumalla V, Chevliakov MV, Shewach DS, Ensminger WD, El-Sayed ME. N-acetylgalactosamine-functionalized dendrimers as hepatic cancer cell-targeted carriers. *Biomaterials*. 2011;32:4118-4129

106. Kobayashi H, Brechbiel MW. Nano-sized mri contrast agents with dendrimer cores. *Advanced Drug Delivery Reviews*. 2005;57:2271-2286

107. Sato N, Kobayashi H, Hiraga A, Saga T, Togashi K, Konishi J, Brechbiel MW. Pharmacokinetics and enhancement patterns of macromolecular mr contrast agents with various sizes of polyamidoamine dendrimer cores. *Magn Reson Med*. 2001;46:1169-1173

108. Liu J, Zhou J, Luo Y. Sirna delivery systems based on neutral cross-linked dendrimers. *Bioconjug Chem*. 2012;23:174-183

109. Han L, Zhang A, Wang H, Pu P, Jiang X, Kang C, Chang J. Tat-bmps-pamam conjugates enhance therapeutic effect of small interference rna on u251 glioma cells in vitro and in vivo. *Human gene therapy*. 2010;21:417-426

110. Demeule M, Currie JC, Bertrand Y, Che C, Nguyen T, Regina A, Gabathuler R, Castaigne JP, Beliveau R. Involvement of the low-density lipoprotein receptor-related protein in the transcytosis of the brain delivery vector angiopep-2. *J Neurochem*. 2008;106:1534-1544

111. Ke W, Shao K, Huang R, Han L, Liu Y, Li J, Kuang Y, Ye L, Lou J, Jiang C. Gene delivery targeted to the brain using an angiopep-conjugated polyethyleneglycol-modified polyamidoamine dendrimer. *Biomaterials*. 2009;30:6976-6985

112. Huang S, Li J, Han L, Liu S, Ma H, Huang R, Jiang C. Dual targeting effect of angiopep-2-modified, DNA-loaded nanoparticles for glioma. *Biomaterials*. 2011;32:6832-6838

113. Darbre T, Reymond JL. Glycopeptide dendrimers for biomedical applications. *Current topics in medicinal chemistry*. 2008;8:1286-1293

114. Lagnoux D, Darbre T, Schmitz ML, Reymond JL. Inhibition of mitosis by glycopeptide dendrimer conjugates of colchicine. *Chemistry*. 2005;11:3941-3950

115. Agrawal P, Gupta U, Jain NK. Glycoconjugated peptide dendrimers-based nanoparticulate system for the delivery of chloroquine phosphate. *Biomaterials*. 2007;28:3349-3359

116. Bhadra D, Yadav AK, Bhadra S, Jain NK. Glycodendrimeric nanoparticulate carriers of primaquine phosphate for liver targeting. *International journal of pharmaceutics*. 2005;295:221-233

117. Sebestik J, Niederhafner P, Jezek J. Peptide and glycopeptide dendrimers and analogous dendrimeric structures and their biomedical applications. *Amino acids*. 2011;40:301-370

118. Comelli EM, Head SR, Gilmartin T, Whisenant T, Haslam SM, North SJ, Wong NK, Kudo T, Narimatsu H, Esko JD, Drickamer K, Dell A, Paulson JC. A focused microarray approach to functional glycomics: Transcriptional regulation of the glycome. *Glycobiology*. 2006;16:117-131

119. Raman R, Venkataraman M, Ramakrishnan S, Lang W, Raguram S, Sasisekharan R. Advancing glycomics: Implementation strategies at the consortium for functional glycomics. *Glycobiology*. 2006;16:82R-90R

120. Sahoo S, Losordo DW. Exosomes and cardiac repair after myocardial infarction. *Circ Res*. 2014;114:333-344

121. Johnstone RM, Adam M, Hammond JR, Orr L, Turbide C. Vesicle formation during reticulocyte maturation. Association of plasma membrane activities with released vesicles (exosomes). *The Journal of biological chemistry*. 1987;262:9412-9420

122. Thery C, Duban L, Segura E, Veron P, Lantz O, Amigorena S. Indirect activation of naive cd4+ t cells by dendritic cell-derived exosomes. *Nature immunology*. 2002;3:1156-1162

123. Thery C, Zitvogel L, Amigorena S. Exosomes: Composition, biogenesis and function. *Nature reviews. Immunology*. 2002;2:569-579

124. Valadi H, Ekstrom K, Bossios A, Sjostrand M, Lee JJ, Lotvall JO. Exosome-mediated transfer of mrnas and micrornas is a novel mechanism of genetic exchange between cells. *Nat Cell Biol*. 2007;9:654-U672

125. Boon RA, Vickers KC. Intercellular transport of micrornas. *Arterioscl Throm Vas*. 2013;33:186-192

126. Vickers KC, Palmisano BT, Shoucri BM, Shamburek RD, Remaley AT. Micrornas are transported in plasma and delivered to recipient cells by high-density lipoproteins. *Nat Cell Biol*. 2011;13:423-U182

127. Fichtlscherer S, Zeiher AM, Dimmeler S. Circulating micrornas biomarkers or mediators of cardiovascular diseases? *Arterioscl Throm Vas*. 2011;31:2383-2390

128. Ohshima K, Inoue K, Fujiwara A, Hatakeyama K, Kanto K, Watanabe Y, Muramatsu K, Fukuda Y, Ogura S, Yamaguchi K, Mochizuki T. Let-7 microrna family is selectively secreted into the extracellular environment via exosomes in a metastatic gastric cancer cell line. *Plos One*. 2010;5

129. Alvarez-Erviti L, Seow Y, Yin H, Betts C, Lakhal S, Wood MJ. Delivery of sirna to the mouse brain by systemic injection of targeted exosomes. *Nat Biotechnol*. 2011;29:341-345

130. Skog J, Wurdinger T, van Rijn S, Meijer DH, Gainche L, Sena-Esteves M, Curry WT, Jr., Carter BS, Krichevsky AM, Breakefield XO. Glioblastoma microvesicles transport rna and proteins that promote tumour growth and provide diagnostic biomarkers. *Nat Cell Biol*. 2008;10:1470-1476

131. Montecalvo A, Larregina AT, Shufesky WJ, Stolz DB, Sullivan ML, Karlsson JM, Baty CJ, Gibson GA, Erdos G, Wang Z, Milosevic J, Tkacheva OA, Divito SJ, Jordan R, Lyons-Weiler J, Watkins SC, Morelli AE. Mechanism of transfer of functional micrornas between mouse dendritic cells via exosomes. *Blood*. 2012;119:756-766

132. Parolini I, Federici C, Raggi C, Lugini L, Palleschi S, De Milito A, Coscia C, Iessi E, Logozzi M, Molinari A, Colone M, Tatti M, Sargiacomo M, Fais S. Microenvironmental ph is a key factor for exosome traffic in tumor cells. *J Biol Chem*. 2009;284:34211-34222

133. Witwer KW, Buzas EI, Bemis LT, Bora A, Lasser C, Lotvall J, Nolte-'t Hoen EN, Piper MG, Sivaraman S, Skog J, Thery C, Wauben MH, Hochberg F. Standardization of sample collection, isolation and analysis methods in extracellular vesicle research. *Journal of extracellular vesicles*. 2013;2

134. Lai CP, Breakefield XO. Role of exosomes/microvesicles in the nervous system and use in emerging therapies. *Frontiers in physiology*. 2012;3:228

135. Barile L, Gherghiceanu M, Popescu LM, Moccetti T, Vassalli G. Ultrastructural evidence of exosome secretion by progenitor cells in adult mouse myocardium and adult human cardiospheres. *Journal of biomedicine & biotechnology*. 2012;2012:354605

136. Manole CG, Cismasiu V, Gherghiceanu M, Popescu LM. Experimental acute myocardial infarction: Telocytes involvement in neo-angiogenesis. *Journal of cellular and molecular medicine*. 2011;15:2284-2296

137. Mackie AR, Klyachko E, Thorne T, Schultz KM, Millay M, Ito A, Kamide CE, Liu T, Gupta R, Sahoo S, Misener S, Kishore R, Losordo DW. Sonic hedgehog-

modified human cd34+ cells preserve cardiac function after acute myocardial infarction. *Circ Res*. 2012;111:312-321

138. Sahoo S, Klychko E, Thorne T, Misener S, Schultz KM, Millay M, Ito A, Liu T, Kamide C, Agrawal H, Perlman H, Qin G, Kishore R, Losordo DW. Exosomes from human cd34(+) stem cells mediate their proangiogenic paracrine activity. *Circ Res*. 2011;109:724-728

139. Zhang H-G. *Emerging concepts of tumor exosome-mediated cell-cell communication*. New York: Springer; 2013.

140. Vrijsen KR, Sluijter JP, Schuchardt MW, van Balkom BW, Noort WA, Chamuleau SA, Doevendans PA. Cardiomyocyte progenitor cell-derived exosomes stimulate migration of endothelial cells. *Journal of cellular and molecular medicine*. 2010;14:1064-1070

141. Chen L, Wang Y, Pan Y, Zhang L, Shen C, Qin G, Ashraf M, Weintraub N, Ma G, Tang Y. Cardiac progenitor-derived exosomes protect ischemic myocardium from acute ischemia/reperfusion injury. *Biochemical and biophysical research communications*. 2013;431:566-571

142. Lloyd-Jones D, Adams RJ, Brown TM, Carnethon M, Dai S, De Simone G, Ferguson TB, Ford E, Furie K, Gillespie C. Heart disease and stroke statistics--2010 update: A report from the american heart association. *Circulation*. 2010;121:e46

143. Maulik N, Yoshida T, Das DK. Oxidative stress developed during the reperfusion of ischemic myocardium induces apoptosis. *Free Radic. Biol. Med.* 1998;24:869-875

144. Bialik S, Geenen DL, Sasson IE, Cheng R, Horner JW, Evans SM, Lord EM, Koch CJ, Kitsis RN. Myocyte apoptosis during acute myocardial infarction in the mouse localizes to hypoxic regions but occurs independently of p53. *Journal of Clinical Investigation*. 1997;100:1363

145. McGill CJ, Brooks G. Cell cycle control mechanisms and their role in cardiac growth. *Cardiovascular Research*. 1995;30:557-569

146. Rumyantsev PP. Interrelations of the proliferation and differentiation processes during cardiac myogenesis and regeneration. *International Review of Cytology*. 1977;51:187-273

147. Kajstura J, Leri A, Finato N, Di Loreto C, Beltrami CA, Anversa P. Myocyte proliferation in end-stage cardiac failure in humans. *Proceedings of the National Academy of Sciences of the United States of America*. 1998;95:8801

148. Park M, Shen YT, Gaussin V, Heyndrickx GR, Bartunek J, Resuello RRG, Natividad FF, Kitsis RN, Vatner DE, Vatner SF. Apoptosis predominates in nonmyocytes in heart failure. *American Journal of Physiology-Heart and Circulatory Physiology*. 2009;297:H785

149. Maulik N, Engelman RM, Rousou JA, Flack III JE, Deaton D, Das DK. Ischemic preconditioning reduces apoptosis by upregulating anti-death gene bcl-2. *Circulation*. 1999;100:II-369

150. Jolly S, Kane W, Bailie M, Abrams G, Lucchesi B. Canine myocardial reperfusion injury. Its reduction by the combined administration of superoxide dismutase and catalase. *Circ Res*. 1984;54:277

151. Andreka P, Zang J, Dougherty C, Slepak TI, Webster KA, Bishopric NH. Cytoprotection by jun kinase during nitric oxide-induced cardiac myocyte apoptosis. *Circ Res*. 2001;88:305

152. Minamino T, Yujiri T, Papst PJ, Chan ED, Johnson GL, Terada N. Mekk1 suppresses oxidative stress-induced apoptosis of embryonic stem cell-derived cardiac myocytes. *Proceedings of the National Academy of Sciences of the United States of America*. 1999;96:15127

153. Franke TF, Kaplan DR, Cantley LC. Pi3k: Downstream aktion blocks apoptosis. *Cell*. 1997;88:435

154. Wang Y, Huang S, Sah VP, Ross J, Brown JH, Han J, Chien KR. Cardiac muscle cell hypertrophy and apoptosis induced by distinct members of the p38 mitogen-activated protein kinase family. *Journal of Biological Chemistry*. 1998;273:2161

155. Chua CC, Gao J, Ho YS, Xiong Y, Xu X, Chen Z, Hamdy RC, Chua BHL. Overexpression of iap-2 attenuates apoptosis and protects against myocardial ischemia/reperfusion injury in transgenic mice. *Biochimica et Biophysica Acta (BBA)-Molecular Cell Research*. 2007;1773:577-583

156. Matherne GP, Linden J, Byford AM, Gauthier NS, Headrick JP. Transgenic a1 adenosine receptor overexpression increases myocardial resistance to ischemia. *Proceedings of the National Academy of Sciences of the United States of America*. 1997;94:6541

157. Matsui T, Tao J, del Monte F, Lee KH, Li L, Picard M, Force TL, Franke TF, Hajjar RJ, Rosenzweig A. Akt activation preserves cardiac function and prevents injury after transient cardiac ischemia in vivo. *Circulation*. 2001;104:330

158. Vemuri S, Rhodes C. Preparation and characterization of liposomes as therapeutic delivery systems: A review. *Pharmaceutica Acta Helvetiae*. 1995;70:95-111

159. Seshadri G, Sy JC, Brown M, Dikalov S, Yang SC, Murthy N, Davis ME. The delivery of superoxide dismutase encapsulated in polyketal microparticles to rat myocardium and protection from myocardial ischemia-reperfusion injury. *Biomaterials*. 2010;31:1372-1379

160. Yuan XB, Gu MQ, Kang CS, Zhao YH, Tian NJ, Pu PY, Sheng J. Surface biofunctionalization of pla nanoparticles through amphiphilic polysaccharide coating and ligand coupling: Evaluation of biofunctionalization and drug releasing behavior. *Carbohyd Polym*. 2007;67:417-426

161. Granger BL, Lazarides E. Desmin and vimentin coexist at the periphery of the myofibril z disc. *Cell*. 1979;18:1053-1063

162. Li Z, Mericskay M, Agbulut O, Butler-Browne G, Carlsson L, Thornell LE, Babinet C, Paulin D. Desmin is essential for the tensile strength and integrity of myofibrils but not for myogenic commitment, differentiation, and fusion of skeletal muscle. *The Journal of Cell Biology*. 1997;139:129-144

163. Bogoyevitch MA, Gillespie-Brown J, Ketterman AJ, Fuller SJ, Ben-Levy R, Ashworth A, Marshall CJ, Sugden PH. Stimulation of the stress-activated mitogen-activated protein kinase subfamilies in perfused heart. P38/rk mitogen-activated protein kinases and c-jun n-terminal kinases are activated by ischemia/reperfusion. *Circulation research*. 1996;79:162-173

164. Pombo CM, Bonventre JV, Avruch J, Woodgett JR, Kyriakis JM, Force T. The stress-activated protein kinases are major c-jun amino-terminal kinases activated by ischemia and reperfusion. *The Journal of biological chemistry*. 1994;269:26546-26551

165. Yin T, Sandhu G, Wolfgang CD, Burrier A, Webb RL, Rigel DF, Hai T, Whelan J. Tissue specific pattern of stress kinase activation in ischemia/reperfused heart and kidney. *Journal of Biological Chemistry*. 1997;272:19943-19950

166. Amado LC, Saliaris AP, Schuleri KH, St John M, Xie JS, Cattaneo S, Durand DJ, Fitton T, Kuang JQ, Stewart G, Lehrke S, Baumgartner WW, Martin BJ, Heldman AW, Hare JM. Cardiac repair with intramyocardial injection of allogeneic mesenchymal stem cells after myocardial infarction. *Proceedings of the National Academy of Sciences of the United States of America*. 2005;102:11474-11479

167. Krause K, Jaquet K, Schneider C, Haupt S, Lioznov MV, Otte KM, Kuck KH. Percutaneous intramyocardial stem cell injection in patients with acute myocardial infarction: First-in-man study. *Heart*. 2009;95:1145-1152

168. Herreros J, Prosper F, Perez A, Gavira JJ, Garcia-Velloso MJ, Barba J, Sanchez PL, Canizo C, Rabago G, Marti-Climent JM, Hernandez M, Lopez-Holgado N, Gonzalez-Santos JM, Martin-Luengo C, Alegria E. Autologous intramyocardial injection of cultured skeletal muscle-derived stem cells in patients with non-acute myocardial infarction. *Eur Heart J*. 2003;24:2012-2020

169. Li Q, Li B, Wang X, Leri A, Jana KP, Liu Y, Kajstura J, Baserga R, Anversa P. Overexpression of insulin-like growth factor-1 in mice protects from myocyte death after infarction, attenuating ventricular dilation, wall stress, and cardiac hypertrophy. *J Clin Invest*. 1997;100:1991-1999

170. Sabbah HN, Sharov VG, Gupta RC, Todor A, Singh V, Goldstein S. Chronic therapy with metoprolol attenuates cardiomyocyte apoptosis in dogs with heart failure. *Journal of the American College of Cardiology*. 2000;36:1698-1705

171. Jones SP, Zachara NE, Ngoh GA, Hill BG, Teshima Y, Bhatnagar A, Hart GW, Marban E. Cardioprotection by n-acetylglucosamine linkage to cellular proteins. *Circulation*. 2008;117:1172

172. Gray WD, Che P, Brown M, Ning X, Murthy N, Davis ME. N-acetylglucosamine conjugated to nanoparticles enhances myocyte uptake and improves delivery of a small molecule p38 inhibitor for post-infarct healing. *Journal of cardiovascular translational research*. 2011;4:631-643

173. Yan Y, Such GK, Johnston APR, Best JP, Caruso F. Engineering particles for therapeutic delivery: Prospects and challenges. *ACS Nano*. 2012;6:3663-3669

174. Astruc D, Boisselier E, Ornelas C. Dendrimers designed for functions: From physical, photophysical, and supramolecular properties to applications in sensing, catalysis, molecular electronics, photonics, and nanomedicine. *Chemical reviews*. 2010;110:1857-1959

175. Liu J, Gray WD, Davis ME, Luo Y. Peptide- and saccharide-conjugated dendrimers for targeted drug delivery: A concise review. *Interface Focus*. 2012;2:307-324

176. Soliman G, Sharma A, Maysinger D, Kakkar A. Dendrimers and miktoarm polymers based multivalent nanocarriers for efficient and targeted drug delivery. *Chemical Communications*. 2011;47:9572-9587

177. Tomalia D. Birth of a new macromolecular architecture: Dendrimers as quantized building blocks for nanoscale synthetic polymer chemistry. *Progress in Polymer Science*. 2005;30:294-324

178. Waite CL, Roth CM. Pamam-rgd conjugates enhance sirna delivery through a multicellular spheroid model of malignant glioma. *Bioconjugate Chemistry*. 2009;20:1908-1916

179. Dufès C, Uchegbu I, Schatzlein A. Dendrimers in gene delivery. *Advanced Drug Delivery Reviews*. 2005;57:2177-2202

180. Liu X, Liu J, Luo Y. Facile glycosylation of dendrimers for eliciting specific cell–material interactions. *Polymer Chemistry*. 2012;3:310-313

181. Shukla R, Thomas T, Peters J, Kotlyar A, Myc A, Baker Jr J. Tumor angiogenic vasculature targeting with pamam dendrimer–rgd conjugates. *Chemical Communications*. 2005:5739-5741

182. Wolfenden ML, Cloninger MJ. Carbohydrate-functionalized dendrimers to investigate the predictable tunability of multivalent interactions. *Bioconjugate Chemistry*. 2006;17:958-966

183. Schneider CA, Rasband WS, Eliceiri KW. Nih image to imagej: 25 years of image analysis. *Nature Methods*. 2012;9:671-675

184. Bumcrot D, Manoharan M, Koteliansky V, Sah DWY. Rnai therapeutics: A potential new class of pharmaceutical drugs. *Nature Chemical Biology*. 2006;2:711-719

185. Pecot C, Calin G, Coleman R, Lopez-Berestein G, Sood A. Rna interference in the clinic: Challenges and future directions. *Nature Reviews Cancer*. 2010;11:59-67

186. Gillies ER, Dy E, Fréchet JMJ, Szoka FC. Biological evaluation of polyester dendrimer: Poly(ethylene oxide) "bow-tie" hybrids with tunable molecular weight and architecture. *Molecular Pharmaceutics*. 2005;2:129-138

187. Gillies ER, Fréchet JMJ. Designing macromolecules for therapeutic applications: Polyester dendrimerpoly(ethylene oxide) "bow-tie" hybrids with tunable molecular weight and architecture. *Journal of the American Chemical Society*. 2002;124:14137-14146

188. Wu P, Malkoch M, Hunt JN, Vestberg R, Kaltgrad E, Finn MG, Fokin VV, Sharpless KB, Hawker CJ. Multivalent, bifunctional dendrimers prepared by click chemistry. *Chemical Communications*. 2005:5775-5777

189. Gaertner HF, Cerini F, Kamath A, Rochat A-F, Siegrist C-A, Menin L, Hartley O. Efficient orthogonal bioconjugation of dendrimers for synthesis of bioactive nanoparticles. *Bioconjugate Chemistry*. 2011;22:1103-1114

190. Tomalia D, Huang B, Swanson D, Brothers H, Klimash J. Structure control within poly (amidoamine) dendrimers: Size, shape and regio-chemical mimicry of globular proteins. *Tetrahedron*. 2003;59:3799-3813

191. Gray WD, Wu RJ, Yin X, Zhou J, Davis ME, Luo Y. Dendrimeric bowties featuring hemispheric-selective decoration of ligands for microrna-based therapy. *Biomacromolecules*. 2013;14:101-109

192. Stasko NA, Johnson CB, Schoenfisch MH, Johnson TA, Holmuhamedov EL. Cytotoxicity of polypropylenimine dendrimer conjugates on cultured endothelial cells. *Biomacromolecules*. 2007;8:3853-3859

193. Hunter AC. Molecular hurdles in polyfectin design and mechanistic background to polycation induced cytotoxicity. *Advanced Drug Delivery Reviews*. 2006;58:1523-1531

194. Almutairi A, Rossin R, Shokeen M, Hagooly A, Ananth A, Capoccia B, Guillaudeu S, Abendschein D, Anderson C, Welch M. Biodegradable dendritic positron-emitting nanoprobes for the noninvasive imaging of angiogenesis. *Proceedings of the National Academy of Sciences of the United States of America*. 2009;106:685-690

195. Boswell C, Eck P, Regino C, Bernardo M, Wong K, Milenic D, Choyke P, Brechbiel M. Synthesis, characterization, and biological evaluation of integrin αvβ3-targeted pamam dendrimers. *Molecular Pharmaceutics*. 2008;5:527-539

196. Pandita D, Santos J, Rodrigues J, Pêgo A, Granja P, Tomás H. Gene delivery into mesenchymal stem cells: A biomimetic approach using rgd nanoclusters based on poly (amidoamine) dendrimers. *Biomacromolecules*. 2011;12:472-481

197. Feng R, Chen X, Yu Y, Su L, Yu B, Li J, Cai Q, Yan M, Liu B, Zhu Z. Mir-126 functions as a tumour suppressor in human gastric cancer. *Cancer letters*. 2010;298:50-63

198. Zernecke A, Bidzhekov K, Noels H, Shagdarsuren E, Gan L, Denecke B, Hristov M, Köppel T, Jahantigh MN, Lutgens E, Wang S, Olson EN, Schober A, Weber C. Delivery of microrna-126 by apoptotic bodies induces cxcl12-dependent vascular protection. *Science Signaling*. 2009;2:ra81

199. Harnprasopwat R, Ha D, Toyoshima T, Lodish H, Tojo A, Kotani A. Alteration of processing induced by a single nucleotide polymorphism in pri-mir-126. *Biochemical and Biophysical Research Communications*. 2010;399:117-122

200. Fish J, Santoro M, Morton S, Yu S, Yeh R, Wythe J, Ivey K. Mir-126 regulates angiogenic signaling and vascular integrity. *Developmental Cell*. 2008;15:272-284

201. Oglesby IK, Bray IM, Chotirmall SH, Stallings RL, O'Neill SJ, McElvaney NG, Greene CM. Mir-126 is downregulated in cystic fibrosis airway epithelial cells and regulates tom1 expression. *Journal of Immunology*. 2010;184:1702-1709

202. Aplin AE, Howe A, Alahari SK, Juliano RL. Signal transduction and signal modulation by cell adhesion receptors: The role of integrins, cadherins, immunoglobulin-cell adhesion molecules, and selectins. *Pharmacological Reviews*. 1998;50:197-263

203. Aizpurua JM, Ganboa JI, Palomo C, Loinaz I, Oyarbide J, Fernandez X, Balentová E, Fratila RM, Jiménez A, Miranda JI, Laso A, Ávila S, Castrillo JL. Cyclic rgd β-lactam peptidomimetics induce differential gene expression in human endothelial cells. *ChemBioChem*. 2011;12:401-405

204. Kuehbacher A, Urbich C, Zeiher AM, Dimmeler S. Role of dicer and drosha for endothelial microrna expression and angiogenesis. *Circulation research*. 2007;101:59-68

205. Bonauer A, Carmona G, Iwasaki M, Mione M, Koyanagi M, Fischer A, Burchfield J, Fox H, Doebele C, Ohtani K. Microrna-92a controls angiogenesis and functional recovery of ischemic tissues in mice. *Science*. 2009;324:1710

206. Chen Y, Gorski DH. Regulation of angiogenesis through a microrna (mir-130a) that down-regulates antiangiogenic homeobox genes gax and hoxa5. *Blood*. 2008;111:1217-1226

207. Anand S, Majeti B, Acevedo L, Murphy E, Mukthavaram R, Scheppke L, Huang M, Shields D, Lindquist J, Lapinski P. Microrna-132-mediated loss of p120rasgap activates the endothelium to facilitate pathological angiogenesis. *Nature Medicine*. 2010;16:909-914

208. Caporali A, Emanueli C. Microrna regulation in angiogenesis. *Vascular Pharmacology*. 2011;55:1-8

209. Zhu H, Fan G-C. Extracellular/circulating micrornas and their potential role in cardiovascular disease. *American Journal of Cardiovascular Disease*. 2011;1:138-149

210. Gnecchi M, He H, Liang OD, Melo LG, Morello F, Mu H, Noiseux N, Zhang L, Pratt RE, Ingwall JS, Dzau VJ. Paracrine action accounts for marked protection of ischemic heart by akt-modified mesenchymal stem cells. *Nat Med*. 2005;11:367-368

211. Gnecchi M, He H, Noiseux N, Liang OD, Zhang L, Morello F, Mu H, Melo LG, Pratt RE, Ingwall JS, Dzau VJ. Evidence supporting paracrine hypothesis for akt-modified mesenchymal stem cell-mediated cardiac protection and functional improvement. *FASEB journal : official publication of the Federation of American Societies for Experimental Biology*. 2006;20:661-669

212. Gnecchi M, Zhang Z, Ni A, Dzau VJ. Paracrine mechanisms in adult stem cell signaling and therapy. *Circ Res*. 2008;103:1204-1219

213. Zernecke A, Bidzhekov K, Noels H, Shagdarsuren E, Gan L, Denecke B, Hristov M, Koppel T, Jahantigh MN, Lutgens E, Wang S, Olson EN, Schober A, Weber C. Delivery of microrna-126 by apoptotic bodies induces cxcl12-dependent vascular protection. *Sci Signal*. 2009;2:ra81

214. Li X, Arslan F, Ren Y, Adav SS, Poh KK, Sorokin V, Lee CN, de Kleijn D, Lim SK, Sze SK. Metabolic adaptation to a disruption in oxygen supply during myocardial ischemia and reperfusion is underpinned by temporal and quantitative changes in the cardiac proteome. *Journal of proteome research*. 2012;11:2331-2346

215. Scheurer SB, Rybak JN, Rosli C, Neri D, Elia G. Modulation of gene expression by hypoxia in human umbilical cord vein endothelial cells: A transcriptomic and proteomic study. *Proteomics*. 2004;4:1737-1760

216. Elbashir SM, Harborth J, Lendeckel W, Yalcin A, Weber K, Tuschl T. Duplexes of 21-nucleotide rnas mediate rna interference in cultured mammalian cells. *Nature*. 2001;411:494-498

217. Mittelbrunn M, Sanchez-Madrid F. Intercellular communication: Diverse structures for exchange of genetic information. *Nature reviews. Molecular cell biology*. 2012;13:328-335

218. Tauro BJ, Greening DW, Mathias RA, Ji H, Mathivanan S, Scott AM, Simpson RJ. Comparison of ultracentrifugation, density gradient separation, and immunoaffinity capture methods for isolating human colon cancer cell line lim1863-derived exosomes. *Methods*. 2012;56:293-304

219. Valadi H, Ekstrom K, Bossios A, Sjostrand M, Lee JJ, Lotvall JO. Exosome-mediated transfer of mrnas and micrornas is a novel mechanism of genetic exchange between cells. *Nat Cell Biol*. 2007;9:654-659

220. Weber JA, Baxter DH, Zhang S, Huang DY, Huang KH, Lee MJ, Galas DJ, Wang K. The microrna spectrum in 12 body fluids. *Clinical chemistry*. 2010;56:1733-1741

221. Kuwabara Y, Ono K, Horie T, Nishi H, Nagao K, Kinoshita M, Watanabe S, Baba O, Kojima Y, Shizuta S, Imai M, Tamura T, Kita T, Kimura T. Increased microrna-1 and microrna-133a levels in serum of patients with cardiovascular disease indicate myocardial damage. *Circulation. Cardiovascular genetics*. 2011;4:446-454

222. Arroyo JD, Chevillet JR, Kroh EM, Ruf IK, Pritchard CC, Gibson DF, Mitchell PS, Bennett CF, Pogosova-Agadjanyan EL, Stirewalt DL, Tait JF, Tewari M. Argonaute2 complexes carry a population of circulating micrornas independent of vesicles in human plasma. *Proceedings of the National Academy of Sciences of the United States of America*. 2011;108:5003-5008

223. Kroh EM, Parkin RK, Mitchell PS, Tewari M. Analysis of circulating microrna biomarkers in plasma and serum using quantitative reverse transcription-pcr (qrt-pcr). *Methods*. 2010;50:298-301

224. Mittelbrunn M, Gutierrez-Vazquez C, Villarroya-Beltri C, Gonzalez S, Sanchez-Cabo F, Gonzalez MA, Bernad A, Sanchez-Madrid F. Unidirectional transfer of microrna-loaded exosomes from t cells to antigen-presenting cells. *Nature communications*. 2011;2:282

225. Thery C, Amigorena S, Raposo G, Clayton A. Isolation and characterization of exosomes from cell culture supernatants and biological fluids. *Current protocols in cell biology / editorial board, Juan S. Bonifacino ... [et al.]*. 2006;Chapter 3:Unit 3 22

226. Muller G, Jung C, Straub J, Wied S, Kramer W. Induced release of membrane vesicles from rat adipocytes containing glycosylphosphatidylinositol-anchored microdomain and lipid droplet signalling proteins. *Cellular signalling*. 2009;21:324-338

227. Malik ZA, Kott KS, Poe AJ, Kuo T, Chen L, Ferrara KW, Knowlton AA. Cardiac myocyte exosomes: Stability, hsp60, and proteomics. *American journal of physiology. Heart and circulatory physiology*. 2013;304:H954-965

228. Park JE, Tan HS, Datta A, Lai RC, Zhang H, Meng W, Lim SK, Sze SK. Hypoxic tumor cell modulates its microenvironment to enhance angiogenic and metastatic potential by secretion of proteins and exosomes. *Molecular & cellular proteomics : MCP*. 2010;9:1085-1099

229. Schorey JS, Bhatnagar S. Exosome function: From tumor immunology to pathogen biology. *Traffic*. 2008;9:871-881

230. Fruhbeis C, Frohlich D, Kramer-Albers EM. Emerging roles of exosomes in neuron-glia communication. *Frontiers in physiology*. 2012;3:119

231. Arslan F, Lai RC, Smeets MB, Akeroyd L, Choo A, Aguor EN, Timmers L, van Rijen HV, Doevendans PA, Pasterkamp G, Lim SK, de Kleijn DP. Mesenchymal stem cell-derived exosomes increase atp levels, decrease oxidative stress and activate pi3k/akt pathway to enhance myocardial viability and prevent adverse remodeling after myocardial ischemia/reperfusion injury. *Stem cell research*. 2013;10:301-312

232. Garbern JC, Lee RT. Cardiac stem cell therapy and the promise of heart regeneration. *Cell stem cell*. 2013;12:689-698

233. Segers VF, Lee RT. Stem-cell therapy for cardiac disease. *Nature*. 2008;451:937-942

234. Passier R, van Laake LW, Mummery CL. Stem-cell-based therapy and lessons from the heart. *Nature*. 2008;453:322-329

235. Matsuura K, Honda A, Nagai T, Fukushima N, Iwanaga K, Tokunaga M, Shimizu T, Okano T, Kasanuki H, Hagiwara N, Komuro I. Transplantation of cardiac progenitor cells ameliorates cardiac dysfunction after myocardial infarction in mice. *J Clin Invest*. 2009;119:2204-2217

236. Tang XL, Rokosh G, Sanganalmath SK, Yuan F, Sato H, Mu J, Dai S, Li C, Chen N, Peng Y, Dawn B, Hunt G, Leri A, Kajstura J, Tiwari S, Shirk G, Anversa P, Bolli R. Intracoronary administration of cardiac progenitor cells alleviates left ventricular dysfunction in rats with a 30-day-old infarction. *Circulation*. 2010;121:293-305

237. Urbich C, Aicher A, Heeschen C, Dernbach E, Hofmann WK, Zeiher AM, Dimmeler S. Soluble factors released by endothelial progenitor cells promote migration of endothelial cells and cardiac resident progenitor cells. *J Mol Cell Cardiol*. 2005;39:733-742

238. Tang YL, Zhu W, Cheng M, Chen L, Zhang J, Sun T, Kishore R, Phillips MI, Losordo DW, Qin G. Hypoxic preconditioning enhances the benefit of cardiac progenitor cell therapy for treatment of myocardial infarction by inducing cxcr4 expression. *Circ Res*. 2009;104:1209-1216

239. Bonauer A, Dimmeler S. The microrna-17-92 cluster: Still a miracle? *Cell Cycle*. 2009;8:3866-3873

240. Mendell JT. Miriad roles for the mir-17-92 cluster in development and disease. *Cell*. 2008;133:217-222

241. Staszel T, Zapala B, Polus A, Sadakierska-Chudy A, Kiec-Wilk B, Stepien E, Wybranska I, Chojnacka M, Dembinska-Kiec A. Role of micrornas in endothelial cell pathophysiology. *Polskie Archiwum Medycyny Wewnetrznej*. 2011;121:361-366

242. Zhu H, Fan GC. Role of micrornas in the reperfused myocardium towards post-infarct remodelling. *Cardiovasc Res*. 2012;94:284-292

243. Puissegur MP, Mazure NM, Bertero T, Pradelli L, Grosso S, Robbe-Sermesant K, Maurin T, Lebrigand K, Cardinaud B, Hofman V, Fourre S, Magnone V, Ricci JE, Pouyssegur J, Gounon P, Hofman P, Barbry P, Mari B. Mir-210 is overexpressed in late stages of lung cancer and mediates mitochondrial alterations associated with modulation of hif-1 activity. *Cell death and differentiation*. 2011;18:465-478

244. Hu S, Huang M, Li Z, Jia F, Ghosh Z, Lijkwan MA, Fasanaro P, Sun N, Wang X, Martelli F, Robbins RC, Wu JC. Microrna-210 as a novel therapy for treatment of ischemic heart disease. *Circulation*. 2010;122:S124-131

245. Hood JL, San RS, Wickline SA. Exosomes released by melanoma cells prepare sentinel lymph nodes for tumor metastasis. *Cancer research*. 2011;71:3792-3801

246. Deregibus MC, Cantaluppi V, Calogero R, Lo Iacono M, Tetta C, Biancone L, Bruno S, Bussolati B, Camussi G. Endothelial progenitor cell derived microvesicles activate an angiogenic program in endothelial cells by a horizontal transfer of mrna. *Blood*. 2007;110:2440-2448

247. Hill JA, Olson EN. Cardiac plasticity. *The New England journal of medicine*. 2008;358:1370-1380

248. Leask A, Abraham DJ. Tgf-beta signaling and the fibrotic response. *FASEB journal : official publication of the Federation of American Societies for Experimental Biology*. 2004;18:816-827

249. Brigstock DR. Connective tissue growth factor (ccn2, ctgf) and organ fibrosis: Lessons from transgenic animals. *Journal of cell communication and signaling*. 2010;4:1-4

250. Liu S, Shi-wen X, Abraham DJ, Leask A. Ccn2 is required for bleomycin-induced skin fibrosis in mice. *Arthritis and rheumatism*. 2011;63:239-246

251. Pandit KV, Corcoran D, Yousef H, Yarlagadda M, Tzouvelekis A, Gibson KF, Konishi K, Yousem SA, Singh M, Handley D, Richards T, Selman M, Watkins SC, Pardo A, Ben-Yehudah A, Bouros D, Eickelberg O, Ray P, Benos PV, Kaminski N. Inhibition and role of let-7d in idiopathic pulmonary fibrosis. *American journal of respiratory and critical care medicine*. 2010;182:220-229

252. Kodama T, Takehara T, Hikita H, Shimizu S, Shigekawa M, Tsunematsu H, Li W, Miyagi T, Hosui A, Tatsumi T, Ishida H, Kanto T, Hiramatsu N, Kubota S, Takigawa M, Tomimaru Y, Tomokuni A, Nagano H, Doki Y, Mori M, Hayashi N. Increases in p53 expression induce ctgf synthesis by mouse and human hepatocytes and result in liver fibrosis in mice. *J Clin Invest*. 2011;121:3343-3356

253. van Almen GC, Verhesen W, van Leeuwen RE, van de Vrie M, Eurlings C, Schellings MW, Swinnen M, Cleutjens JP, van Zandvoort MA, Heymans S, Schroen B. Microrna-18 and microrna-19 regulate ctgf and tsp-1 expression in age-related heart failure. *Aging cell*. 2011;10:769-779

254. Betel D, Wilson M, Gabow A, Marks DS, Sander C. The microrna.Org resource: Targets and expression. *Nucleic acids research*. 2008;36:D149-153

255. Spinetti G, Fortunato O, Caporali A, Shantikumar S, Marchetti M, Meloni M, Descamps B, Floris I, Sangalli E, Vono R, Faglia E, Specchia C, Pintus G, Madeddu P, Emanueli C. Microrna-15a and microrna-16 impair human circulating proangiogenic cell functions and are increased in the proangiogenic cells and serum of patients with critical limb ischemia. *Circ Res*. 2013;112:335-346

256. Ngoh GA, Hamid T, Prabhu SD, Jones SP. O-glcnac signaling attenuates er stress-induced cardiomyocyte death. *American journal of physiology. Heart and circulatory physiology*. 2009;297:H1711-1719

257. Zafir A, Readnower R, Long BW, McCracken J, Aird A, Alvarez A, Cummins TD, Li Q, Hill BG, Bhatnagar A, Prabhu SD, Bolli R, Jones SP. Protein o-glcnacylation is a novel cytoprotective signal in cardiac stem cells. *Stem Cells*. 2013;31:765-775

258. Lee I, Park M, Kim Y, Hwang O, Khang G, Lee D. Ketal containing amphiphilic block copolymer micelles as ph-sensitive drug carriers. *International journal of pharmaceutics*. 2013;448:259-266

259. Liu J, Gu C, Cabigas EB, Pendergrass KD, Brown ME, Luo Y, Davis ME. Functionalized dendrimer-based delivery of angiotensin type 1 receptor sirna for preserving cardiac function following infarction. *Biomaterials*. 2013;34:3729-3736

260. Shenoi RA, Lai BF, Imran ul-haq M, Brooks DE, Kizhakkedathu JN. Biodegradable polyglycerols with randomly distributed ketal groups as multi-functional drug delivery systems. *Biomaterials*. 2013;34:6068-6081

261. Shenoi RA, Narayanannair JK, Hamilton JL, Lai BF, Horte S, Kainthan RK, Varghese JP, Rajeev KG, Manoharan M, Kizhakkedathu JN. Branched multifunctional polyether polyketals: Variation of ketal group structure enables unprecedented control over polymer degradation in solution and within cells. *Journal of the American Chemical Society*. 2012;134:14945-14957

262. Sohn YD, Somasuntharam I, Che PL, Jayswal R, Murthy N, Davis ME, Yoon YS. Induction of pluripotency in bone marrow mononuclear cells via polyketal nanoparticle-mediated delivery of mature micrornas. *Biomaterials*. 2013;34:4235-4241

263. Somasuntharam I, Boopathy AV, Khan RS, Martinez MD, Brown ME, Murthy N, Davis ME. Delivery of nox2-nadph oxidase sirna with polyketal nanoparticles for improving cardiac function following myocardial infarction. *Biomaterials*. 2013;34:7790-7798

264. Wang Y, Chang B, Yang W. Ph-sensitive polyketal nanoparticles for drug delivery. *Journal of nanoscience and nanotechnology*. 2012;12:8266-8275

265. Whiting BT, Coates GW. Synthesis and polymerization of bicyclic ketals: A practical route to high-molecular weight polyketals. *Journal of the American Chemical Society*. 2013;135:10974-10977

VITA

WARREN DALE GRAY

Originally hailing from Oregon City, OR—the end of the Oregon Trail—Warren's first educational experiences were in music (violin lessons), biology (calf birthing), horticulture (flower and vegetable farming), exercise (chasing—and being chased by—his siblings) and fear-conquering (egg collection from the chicken coop). In his teens, he won baking competitions at the county fair and sang, dance, and acted in numerous high school stage productions. At Oregon State University (OSU), he studied chemical engineering and took enough gymnastics classes to unofficially minor. At OSU, he conducted research under Dr. Joseph McGuire on protein adsorption at interfaces. Warren lived for two years in Louisiana, where he served as a missionary for the Church of Jesus Christ of Latter-day Saints and was involved in Hurricane Katrina recuperation. During his graduate years, he was a student at Georgia Institute of Technology, Emory University, and Peking University. Additionally, he took up ballet and swimming, ran three 24-hour relay races in Georgia and Tennesse, and hiked on the Appalachian Trail, in the Great Smoky Mountains, and along the Blue Ridge Parkway. In China, he searched for the best kung pao chicken and managed with (very) broken Mandarin.

Warren and his wife, Whitney, expect to live a life full of adventures.